POLYMERIZED BENTONITES AND THEIR APPLICATIONS IN GEOSYNTHETIC CLAY LINER

July 2018

Department of Science and Advanced Technology
Graduate School of Science and Engineering
Saga University

NUTTHACHAI PRONGMANEE

Polymerized Bentonites and Their Applications in Geosynthetic Clay Liner

A dissertation submitted in partial fulfillment of the requirement for the degree of Doctor of Philosophy in Geotechnical Engineering

By

NUTTHACHAI PRONGMANEE

Examination Committee:	Prof. Jinchun Chai (Supervisor) Prof. Takenori Hino Associate Prof. Akira Sakai Associate Prof. Daisuke Suetsugu Prof. Shuilong Shen (External Examiner) Shanghai Jiao Tong University, Chaina
Nationality:	Thai
Previous Degrees:	Bachelor of Civil Engineering Suranaree University of Technology (SUT), Nakhon Ratchasima, Thailand Master in Geotecnical Engineering Asian Institute of Technology (AIT), Pathum Thani, Thailand
Scholarship Donor:	MEXT (Ministry of Education, Culture, Sports, Science, and Technology)

Department of Science and Advanced Technology
Graduate School of Science and Engineering
Saga University, Japan

ACKNOWLEDGEMENT

I express deepest gratitude to my supervisor Professor Jin-Chun Chai for his guidance, and suggestions during study. I am grateful to my former supervisors, Professor Dennes T. Bergado, Professor Suksun Horpibulsuk and Dr. Thayanan Boonyarak.

I am also thankful to the examination committee members, Prof. Takenori Hino, Associate Prof. Akira Sakai, Associate Prof. Daisuke Suetsugu and Prof. Shuilong Shen (External Examiner) for their valuable suggestions and comments on the dissertation. Special thanks to Mr. Akinori Saito for his technical support. I am also grateful to Assist. Prof. Takehito Negami for scanning electron microscope (SEM) images.

I would like to acknowledge to the scholarship grant provided by MEXT (Ministry of Education, Culture, Sports, Science, and Technology) for the opportunity and financial support of my study in Saga University.

I am grateful to my seniors, Dr. Apichat Suddeepong, Dr. Sailesh Shrestha, Dr. Nachanok Chanmee, and Dr. Yang Zhou. I am also thanks to my colleagues, Mr. Krisana Kobwittaya, Mr. Yi-Tian Lu, Mr. Peerapat Khaimook, Mr. Hong-Tao Fu, Mr. Takaharu Ide, and Mr. Yuto Toko for kindly helping.

I express a lot of gratefulness to my mother for her inspiration and all necessary helps. Finally, I dedicated this work to my father.

ABSTRACT

To increase the swell potential of bentonite in high cation concentration solutions and corrosive solutions, effectiveness of polymerizing bentonites was investigated experimentally. Firstly, the optimum conditions for producing polymerized bentonite (PB) were investigated systematically by varying initiator type, pH value, monomer to initiator ratio etc. Free swelling index (FSI) of the produced PB is used as an index to judge the optimum conditions. The proposed optimum conditions are using the free radical polymerization method, with sodium acrylate as the monomer and KPS as the initiator, pH of 7, the initiator (*I*) to monomer (*M*) ratio, *I/M,* of 0.2 and the monomer content of 10%.

The result of X-ray diffraction (XRD) pattern of the PB indicates that polymerizing the sodium polyacrylate onto the bentonite particles does not modify the interlayer spacing of the bentonite. Additionally, scanning electron microscope (SEM) image of the PB showed rounder edges compared with that of the untreated bentonite (UB). It is considered that the polymer coated onto the bentonite particles.

The properties of the PB in aggressive chemical solutions were investigated subsequently through a series of consolidation test, permeability (*k*) test, and swelling pressure test by considering effect of cation concentration, valence of cation and pH levels of the solutions. The test results indicated that the PB had higher compression index (C_c), swelling index (C_s), and lower coefficient of consolidation (c_v) in the aggressive solutions compared with that of the UB. Under the identical void ratio (*e*), the PB had much lower *k* value than that of the UB. The results of swelling pressure tests, under a comparable initial dry density, PB had higher swelling pressure than that of the UB for all tested liquids. The higher swelling potential of the PB in cationic solutions is that a negatively charged functional group (COO^-) of the sodium polyacrylate may attract to some cations in the solutions before it tries to enter into the interlayer of the bentonite particles. It is suggested that the PB can be used as a core material for a barrier system, such as geosynthetic clay liner (GCL) to be used for aggressive chemical solutions.

Then, the self-healing capacity of the GCL using the PB as core material (PB-GCL) have been investigated experimentally through a series of small scale and large scale leakage rate tests. The results of small scale leakage rate test show that the PB-GCL specimens had higher self-healing capacity than that of the corresponding GCL specimens using the UB (UB-

GCL). Especially, when using 0.6 M $CaCl_2$ solution, for a 20 mm in diameter damage hole, the UB-GCL specimen gave a zero-healing ratio (healed damage area/total damage area), but the PB-GCL specimen resulted in about 76% healing ratio. The self-healing capacity of the PB-GCL and the UB-GCL was then investigated by considering of the effect of the pH level through a series of large scale leakage rate test. The test results showed that the PB-GCL resulted in the higher self-healing capacity compared with that of the UB-GCL, and consequently lower permeability of damage hole (k_{hole}) in all tested solutions. It is very interesting to note that the PB-GCL had increasing in the barrier performance when interacted with a corrosive alkaline solution (pH =13), i.e. higher swelling potential, lower permeability compared to that in deionized water. The possible reason is that the increasing in OH^- concentration increases the repulsive force between the chained anionic polymer, and resulting in increase in swelling capacity. Based on test results in this study, the PB-GCL can be recommended as an effective barrier for containing an aggressive liquid waste.

TABLE OF CONTENTS

LIST OF TABLES

LIST OF FIGURES

LIST OF NOTATIONS

$1/\kappa$	Thickness of double layer
k_b	Boltzmann constant
T	Absolute temperature
n	Molar concentration of ions in pore fluid
ε_0	Elementary charge
v	Ionic valence
e_e	Elementary electric charge
k	Permeability or hydraulic conductivity
ψ	Permittivity
Q	Flow rate
σ	Overburden pressure
hv	energy of a single photon of frequency v
Δ	Thermal energy
d	Space between layers in the clay lattice
θ	Measured diffraction angle
λ	Wave length of X-ray radiation
AA	Acrylic acid
Na-AA	Sodium acrylate monomer
FSI	Free swelling index
I/M	weight of the initiator (I) to the weight of the monomer (M)
EC	Electro conductivity
pH	Potential of hydrogen
XRD	X-ray diffraction
SEM	Scanning Electron Microscopy
UB	Untreated bentonite
PB	Polymerized bentonite
G	Specific gravity
w_l	Liquids limits
w_p	Plastic limit
σ_v'	Vertical effective stress
w_i	Initial water content

e_i	Initial void ratio
C_c	Compression index
C_s	Swelling index
m_v	Coefficient of volume change
c_v	Coefficients of consolidation
t_{90}	Time at 90% of consolidation
e	Void ratio
V_f	Fluid loss volume
V	Filtrated volume
k_{filter}	Permeability from filter press test
ω	Total filtrate volume
ΔP	Pressure gradient
A_c	Cross-section area
μ	Viscosity of filtrated liquids
c	Thickness of the filter cake
g	Gravity acceleration
ψ_{filter}	Permittivity of filter cake
α	Healing ratio
A_{hole}	Total damage hole area
A_1	Healed area
k_{hole}	Permeability of the damage hole
k_d	Average permeability of the damaged sample
k_{ud}	Permeability of the sample without damage
A_{total}	Total area of the specimen
Q_{ud}	steady flow rate of the undamaged sample
Q_d	steady flow rate of the damage sample
Δh	water head difference
m_b	Dry bentonite mass
w	Water content
n_{i0}	Bulk concentration
n_c^+	Concentration of local cations
n_c^-	Concentration of local anions
c_c^+	Counterions in the aqueous solution

CHAPTER ONE
INTRODUCTION

1.1 Background

Due to rapid urbanization around the world, amount of waste generation is increasing and to treat the waste has become a serious social problem. Wastes (e.g., municipal solid waste (MSW), hazardous waste, wastewater, and others) are mostly generated from household and/or industrial activities every day. There are several methods to treat the wastes. According to data provided by United States Environmental Protection Agency (EPA) (2015), totally 250.9 million tons of MSW were generated in the USA in 2012, in which; (1) 65.3 million tons were diverted to recycling, (2) 21.3 million tons were diverted to composting, and (3) 29.3 million tons were combusted, and (4) the remaining 135.0 million tons (> 50%) were sent to landfills. European countries, such as Italy, Slovakia and England had a total of 49 (Italy), 2 (Slovakia), and 11 (England) incinerators were operating in 2001. While, for landfills were 619, 121 and 232, respectively (Forastiere et al., 2011). Due to almost all MSW can be landfilled, there is an increased demand for landfill construction. Landfill must be carefully designed and constructed to prevent leachate enters nearby environment from a landfill. The lining layer become a very important component of a modern landfill.

Nowadays, geosynthetic clay liners (GCLs) are widely used as a lining material in waste containment systems because its easily to install and low water permeability (k). The GCLs are consisted of a sodium bentonite encased between two layers of geotextiles (GT-GCL) or the bentonite attached to a geomembrane (GM-GCL) by chemical adhesives. The key component that controls hydraulic properties of a GCL (e.g., GT-GCL or damaged GM-GCL) is a thin layer of sodium bentonite. GCLs also have a prominent property of self-healing of damage holes that are caused by several reasons during the field construction (Sari and Chai, 2013).

In the field, GCLs are usually interacted with chemical liquids. Although a sodium bentonite has high swelling ability in water, when it interacts with chemical solutions, especially the solution with high concentration of cations (e.g., seawater, leachates from landfill), the swelling capacity of the sodium bentonite dramatically decreases (Jo et al., 2001; Razakamanantsoa et al., 2012). This is because the chemical solutions can reduce the repulsive

force in the interlayer between bentonite particles (Mitchell and Soga, 2005; Chai and Shen, 2018).

To improve the swelling capacity of the bentonite when interacted with cationic solutions, technique of polymerizing sodium bentonite has been developed (Elhajji et. al., 2001; Razakamanantsoa et al., 2008; Bohnhoff and Shackelford, 2013; Di Emidio et al., 2015). Some researchers confirmed that polymerized bentonite can enhance the swelling capacity of the bentonite against cationic solutions (Di Emidio et al., 2015; Scalia et. al., 2011). An anionic polymer treated bentonite provides both a higher swelling capacity and a lower permeability in cationic solutions compared with that of the untreated bentonite (UB) (Di Emidio et al., 2015; Scalia et al., 2011; Scalia et al., 2014). Sodium polyacrylate is an anionic polymer, which has much higher water absorption ability compared with bentonites (Kong et al., 2017), and widely used for producing the polymerized bentonite (PB) (Scalia et al., 2011; Scalia et al., 2014; Özhan, 2017).

1.2 Problem statement

There are very few researchers have reported the optimum conditions (e.g., initiator type, amount of initiator, pH, monomer content, etc.) for polymerizing the bentonite to result in better hydraulic properties against high concentration cation solutions for liner application. Also, there is no comprehensive research regarding the self-healing capacity of GCLs using polymerized bentonites in various chemical liquids.

1.3 Objectives

The objectives of this dissertation are (1) establish the optimum conditions for producing the PB to be used in landfill liner system, i.e. initiator type, amount of initiator, monomer content, and pH condition. (2) Investigate the physical properties, microstructure of the PB by swelling pressure tests, permeability tests and consolidation tests, etc. (3) Assesse the performance of the GCL using the PB through a series of the leakage rate tests using high cation concentration solutions, strong acid solutions (pH = 1 and 3) and strong alkaline solutions (pH = 11 and 13).

The objectives have been achieved by the following steps:

(1) Optimum conditions for producing PB

The optimum conditions were investigated by a series of the free swelling index (FSI) test using the PBs produced by varying of initiator types, amount of the initiator, monomer contents and the pH values. Then, the effectiveness of the proposed optimum conditions was examined by other bentonites with FSI value less than 24 ml/2g. FSI > 24 ml/2g is one of the criterion for a bentonite to be used in GCLs.

(2) Properties of the PB.

The produced PB using the proposed optimum conditions was tested on the physical properties, micro-structure and hydraulic properties (fluid loss, swelling pressure and permeability). The nine (9) different liquids were used to evaluate the performance of the PB material compared with that of the untreated bentonite (UB).

(3) Performances of the GCL

The PB was adopted as the core material for a GT-GCL. The reproduced PB-GCL and UB-GCL were investigated on the self-healing capacity through a series of the leakage rate tests (small-scale and large-scale tests). The performance of the PB-GCL was checked by permeating several chemical solutions, such as, aggressive cationic solutions (0.6 M NaCl, 0.6 M $CaCl_2$), and the corrosive wastes (e.g., pH = 1 and pH = 13).

1.4 Organization of the dissertation

The dissertation contains five chapters. The introductory Chapter 1 describes the background, objectives of the dissertation. Chapter 2 reviews the literatures about GCLs, the polymerization techniques, and the behavior of polymer-clay composite. Chapter 3 presents laboratory test results of PB as well as the proposed optimum conditions for producing the PB. Chapter 4 presents the performance of the GCL using PB as the core, i.e. PB-GCL, in different chemical solutions. Finally, the conclusions drawn from this study and recommendations for future works are given in Chapter 5. The flowchart and contents of this dissertation is given in Fig. 1.1.

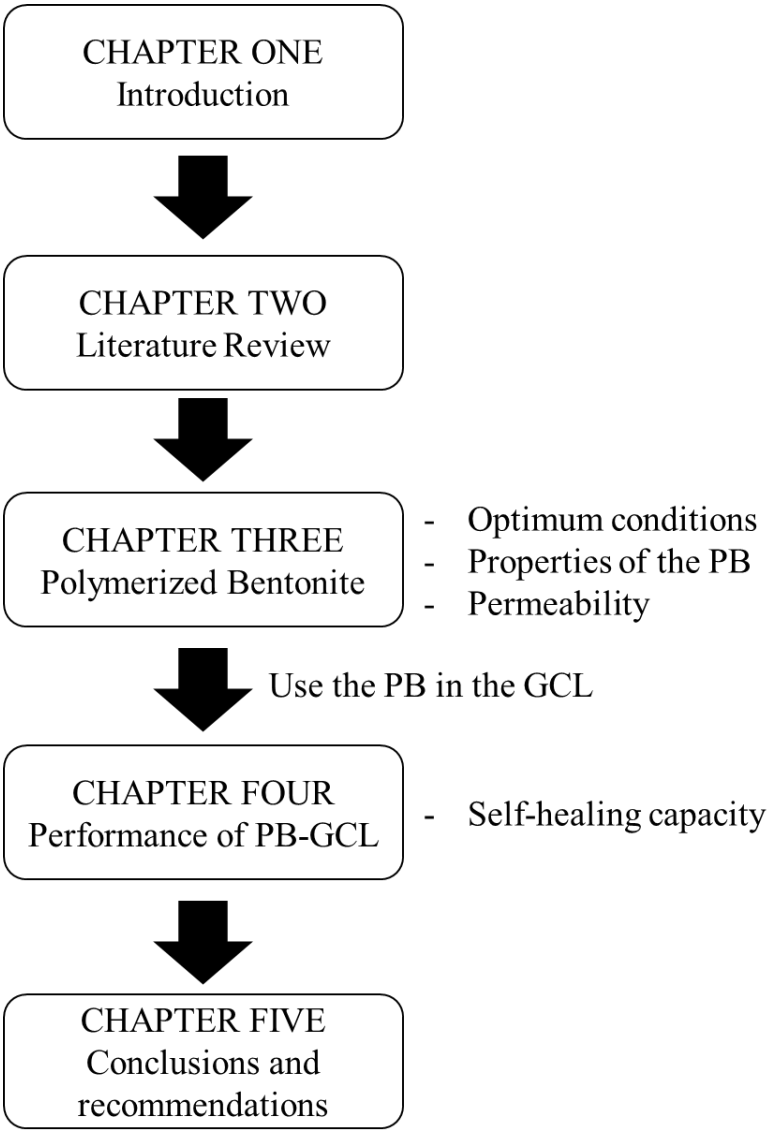

Fig. 1.1. Flowchart of this study

CHAPTER TWO
LITERATURE REVIEW

2.1 Introduction

Nowadays, geosynthetic clay liners (GCLs) have been widely used in landfill applications because its low permeability (*k*), easy installation and cost effective. The GCLs are usually consisted of a layer of sodium bentonite encased with the cover and the carrier geotextiles (GT-GCLs), or the bentonite glued to a geomembrane (GM-GCLs). The core layer "sodium bentonite" has high swelling and low *k* value, which controls the barrier properties of a GCL.

However, the swelling capacity of the sodium bentonite is decreased when interacted with chemical solutions, especially cationic solutions. Therefore, polymerized bentonite (PB) technique has been effectively used to improve the properties of sodium bentonite against chemical solutions (Bohnhoff and Shackelford, 2013; Di Emidio et al., 2015). The reported results about the performance of GCLs, the methods for polymerizing bentonite as well as the properties of the polymerized bentonite are reviewed first. Then, the limitation of the current methods as swell as the issues further researches being needed are discussed.

2.2 Geosynthetics clay liners (GCLs)

Geosynthetic clay liners (GCLs) are manufactured composite material, which is typically composed of a low permeability bentonite layer sandwiched between carrier and cover geotextiles (GT-GCL) or bonded to a geomembrane by adhesive glue (GM-GCL). In the presence of water, the bentonite layer can swell and create a very low permeability ($k \sim 10^{-10}$ to 10^{-12} m/s (Shackelford et al., 2010)) barrier. The engineering function of a GCL is used as a hydraulic barrier to water, leachate or other liquids and sometimes gases.

2.2.1 Geomembrane-supported GCLs (GM-GCLs)

For the GM-GCLs, the bentonite clay is admixed with an adhesive, and it glued to a smooth or texture surface of a geomembrane as shown in Fig. 2.1. There are two common types of geomembrane used for lining systems i.e., high-density polyethylene (HDPE), and linear low-density polyethylene (LLDPE). The HDPE provides low permeability, UV resistant (especially with carbon black and antioxidants) and high chemical resistant. The HDPE

geomembrane is most widely used in civil engineering applications. For LLDPE, it has high elongation capability, which made the LLDPE more flexible than the HPDE.

Fig. 2.1 Cross section of GM-GCLs (modified from Daniel, 1993)

2.2.2 Geotextile-encased GCLs (GT-GCLs)

GT-GCLs can be divided into three categories, (1) adhesive-bonded, (2) stitch-bonded and (3) needle-punched as shown in Figs. 2.2(a) to (c). Fig. 2.2(a) illustrates a bentonite is mixed with an adhesive which is bonded with upper and lower geotextiles. Fig. 2.2(b) illustrates a stitch-bonded type where layer of a bentonite layer is supported by upper and lower geotextiles and they are joined by continuous sewing in discrete rows throughout the machine direction of the product. Fig. 2.2c illustrates a bentonite is sandwiched by upper and lower surfaces and they are needle punched together.

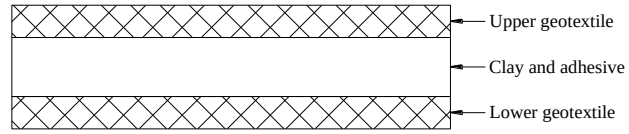

a) Clay bound with adhesive to upper and lower geotextile

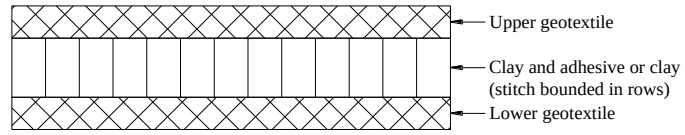

b) Clay stitch bonded between upper and lower geotextile

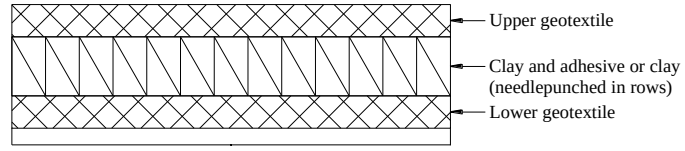

c) Clay needledpunched through upper and lower geotextile

Fig. 2.2(a) to (c) Cross section of GT-GCLs (modified from EPA, 2001)

2.2.3 Bentonite

Bentonite is a highly expansive clay, usually generated from weathering of volcanic ash, and it consists mainly of montmorillonite mineral (approximately 65 to 90% of montmorillonite, (Shackelford et al., 2000). Bentonite is used for a variety of purposes (e.g., civil and environmental engineering, agriculture, cosmetic, etc.). For engineering purpose, it is mostly used for lining material (i.e., GCLs), drilling mud and absorbent due to its highly colloidal and expansion capacity.

There are several types of bentonite and each one is defined the name by a majority cation carried by the bentonite particles, such as sodium (Na^+), potassium (K^+), calcium (Ca^{2+}) and aluminium (Al^{3+}). There are two common bentonites, which is widely used for civil and environmental engineering, i.e. sodium (Na^+) and calcium (Ca^{2+}) bentonites. The Na^+-bentonite is highly expansible in water, while calcium bentonite is generally used as an adsorbent of ions in chemical solution due to its high cation exchange capacity. Regarding to the barrier properties (e.g., swelling, permeability, self-healing), the Na^+-bentonite is mostly used as a lining material (Razakamanantsao et al., 2012).

(1) Bentonite composition and structure

In general, clay minerals have very small particle with net-negatively charge on their surface, which is balanced by the adsorption of cations. The basic unit of clay mineral are the silicon tetrahedron (Fig. 2.3a) and the aluminum or magnesium octahedron (Fig. 2.3b).

Montmorillonite knows as 2:1 clay structure, which is an octahedral sheet sandwiched by two layers of silicon tetrahedron sheets as shown diagrammatically in three dimensions in Fig. 2.4. The bonding between the particles is van der Waals forces. These bonds are weak and can be easily separated by adsorption of water molecules. As shown in Fig. 2.4, the d-spacing is created by balancing between the attractive (van der Waals) and the electrical repulsive force when it absorbs water molecules, and the d-spacing is varying on the degree of saturation. The d-spacing of the montmorillonite structure can be from approximately of 9.6 Å to complete separation (after Mitchell and Soga, 2005).

(2) Diffuse double layer (DDL)

For dry clay particles, some adsorbed cations are tightly adsorbed on surfaces of negative charged clay particles. When the clay absorbs water molecules from a solution, the salt precipitates can go into the solution, and it try to diffuse away for equalizing concentrations

throughout the pore fluid. The escaping tendency due to diffusion and the opposing electrostatic attraction leads to ion distributions adjacent to a single clay particle in suspension as shown in Fig. 2.5.

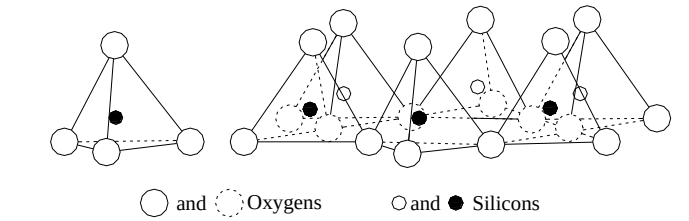

(a) Silicon tetrahedron

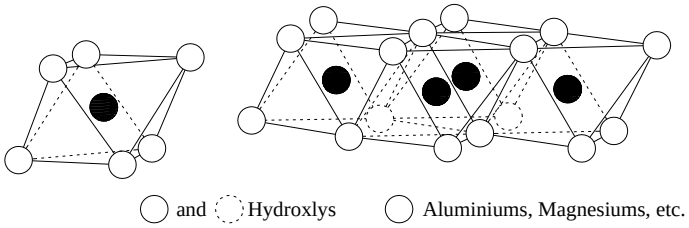

(b) Aluminum or magnesium octahedron

Fig. 2.3 Unit and sheet structure (a) silicon tetrahedron (b) aluminium or magnesium octahedron (after Mitchell and Soga, 2005)

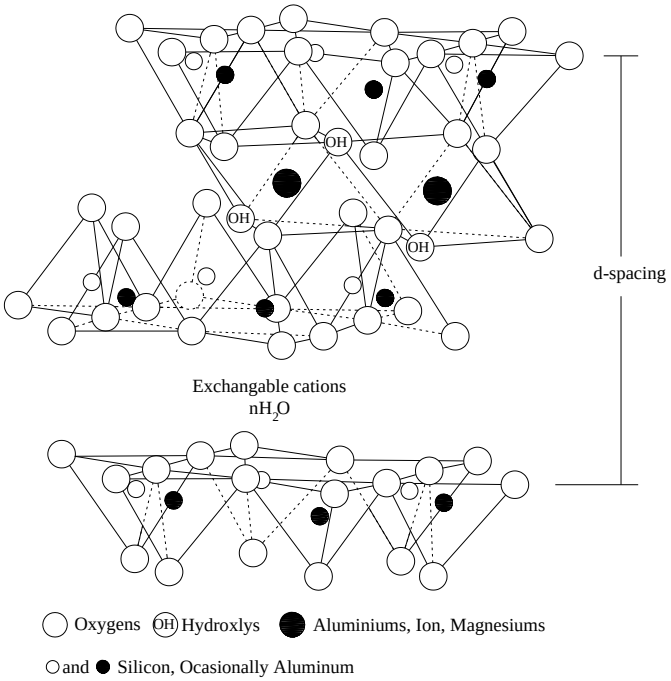

Fig. 2.4 Montmorillonite structure (after Mitchell and Soga, 2005)

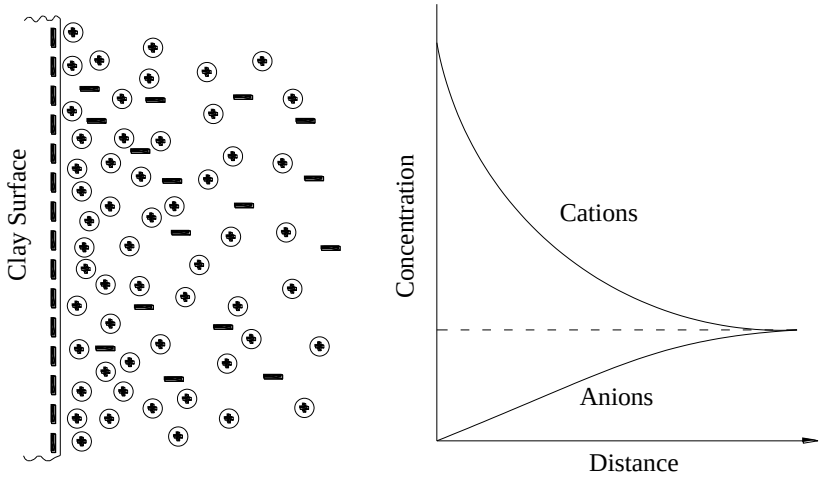

Fig. 2.5 Ion distribution in diffuse double layer (after Mitchell and Soga, 2005)

The diffuse double layer (DDL) theory is often referred to as the Gouy-Chapman theory, and it can reasonably describe only for smectite particles suspended in monovalent electrolyte solution at very low concentration (< 0.001 M) (Sposito, 1989). The idealizing assumptions of the DDL theory are: Firstly, there are no interactions between the ions, and they are considered as point charges; secondly, the charge on the particle surface is considered to have a uniform distribution; and thirdly, the permittivity of the medium adjacent to the particle surface does not depend on their location; lastly, the DDL theory is determined in the one-dimensional condition only and the particle surface must be considered as a plate (i.e., large plan area relative to the thickness of the double layer).

The DDL of clay particles overlap causing interaction between the two diffuse regions as shown Fig. 2.6. The model of two parallel clay plates and the charge distribution has a similar shape and the distance between the two particles is considered as 2d. For negative charged clay particles, $n_c^+ > n_{c0}$ and $n_c^- < n_{c0}$, where n_{c0} is the bulk concentration (ions/m^3), + and – are indicated cations and anions, respectively and c_c^+ is cations (counterions) concentration in an aqueous solution.

The distance from the surface to center of gravity of the diffuse layer is defined as the thickness of the double layer and it is affected by changes on the surface, electrolyte concentration, cation valence, and dielectric constant of the electrolyte, as well as pH and ion size. The thickness of the double layer can be expressed by Eq. (2.1).

$$\frac{1}{\kappa} = \left(\frac{\varepsilon_0 D k_b T}{2 n_0 e \nu^2} \right) \tag{2.1}$$

where, D = dielectric constant of solution; k_b = Boltzmann constant ($k_b = 1.38 \times 10^{-23}$ J/K); T = absolute temperature (Kelvin); n_0 = molar concentration of ions in pore fluid (mole/m^3 multiplied by Avogadro's number, $N_A = 6.023 \times 10^{23}$); ε_0 = elementary charge ($\varepsilon_0 = 4.8 \times 10^{-20}$ $C^2J^{-1}M^{-1}$); v = ionic valence; and e_e = elementary electric charge (=1.602 × 10^{-19} C).

The hydraulic properties (e.g., swelling, hydraulic, etc.) of smectite clay are mainly controlled by $1/\kappa$ value. The higher $1/\kappa$ value, the lower permeability and higher swelling potential.

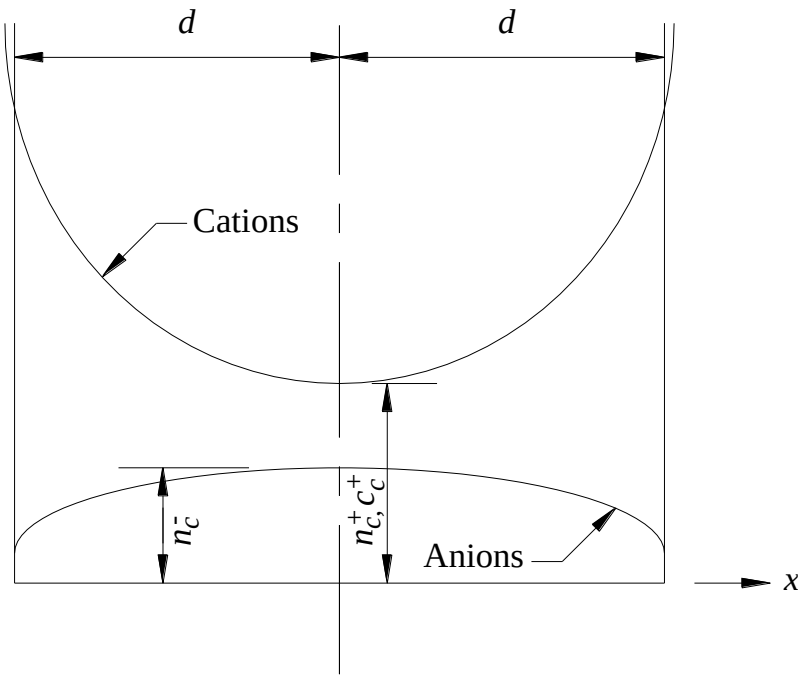

Fig. 2.6 Ion distribution in interacting double layers (after Mitchell and Soga, 2005)

2.2.4 Bentonite-liquids interaction

The swelling of the bentonite occurs when bentonite started to absorb water. Water molecules can be adsorbed on the particle surface through several mechanisms such as, hydrogen bonds, ion hydration, attraction by osmosis and dipole attraction as shown in Figs. 2.7(a) to (c).

As mentioned before, the electrostatic and van der Waals forces holding the layers together are relatively weak. The interlayer cations can be hydrated in aqueous solutions well known as clay swelling. The swelling causes increasing of d-spacing.

In detail, water dipoles have a charge distribution that allows ion hydration. Cations attract the negative side of the water molecule, while anions attract the positive side. If the energy of hydration is less than that of normal water, the water molecule becomes a hydration shell for the ion. Due to the high concentration of ions, the water dipole is strongly attracted to the mineral surface, through diffusion by osmosis. This can cause an arrangement of the dipoles, which leads to a disorientation at the mid-plane region when two particles are close.

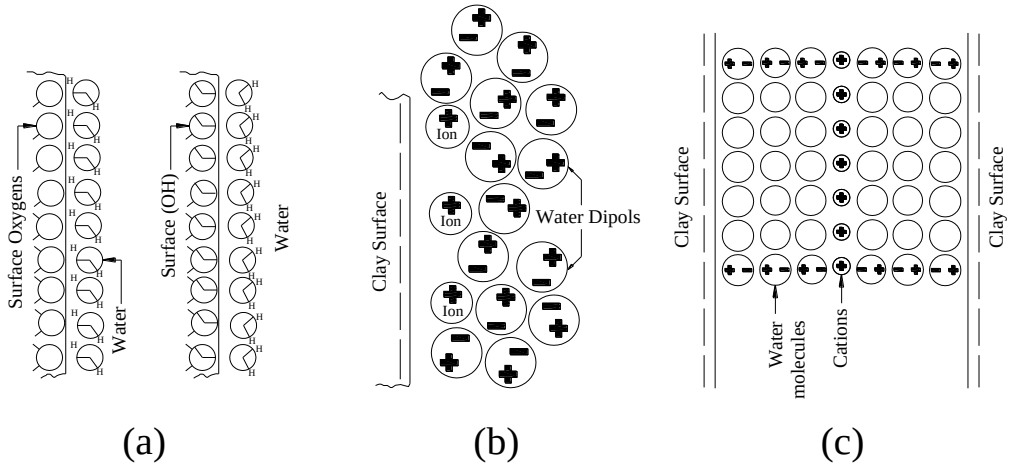

Fig. 2.7 Clay-water interactions (a) hydrogen bonding (b) ion hydration (c) dipole attraction (after Mitchell and Soga, 2005)

Cation valence has an inverse relationship to the thickness of the diffuse double layer. Polyvalent replacing monovalent cations contracts the double layer. Commonly divalent, Ca^{2+} replaces Na^{+} in the sodium bentonite deceasing in the$1/\kappa$ value.

The influence of valence has been shown to be evident in free swelling index tests conducted by Shackelford et al. (2000). The bentonite was hydrated with deionized water and three different 0.025 M chloride solutions (i.e., LiCl, $MgCl_2$, and $AlCl_3$). Results in Fig. 2.8 show the swell volume of each solution.

The highest valence cation, Al^{3+}, has the largest effect on the swelling capacity of the clay, which is consistent with the Eq. (2.1). The swell volume in deionized water is only slightly larger than in the LiCl, due to the monovalent of the cation. The Li^{+} may replace the Na^{+}, but it slightly changes in swell volume because the minimal change in $1/\kappa$ value due to the 1:1 exchange.

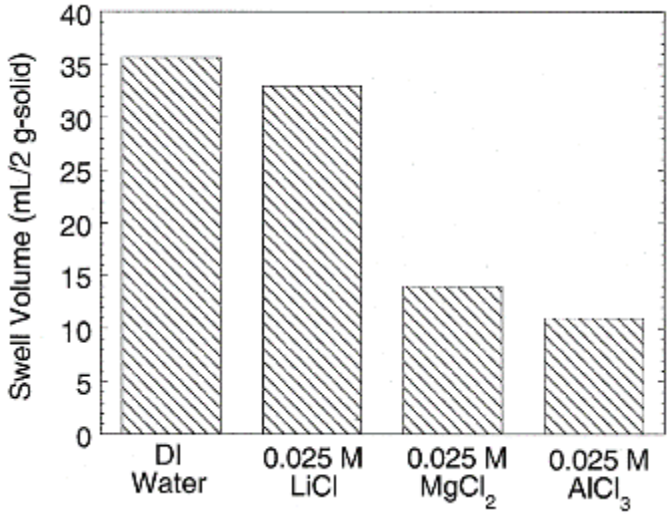

Fig. 2.8 Effect of cation valence on FSI (after Shackelford et al., 2000)

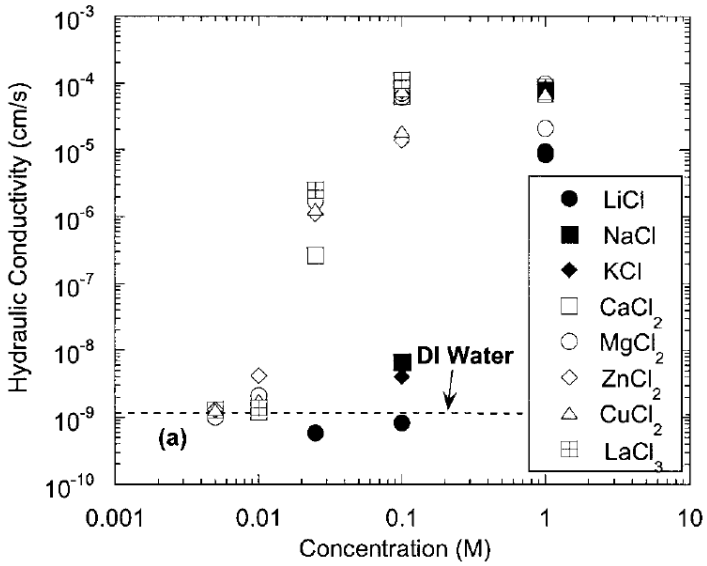

Fig. 2.9 Hydraulic conductivity as function of concentration (after Jo et al., 2001)

Jo et al. (2001) investigated the influence of salt solutions with various concentration, cation valence and pH on hydraulic conductivity (*k*) of geosynthetic clay liners (GCLs). They reported that the *k*-value of the GCL increase with increasing in concentration of solutions. Moreover, they also found that monovalent cations reduce the value of *k* to different degrees depending on the hydrated radius of the cation. It is well known that cations adsorbed on the surface can be replaced by higher cations, but the replacing power of cation also influence on *k*-value due to change in $1/\kappa$ value. For example, under the same chemical concentration, GCL permeated with KCl gave higher *k*-value than that permeated with NaCl solutions (Fig. 2.9).

Typically, the higher valence replaces lower valence cations and ions with smaller ionic radii replace large one, respectively.

The pH level of solutions also affects to the bentonite properties. In Fig. 2.10, by determining only effect of pH (no Ca^{2+}), the results show that swell volume of bentonite trend to decrease in strong acid (pH < 3) and strong basic (pH > 12). This consistent with test results of hydraulic conductivity (*k*) reported in Fig. 2.11. Another researcher, Naka et al. (2012) investigated barrier performance of GCLs against acid rock drained (ARD). They found that the hydraulic conductivity (*k*) of GCL permeated with water was 1.4×10^{-11} m/s and this increased by one order of magnitude with ARD permeation ($k = 5.0 \times 10^{-10}$ m/s).

Presently, there are some research groups successfully improve the bentonite properties against chemical solutions by using polymer and it will give details on section 2.3.

2.2.5 Defects of the GCLs

Although, using of GCLs provides many advantages, but they also have a disadvantage. One of the main disadvantages of GCLs is that in the field during and/or post construction, it may damage locally.

Damages of GM-GCL were founded in the field after removing the waste at Mahoning landfill reported by Evan et al. (1998). There are several large tears (1 to 6 ft) and a lot of small tears (larger than 1 ft). Also, two ruptured at seaming area were found. Geomembrane can be damaged in landfill also. Nosko and Tauze-Foltz (2000) reported result from electrical damage detection systems which installed at more than 300 sites from 16 countries (Fig. 2.12). The study showed that mainly (71 %) damages of geomembrane were caused by stone during installation and the rest by heavy equipment (16 %), inadequate seam (6 %), workers (6 %) and other (1 %).

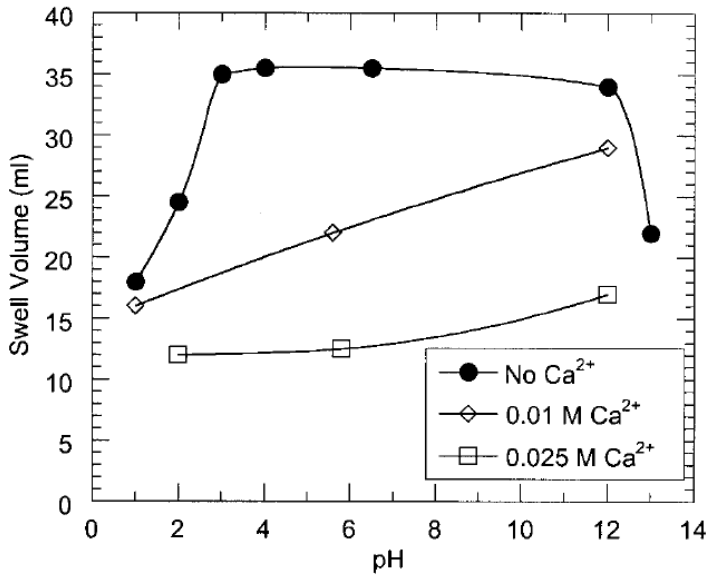

Fig. 2.10 Effect of pH solutions on swelling of sodium bentonite (after Jo et al., 2001)

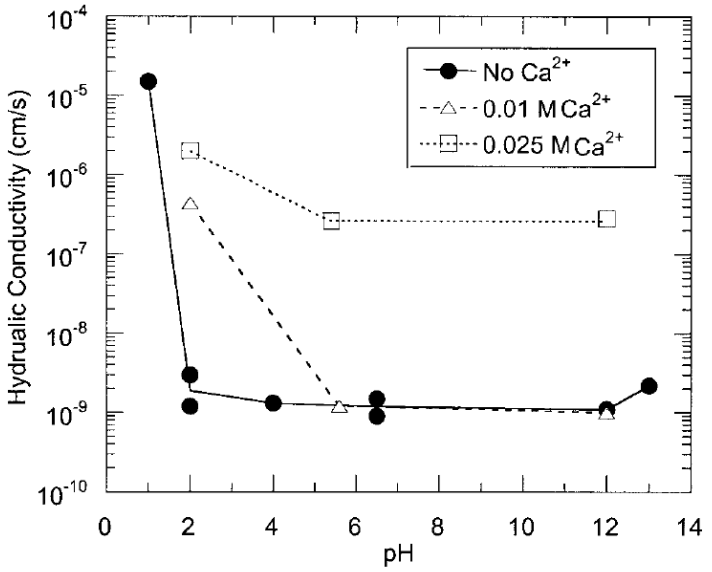

Fig. 2.11 Effect of pH solutions on hydraulic conductivity (after Jo et al., 2001)

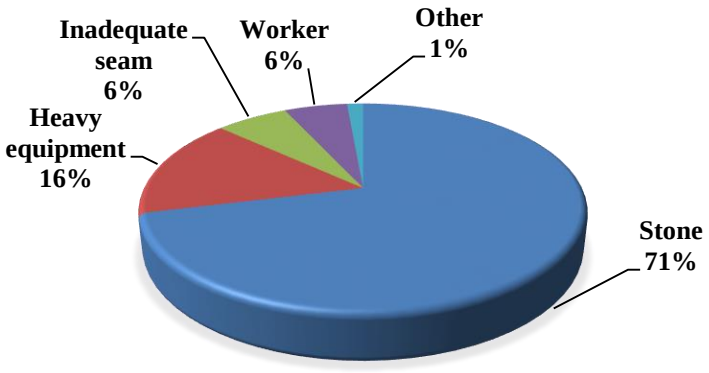

Fig. 2.12 Cause of defects in geomembrane liners after installation of cover layer (data from Nosko and Touze-Foltz (2000))

Mazzieri and Pasqualini (1997) reported that puncturing by plant roots might induce negative impact on the permeability (*k*) of adhesive-bonded GCLs (Fig. 2.13). Fox et al. (1998) performed a field test to investigate of installation damage for GCL. In the field test, the GCLs were laid on subgrade layer, and then covered with sand or gravel. Then, they were hydrated before driving bulldozers on it. After that the tests site were excavated and GCLs samples were taken to laboratory for further investigation.

Fig. 2.13 GCL damaged caused by roots (after Mazzieri and Pasqualini, 1997)

Table 2.1 presents test results of hydraulic conductivity (*k*) of GCLs after simulation of installation damage. Test results show that under gravel soil cover (GCL-1) has the highest *k*-value due to its highest damage level. These results confirmed that GCL may be damaged for lesser cover depths. In addition, increasing cover soil particle size, decreasing thickness of cover soil, increasing water content and number bulldozer pass after hydration can increase the installation damage.

Table 2.1. Hydraulic conductivity for GCLs after field simulation of installation damage (after Fox et al., 1998)

Specimen	Soil cover	Initial thickness (mm)	Final thickness (mm)	Hydraulic conductivity, k (m/s)
GCL-1 S-M, 10 passes	Sand	6.2	5.8	1.9×10^{-11}
GCL-1 G-M, 10 passes	Gravel	10.4	8.9	3.6×10^{-11}
GCL-2 S-M, 10 passes	Sand	9.0	8.4	2.3×10^{-11}
GCL-2 G-M, 10 passes	Gravel	11.0	9.9	1.8×10^{-11}

Wrinkles are also one of the causing factors of possible GCLs defects. Dickson and Brachman (2006) described that wrinkles of geomembrane can induce to non-uniform stress when vertical overburden pressure was applied and lead to damage the GCLs. Fig. 2.14 illustrates the mechanism of GCL defects due to geomembrane wrinkle.

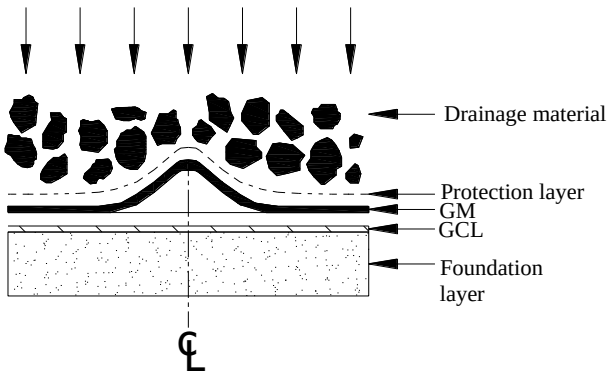

Fig. 2.14 Composite GM/GCL liner with a GM wrinkle (after Dickinson and Brachman, 2006)

Additionally, after installation and before waste coverage, due to day-night temperature variations, water vapor-drop cycles are generated on the GCL, which can cause down-slope erosion of the bentonite resulting in areas without bentonite as shown in Fig. 2.15.

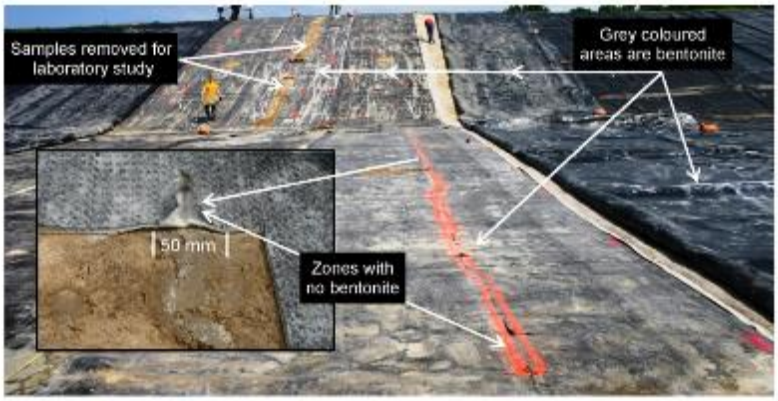

Fig. 2.15 Down slope erosion of GCL (after Rowe et al., 2016)

Although the GCL is easy to be damaged, due to their very high expansion when wet, part or the entire of a damage hole can be healed, and this mechanism is called the "self-healing capacity" (Babu et al., 2001; Sari and Chai 2013).

2.2.6 Self-healing of GCLs

In general, self-healing refers to an ability to automatically repair a damage (e.g., crack, hole, fissure, etc.). In presence of liquids, GCL contains the self-healing ability, which can fully or partially seal a damage. Fig. 2.16 shows a partially healed specimen after laboratory leakage rate test (Sari, 2013).

Fig. 2.16 Photo of healed GT-GCLs after tests (after Sari, 2013)

Several studies in literature have addressed the issue of self-healing of GCLs. Mazzieri and Pasqualini (2000) performed an experimental test program to investigate the permittivity (ψ) of a damaged GCL. Two patterns of defects were simulated, the first damage was introduced by bentonite loss from the geotextile casing, i.e. tearing, and the second damage

was by puncturing. They reported that the damage with losing of bentonite mass had higher severity than that of the puchering type of damage.

Permittivity (ψ) results of damage specimens are compared with that of intact (no damage) specimens as shown in Fig. 2.17. The test results show that ψ value of the damage specimen decrease with permeation time and the steady state (about 200 hours) of ψ value shows slightly increase in ψ compared with that of the undamaged specimen. This is because the damage hole is sealed due to the expansion of hydrated bentonite.

Babu et al. (2001) assessed self-healing capacity of GCL through a series of permittivity test. The permittivity results are shown in Fig. 2.18 and it shows the same trend with the test results reported by Mazzieri and Pasqualini (2000) that the permittivity decrease with elapse time due to self-healing capacity of the GCL. The results confirmed that GCLs with 30 mm-diameter punctures or less still can be fully self-healed.

2.2.7 Factors effect self-healing capacity

There are several influence factors on self-healing capacity of the GCL such as, damage size, overburden stress, damage shape and liquids.

(1) Size of damage

Mazzieri and Pasqualini (2000) investigated effect of damage size on GT-GCL with various circular damage diameters. In Fig. 2.19, the test results of hydraulic conductivity (k) showed increase with increasing of damage hole size. This because the increasing of damage size, the unhealed area of the damage hole was larger. Likewise, Fig. 2.20 showed that the steady flow rate (Q) increase with increasing of size of damage hole (Sari and Chai, 2013).

(2) Overburden pressure (σ)

Mazzieri and Pasqualini (2000) investigated effect of the value of σ on the self-healing capacity of a GT-GCL. The result in Fig. 2.21 shows that the value of k tends to reduce with an increase of σ value, but remained almost constant for σ more than 100 kPa.

Another study on effect of confining of stress on GCL was conducted by Sari and Chai (2013). They reported that two possible effects of σ can be considered. One is the squeezing effect, which tends to push the hydrated bentonite into a damage hole; thus, the self-healing

capacity increases. The other is the constraining effect, which intends to limit the expansion of the bentonite vertically; thus, the self-healing capacity of a GCL decreases.

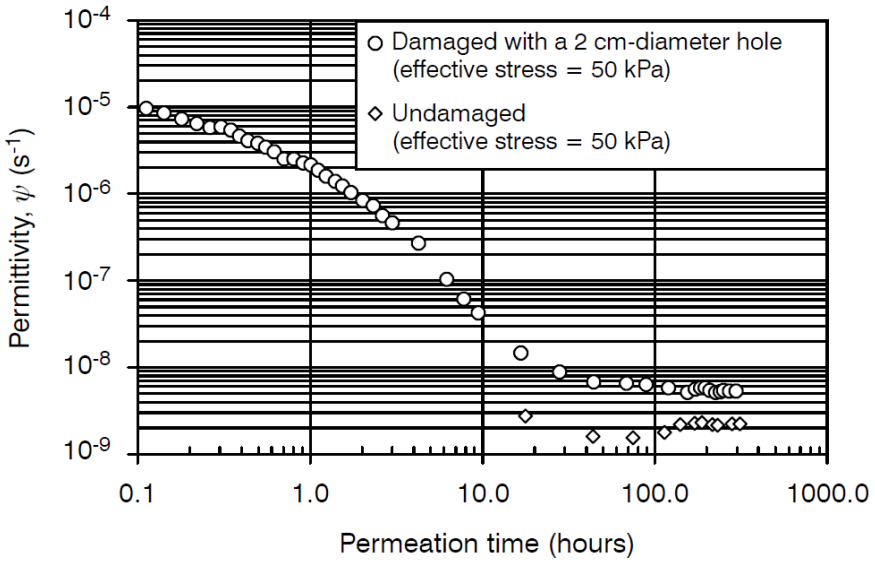

Fig. 2.17 Permittivity of damaged and undamaged GCL specimens under an effective stress of 50 kPa (after Mazzieri and Pasqualini, 2000)

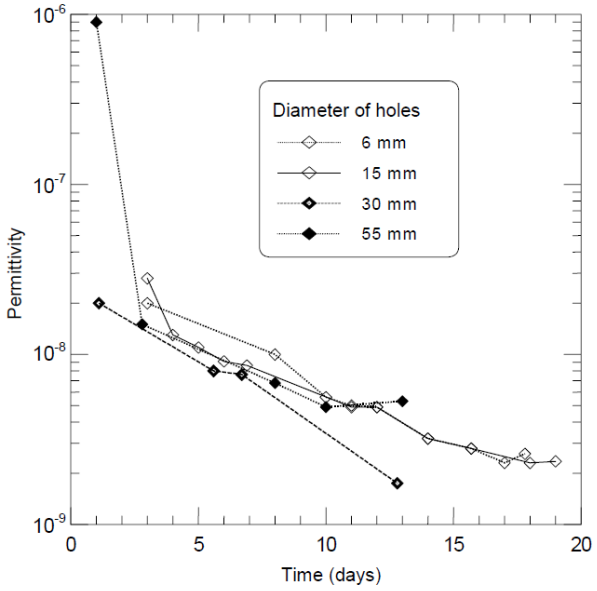

Fig. 2.18 Results of permittivity tests corresponding to different hole diameters (after Babu et al., 2001)

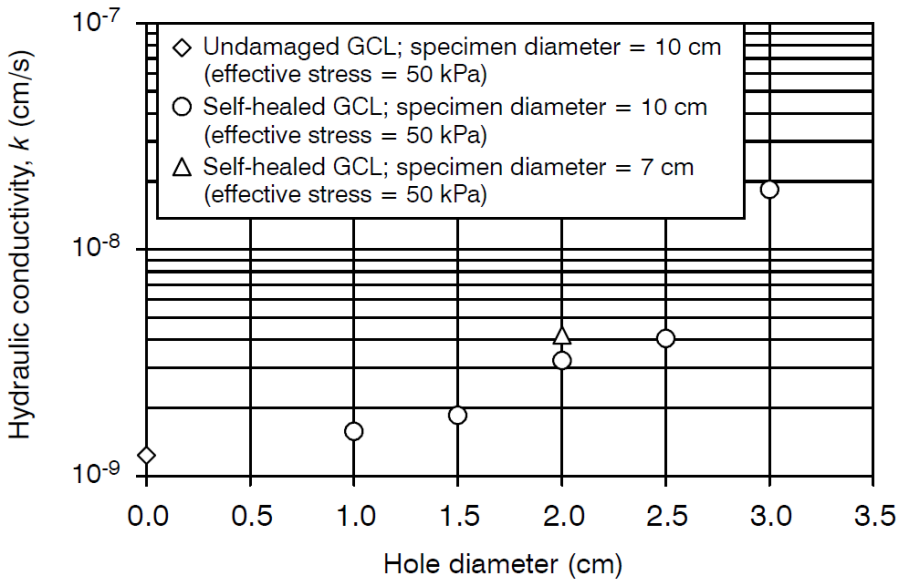

Fig. 2.19 Influence of hole diameter on the hydraulic conductivity of self-healed GCLs specimens (after Mazzieri and Pasqualini, 2000)

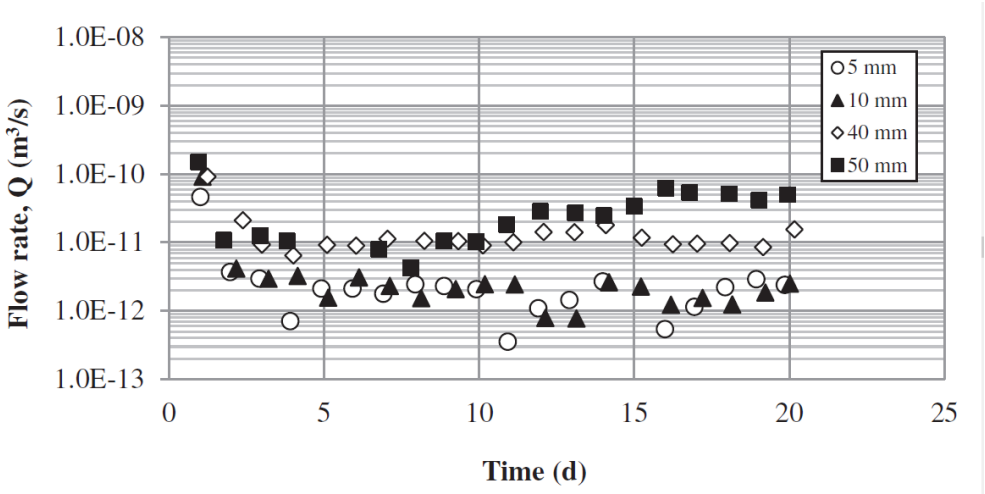

Fig 2.20 Flow rate (Q) of tap water versus elapsed time for GM-GCL with various damage size (after Sari and Chai, 2013)

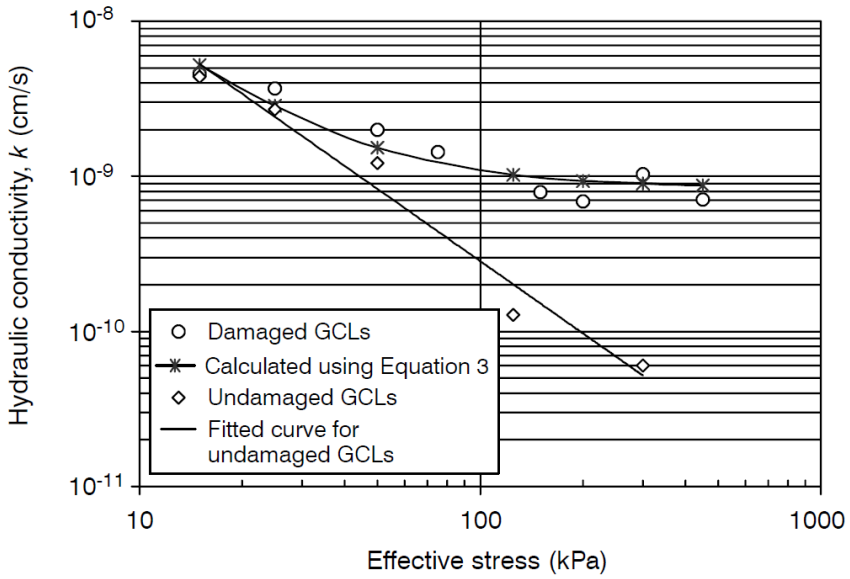

Fig 2.21 Relationship of *k* and effective confining stress (after Mazzieri and Pasqualini, 2000)

(3) Shape

Effect of the shape of a damage hole on the self-healing capacity of the GT-GCL were investigated by Prongmanee and Chai (2017) through a series of a constant head leakage rate tests. Test results confirmed that the damage shape has an influence on the self-healing capacity of the GCL. Under the same damage area, different damage shapes, different self-healing capacity can be obtained. In Fig. 2.22, a circular damage showed higher self-healing capacity compared with a square damage with the same damage area. This is because the "corner effect" of the square damage, i.e. at corners, in term of the hydrated bentonite entering the hole, adjacent perpendicular sides will influence each other and reduce the amount of hydrated bentonite entered the hole (Prongmanee and Chai, 2017).

(4) Liquids

In the field, GCL are usually interacted with chemical liquids other than fresh water. As discussed in the previous section, the chemical substances dissolved in a solution can affect the swelling and permeability (*k*) of the bentonite particles. In a similar way, the self-healing capacity are influenced by the swelling of hydrated bentonite. If the swelling capacity decrease, the self-healing capacity will be reduced.

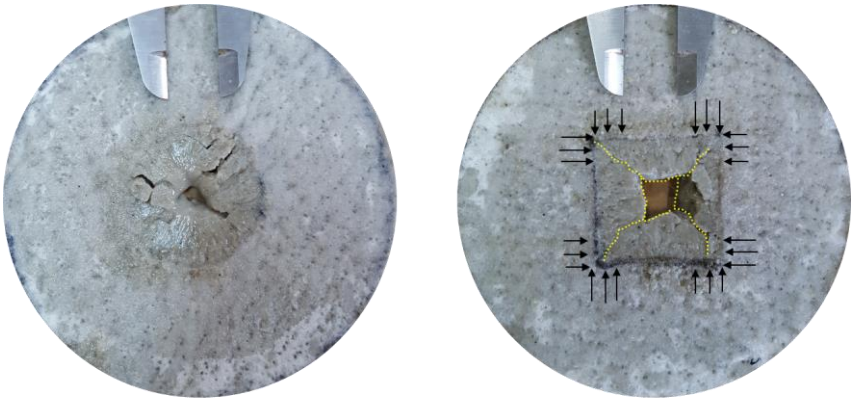

Fig. 2.22 Shape corner effect (after Prongmanee and Chai, 2017)

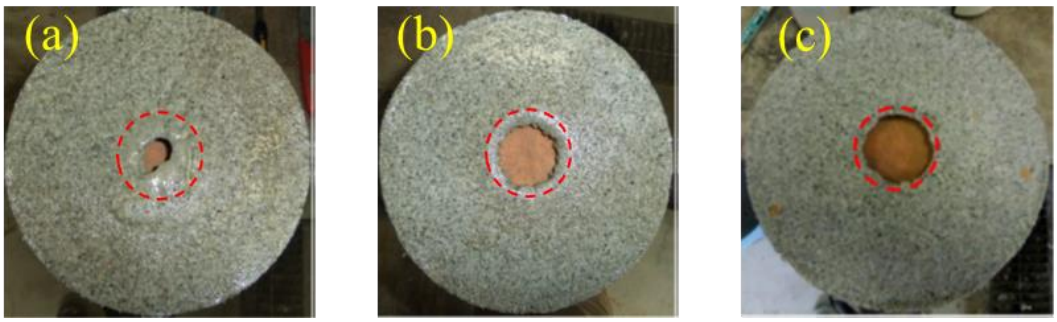

Fig. 2.23 Photos of GM-GCL after leakage rate test, (a) tap-water (b) 0.17 M NaCl solution (c) 0.10 M $CaCl_2$ solution (after Chai et al., 2013)

Ruhl and Daniel (1997) described the behavior of GCLs to permeation with various chemical solutions and leachates. They found that Ca^{2+} was more aggressive to the GCLs than real leachates. Experimental results had shown that Ca^{2+} from dilute solutions can exchange the interlayer Na^{+} ion of bentonite particles, resulting in gradual reducing of thickness of double layer around the bentonite particles, and consequent gradual increase in hydraulic conductivity (Shackelford et al., 2000).

Chai et al. (2013) investigated the effect of liquids on self-healing capacity of GCL by using tap-water, 10 g/l of NaCl solution, 11.1 g/l of $CaCl_2$ solution, and 100 ml/l of ethanol solution. The test results show that the self-healing capacity decrease when permeated in a salt solution and it shows almost not self-healed in $CaCl_2$ solution as shown in Fig. 2.23c. In a similar way, results of permittivity (ψ) increases by increasing in the concentration and valance of cation (i.e., Na^{+} and Ca^{2+}) as shown in Fig. 2.24, while the ethanol solution gave slightly

lower value of ψ than that of the tap water. They explained that the viscosity of the ethanol is higher than that of the tap water.

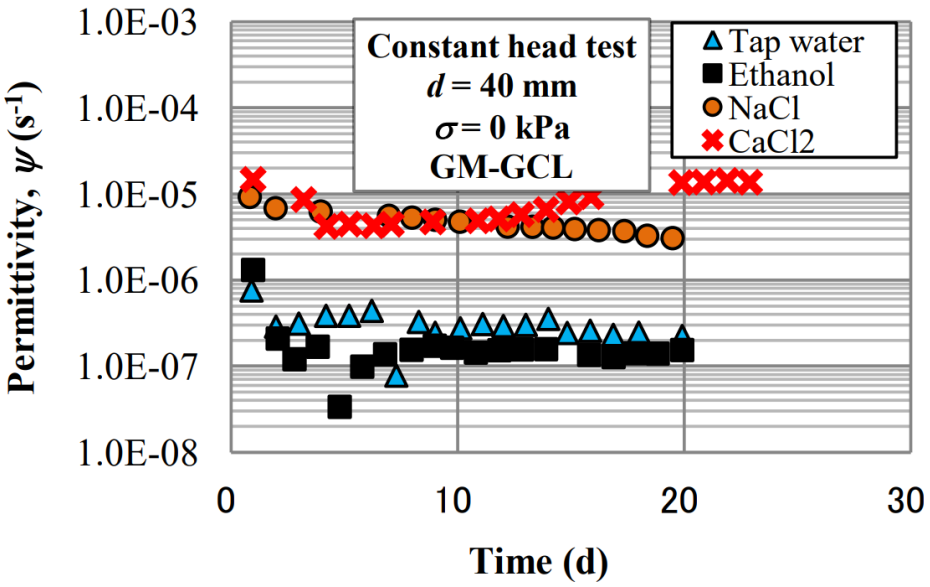

Fig. 2.24 Permittivity versus time (after Chai et al., 2013)

2.3 Polymerized bentonite

2.3.1 Polymer

Polymers are found almost in every material used in human daily life. Polymers are created from many small molecules called monomers. Monomers are linked to form a chain polymer by a chemical reaction called polymerization. According to laboratory synthetic methods, there are generally divided into two classes; (1) step-growth polymerization, and (2) chain-growth polymerization (Sperling, 2005). Due to the long reaction time needed to reach a high yield is a considerable disadvantage for step-growth polymerization as shown in Fig. 2.25. Thus, the chained growth polymerization is mostly used.

For the chain-growth polymerization, growth of the polymer occurs only at an end of the chain. Addition of each monomer unit regenerates the active site (Jenkins et al., 1996). In this method, an activated species (initiator or active monomer) adds one monomer molecule to create a new active center (propagation step), which again adds another monomer molecule to create another active center formed a long chain polymer.

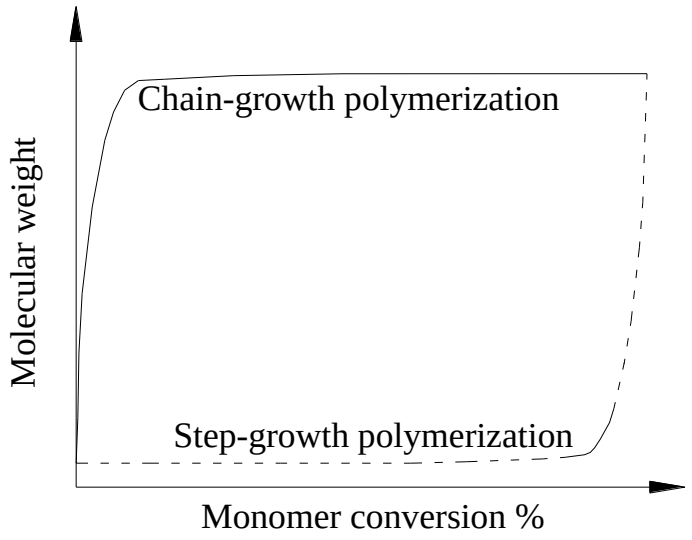

Fig. 2.25 Degree of polymerization as a function of monomer conversion for a chain growth reaction

2.3.2 Functional groups

Some common functional groups were reported in Table 2.2. In structural formulas in Table 2.2, symbols R and R′ indicate to an attached hydrogen or hydrocarbon.

2.3.3 Free-radical polymerization

Free-radical polymerization is a type of chain-growth polymerization, which is a common method for preparing of polymers and composite materials. In 2001, 40 billion of the 110 billion pounds of polymers produced in the United States were produced by free-radical polymerization (Odian, 2004). Figs. 2.26(a) to (c) show the free-radical polymerization steps.

(1) Initiation

Initiation is the first step of the process of polymerization. In the first step, one or two radicals are created from the initiating molecules (Fig. 2.26a). Then, radicals are transferred from the initiator molecules to the monomer units present and created an active center (Fig. 2.26b).

(1.1) Initiators

There are two common types of initiator used for free-radical polymerization i.e., peroxide and azo compound initiators

Table 2.2 List of common functional groups

Chemical class	Group	Formula	Structural formula	Prefix	Suffix	Example
Alkane	Alkyl	$R(CH_2)nH$	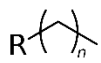	alkyl-	-ane	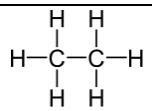 Ethane
Alkene	Alkenyl	$R_2C=CR_2$	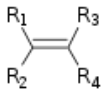	alkenyl-	-ene	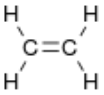 Ethene
Alkyne	Alkynyl	$RC\equiv CR'$	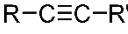	alkynyl-	-yne	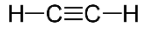 Ethyne
Benzene derivative	Phenyl	RC_6H_5 RPh	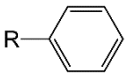	phenyl-	- benzene	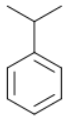 Isopropylbenzene
Azo compound	Azo (Diimide)	RN_2R'	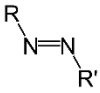	azo-	-diazene	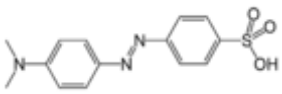 Methyl orange
Peroxide	Peroxy	$ROOR'$	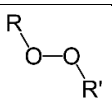	peroxy-	alkyl peroxide	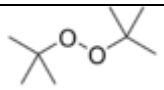 Di-tert-butyl peroxide

Details of free-radical polymerization are summarized as follows:

(a) Initiation

$$I \longrightarrow I^*$$

(b) Propagation

$$I^* + R \longrightarrow IR^* \longrightarrow IR_n^*$$

(c) Termination

$$IR_{n1}{}^{*} + IR_{n2}{}^{*} \longrightarrow IR_{n1}R\text{-}RR_{n2}I$$

I = initiator
R = monomer

Fig. 2.26 Polymerization steps (a) initiation, (b) propagation and (c) termination

(1.1.1) Azo compounds

Azo compounds have R-N=N-R′ structure. It can be produced of two carbon-centered radicals (R• and R'•) and nitrogen gas (N_2) upon heating and/or by irradiation. In Fig. 2.27, a commercial azobisisobutyronitrile (AIBN) is decomposed, and eliminating a molecule of nitrogen gas to form active radicals.

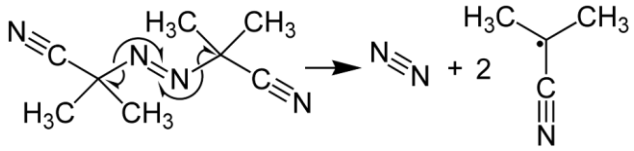

Fig. 2.27 Radicals created from azo-compound

(1.1.2) Peroxide compounds

Peroxide is compound with the structure R-O-O-R′, the common peroxide for initiator is potassium persulfate ($K_2S_2O_8$). Eq. (2.2) shows reaction of generating of active radicals.

$$[O_3SO\text{-}OSO_3]^{2-} \rightleftharpoons 2\,[SO_4]^{\bullet -} \qquad (2.2)$$

(1.2) Initiation methods

(1.2.1) Thermal decomposition

An initiator is heated until a bond is homolytically cleaved, producing two radicals (Fig. 2.28). This method is often used with organic peroxides or azo compounds (Cowie and Arrighi, 2008).

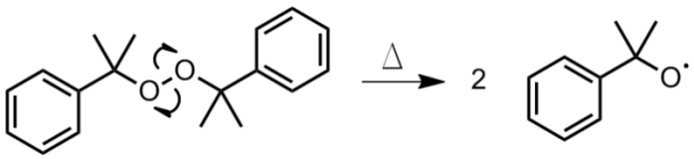

Fig. 2.28 Thermal decomposition of dicumyl peroxide

(1.2.2) Photolysis

Radiation cleaves a bond homolytically, producing two radicals (Fig. 2.29). This method is mostly used with metal iodides, metal alkyls, and azo compounds (Cowie and Arrighi, 2008).

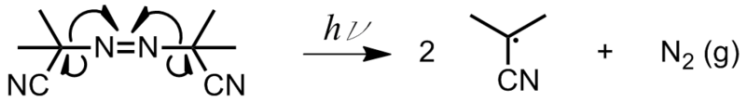

Fig. 2.29 Photolysis of azobisisobutyronitrile (AIBN)

(1.2.3) Redox reactions

A radical is generated by iron as shown in Eq. (2.3) (Cowie and Arrighi, 2008).

$$H_2O_2 + Fe^{2+} \rightarrow Fe^{3+} + HO^- + HO^{\bullet} \quad (2.3)$$

(2) Propagation

In this step, a polymer increases its chain length. After the radical initiator is formed, it attacks a monomer and linked to another monomer to form a chain polymer (Fig. 2.26b).

(3) Termination

Termination step will occur when the reaction is out of monomer contents and other possible mechanisms. Possible termination mechanisms are summarized as follows.

(3.1) Combination between polymer chain

Two active radicals can be combined together to form one long chain (Fig. 2.30). This mode of termination can be monitored by the molecular weight of the final product that the result of molecular weight should be in doubling of usual molecular weight.

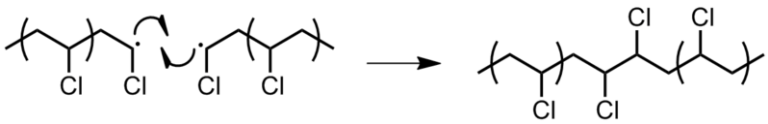

Fig. 2.30 Termination by the combination of two poly (vinyl chloride) (PVC) polymers

(3.2) Radical disproportionation

A hydrogen atom from one chain end is abstracted to another, producing a polymer with a terminal unsaturated group and a polymer with a terminal saturated group (Fig. 2.31).

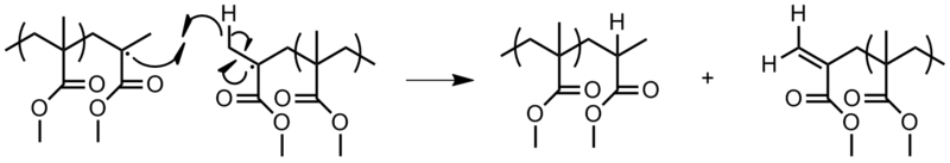

Fig. 2.31 Termination by disproportionation of poly (methyl methacrylate).

(3.3) Combination with active initiator

An active chain end is combined with an initiator radical resulted in termination (Fig. 2.32).

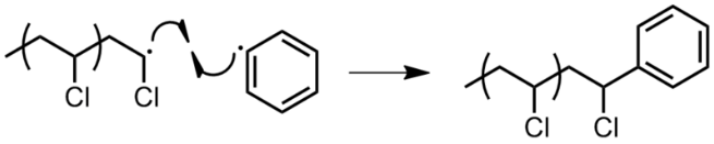

Fig. 2.32 Termination of PVC by reaction with radical initiator.

(3.4) Interaction with impurities or inhibitors.

Oxygen (O_2) molecule is the common inhibitor for free-radical polymerization. The growing chain will react with O_2, producing an oxygen radical, which is much less reactive (Fig. 2.33).

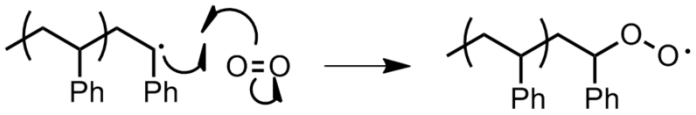

Fig. 2.33 Inhibition of polystyrene propagation due to reaction of polymer with molecular oxygen molecule (O_2).

2.3.4 Polymerization techniques

To produce a high-molecular-weight, uniform product, various methods are used to better control the initiation, propagation, and termination rates during the chain polymerization and also to remove excess concentrated heat during the polymerization. The commercial polymerization techniques included of emulsion polymerization, solution polymerization, suspension polymerization, and precipitation polymerization are widely used.

(1) Emulsion polymerization

Emulsion polymerization is usually starting with an emulsion incorporating water, monomer, and surfactant. The most common type of emulsion polymerization is an oil-in-water

emulsion, in which droplets of monomer (the oil) are emulsified (with surfactants) in a continuous phase of water as shown in Fig. 2.34.

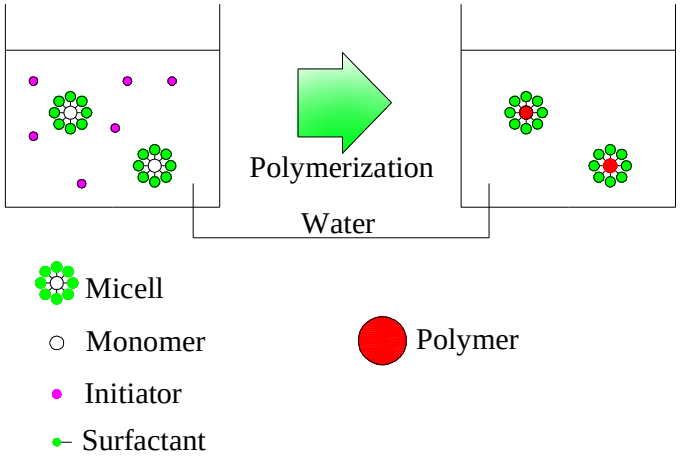

Fig 2.34 Emulsion polymerization

(2) Solution polymerization

In Fig. 2.35, the compositions of the solution polymerization include of monomer, initiator and solvent. In this method, the choosing polymer should be soluble in the chosen solvent. For the advantages of this method, heat released by the reaction is absorbed by the solvent, and so the reaction rate is reduced. The viscosity of the reaction mixture is also reduced, which is not allowing auto acceleration at high monomer concentrations. This process is commonly used in the production of sodium polyacrylate, a superabsorbent polymer used in disposable diapers (Zohuriaan-Mehr and Kabiri, 2008).

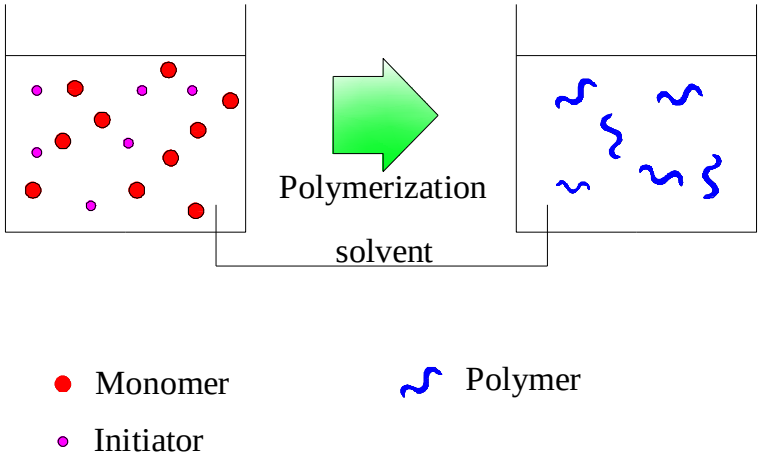

Fig. 2.35 Solution polymerization

(3) Suspension polymerization

Suspension polymerization is a heterogeneous radical polymerization process that uses mechanical agitation to mix a monomer in a liquid phase, while the monomers polymerize, forming spheres of polymer as shown in Fig. 2.36. This process is used in the production of commercial resins, including polyvinyl chloride (PVC), a widely used plastic, styrene resins including polystyrene, expanded polystyrene, and high-impact polystyrene.

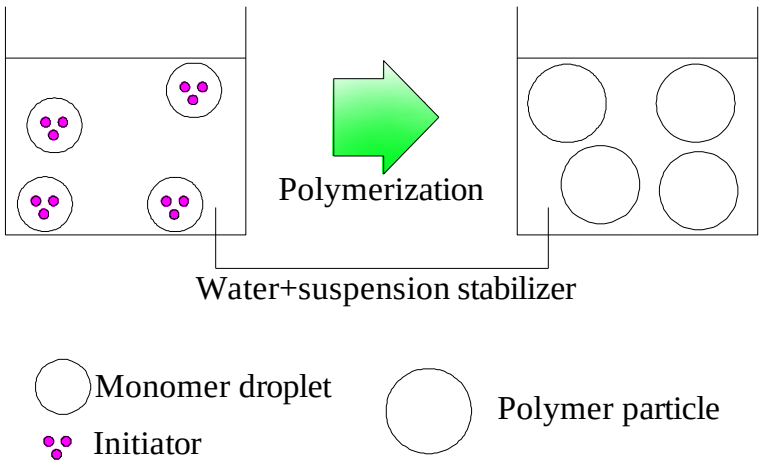

Fig. 2.36 Suspension polymerization

(4) Precipitation polymerization

This polymerization method is a heterogeneous polymerization process that begins initially as a homogeneous system in the continuous phase, where the monomer and initiator are completely soluble, but upon initiation the formed polymer is insoluble and thus precipitates as shown in Fig. 2.37.

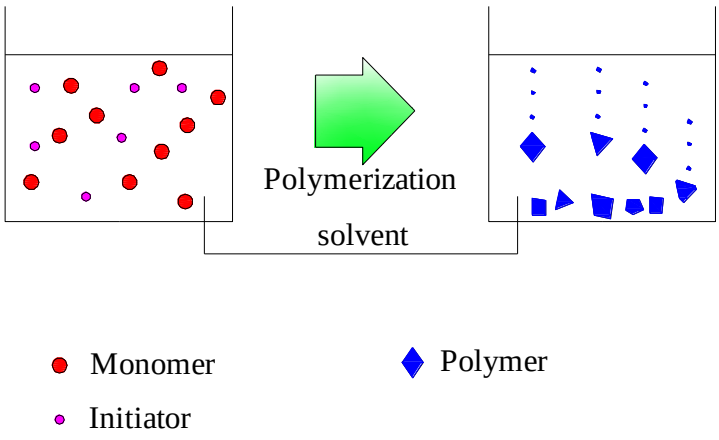

Fig. 2.37 Precipitation polymerization

2.3.5 Clay – polymer composite

A term “composite” is any material made from more than one component. Composite materials are the combination of materials with different structural, physical and chemical properties. Clay/polymer or polymer/clay composite offers many improvements in a wide range of physical and engineering properties. For soil barrier purpose, there are several researchers used polymer treated sodium bentonites (Di Emidio et al., 2015; Ashmawy et al., 2002; Scalia et al., 2011).

2.3.6 Clay-polymer composite structure

Generally, the structures of clay-polymer composite can be classified according to the level of intercalation or exfoliation of polymer chains acted into the micro-structure of clay particles. Various parameters including clay structure, polymer type and preparation method are influencing the properties and structure of the composite.

(1) Phase separated structure

Phase separated structure is obtained when the bentonite particle is interacted with a polymer, but the polymer cannot intercalate into the interlayer of bentonite particles, resulting in the clay particles are coated by the polymer (Fig. 2.38a). The obtained composite structure is considered as “phase separated”. The phase separated clay-polymer composites is in the group of micro composites.

(2) Intercalated structure

Intercalated structure is achieved when one or more polymer chains are inserted into the interlayer of bentonite particles and cause the increasing of the d-spacing, but the stacked structure of the clay particle is still existing, the intercalated bentonite/polymer composite is classified as nanocomposite (Fig. 2.38b).

(3) Exfoliated structure

Exfoliated structure is obtained when the insertion of polymer chains into the d-spacing of the clay causes to the separation of the layers one another and individual layers are dispersed within the polymer matrix (Fig. 2.38c). If the polymer chains cause to the increasing of interlayer spacing more than 80 to 100 Å, the exfoliated structure can be formed (Olad, 2011).

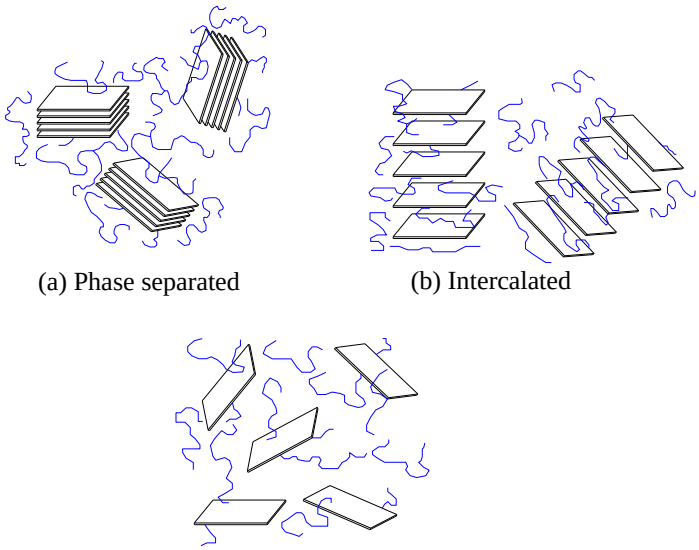

Fig. 2.38 Different structures of obtained clay-polymer composites (after Olad, 2011).

2.3.7 Structural characterization of bentonite-polymer composites

To understand the mechanism of a polymer treated bentonite, micro structure analysis is widely used, such as The X-ray diffraction (XRD) analysis and Scanning Electron Microscope (SEM) image. It is well known that clays show a characteristic peak in the XRD pattern due to their regular layered structures. Using the peak width at half maximum height and peak position (2θ) in the XRD pattern, the d-spacing can be calculated utilizing Bragg's law (Eq. 2.4).

$$2d\text{Sin}\theta = n\lambda \qquad (2.4)$$

where λ is wave length of X-ray radiation used in the diffraction experiments, d is the space between layers in the clay lattice and θ is measured diffraction angle. Any change in the inter-layer of a clay lattice by polymer causes the change in the position, broadness and intensity of the characteristic peak in the XRD pattern. Fig. 2.39 shows the XRD patterns of the sodium bentonite and polystyrene (PS)-sodium bentonite nanocomposites prepared by emulsion polymerization method.

The characteristic peak of the sodium bentonite has been appeared at $2\theta = 7.13°$ corresponding d-spacing of 12.4 Å. The XRD patterns of PS/sodium bentonite nanocomposites containing different clay portion (2 to 6% by weights) show diffraction peaks and lower 2θ degrees, which indicates the increasing of d-spacing.

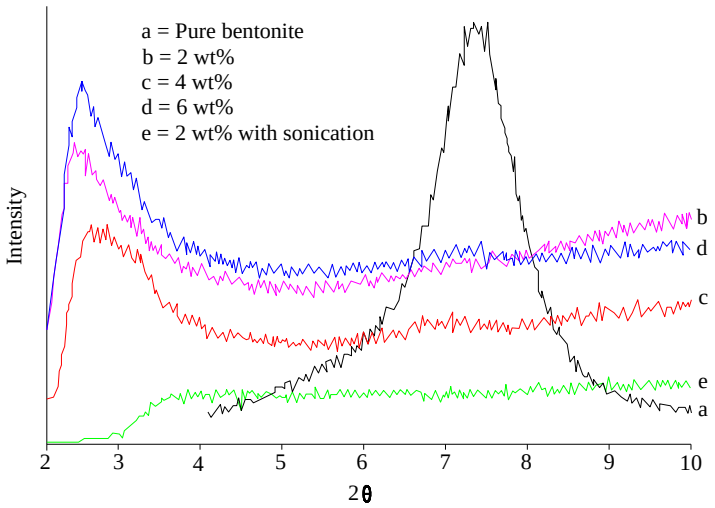

Fig. 2.39 XRD patterns of pure sodium bentonite and PS-sodium bentonite nanocomposites (after Olad, 2011).

2.3.8 Possible mechanisms of polymer treated bentonite

(1) Intercalation and activation of osmotic swell

Onikata and Kondo (1996) intercalated a high polarity aprotic solvent, polycarbonate (PC), within bentonite to form multi-swellable bentonite (MSB). They reported that the diffraction angle (2θ) is shifted to lower value, MSB showed increased d-spacing, illustrating of intercalated PC. Intercalated PC increased bentonite swell by expanding the space between adjacent bentonite platelets, and activating osmotic swell in NaCl solutions up to 0.75 M (Onikata et al., 2000) which is ~0.45 M stronger than the maximum strength which osmotic swell will occur in bentonite (~0.30 M) (Norrish and Quirk, 1954).

(2) Locking of bound cations

Deng et al. (2006) used Fourier-transform infrared spectroscopy (FTIR) spectroscopy to probe the bonds involved in adsorption of an anionic polyelectrolyte to bentonite. Based on the experimental results, they postulated that the mechanism for polyelectrolyte adsorption to bentonite basal surfaces was through exchangeable cation bridging (ECB). In ECB, the anionic polyelectrolyte associates with the cations satisfying the cation exchange capacity (CEC) of the bentonite. Thus, bentonite amended with an intercalated anionic-polyelectrolyte should be more thermodynamically stable to aggressive leachates because the simultaneous association

of the polyelectrolyte with numerous bound cations should effectively “lock” the bound cations in place, thereby reducing cation exchange.

(3) Independently swelling additives

This mechanism considers as the individual swelling potential of each mixture material. Trauger and Darlington (2000) amended sodium bentonite with a super absorbent polymer. However, the water absorptive capacity of superabsorbent polymers is highly sensitive to ionic strength (Buchholz and Graham, 1998). Thus, while a bentonite amended with a superabsorbent polymer may demonstrate a very high swelling capacity in dilute solutions, and may provide minimal supplementary swelling in solutions that are incompatible with bentonite.

2.4 Polymer-bentonite composite in geotechnical engineering

In the literatures, three types of polymers e.g., cationic, anionic and nonionic have been used to treat the bentonite. The properties of bentonite-polymer composite depend on the molecular weight, surface charge and charge density of the polymer. The polymer treated bentonite in the literatures are summarized as follows.

2.4.1 Cationic polymer treated bentonite

Cationic polymer is easy to absorb onto the opposite negatively charge of clay surface (Stuum, 1992) and the schematic of cationic polymer absorbed to the negatively charge clay surface is shown in Fig. 2.40.

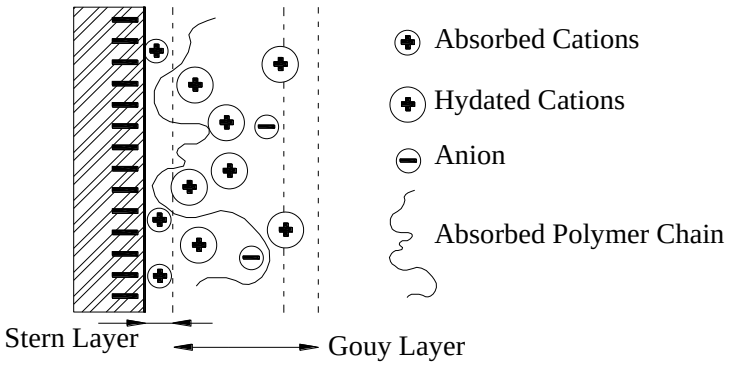

Fig. 2.40 Clay-polymer interaction (after Theng, 1979)

Function of cationic polymer can protect the clay from cation exchange because a cationic polymer chain contains a lot of cation that can be simultaneously exchanged (Theng

1982; Ashmawy et al. 2002). However, the polymer treated with cationic polymer showed higher or similar *k*-value compared with that of the untreated bentonite as shown in Fig. 2.41. This because the cationic polymer tends to aggregate clay particles, and reducing the thickness of double layer around the bentonite particles.

2.4.2 Nonionic polymer treated bentonite

Nonionic polymer can be possible adsorbed to surfaces of the sodium bentonite (Theng, 1979), when the nonionic polymer is added to the clay without the presence of electrolytes, a network of polymer-clay links is formed as shown in Fig. 2.42. Few publications used a nonionic polymer treated bentonite. Shenning (2004) reported that nonionic polymer reduces the free swell index of the bentonite (Fig. 2.43).

2.4.3 Anionic polymer treated bentonite

Adsorption of anionic polymers onto the clay surface is promoted by the presence of polyvalent cations, which act as bridges between the anionic groups on the polymer and the negatively charged sites on the clay as shown in Fig. 2.44. (Mortensen 1960; Theng 1979). Razakamanantsoa et al. (2014) reported that using an anionic polymer mixed with bentonite can be used as a suitable hydraulic barrier, backfill or mud for drilling application.

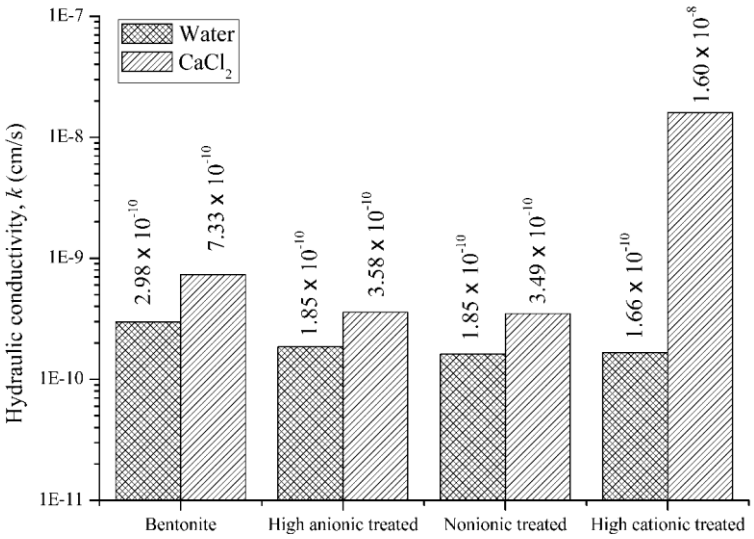

Fig. 2.41 Hydraulic performance of non-treated and polymer treated clays (after McRory and Ashmawy, 2005).

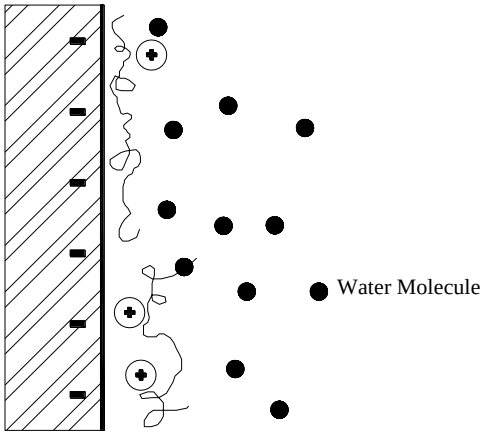

Fig. 2.42 Adsorption of uncharged polymer on clay (after Theng, 1979)

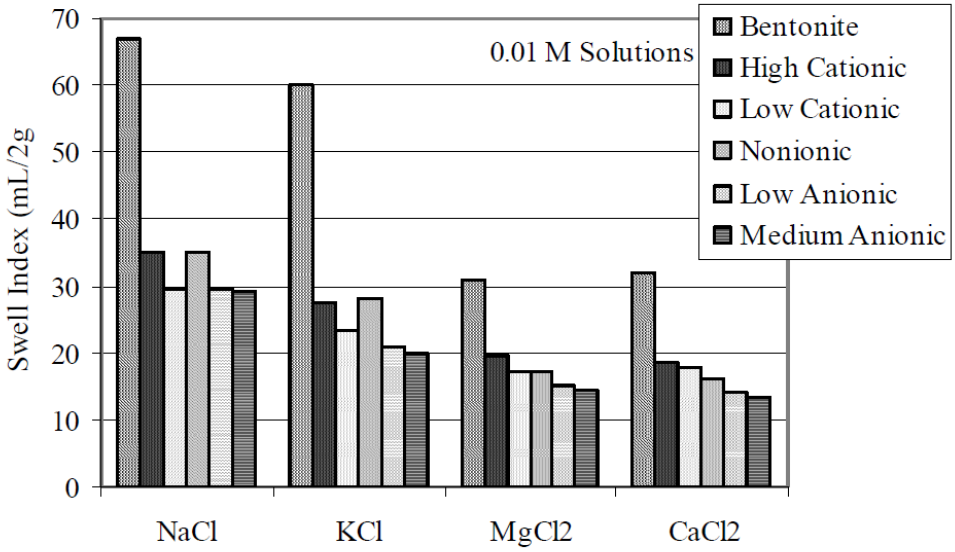

Fig. 2.43 Effect of charge density on swell index (after Schenning, 2004)

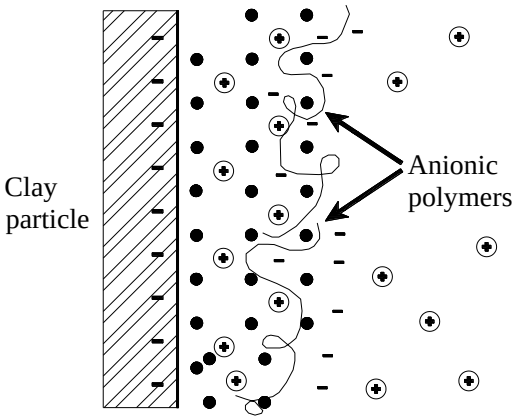

Fig. 2.44 Interaction between anionic polymers and clays (after Theng, 1979)

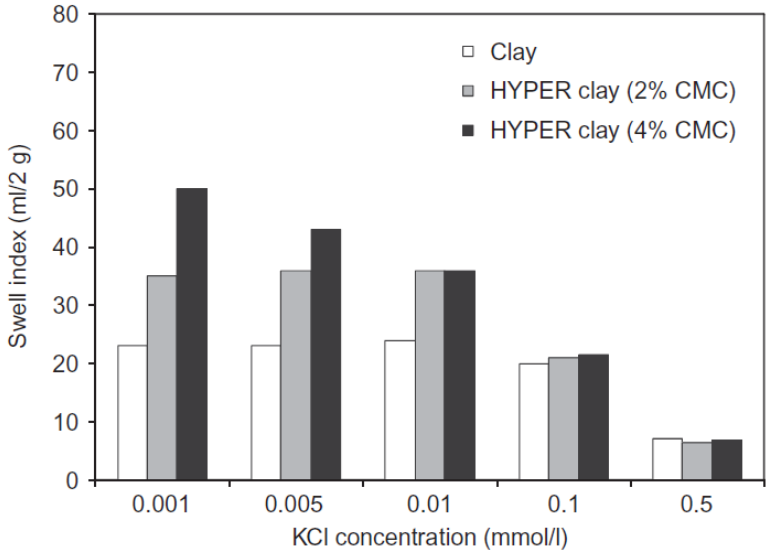

Fig. 2.45 The addition of CMC to the clay improved its swelling ability in KCl solutions (after Di Edimio et al., 2015)

Di Edimio et al. (2015) polymerized a sodium bentonite by using an anionic sodium carboxymethyl cellulose (CMC) with commercial name as HYPER clay. They investigated both swelling and permeability (k). The test results show that the HYPER clay had higher swelling capacity (Fig. 2.45) and a lower permeability (Figs. 2.46(a) and 2.46(b)) compared with that of the untreated bentonite.

2.4.4 Sodium polyacrylate

Sodium polyacrylate, is a sodium salt of polyacrylic acid with the chemical formula $[-CH_2-CH(CO_2Na)-]_n$. Sodium polyacrylate is an anionic polyelectrolyte with negatively charged carboxylic groups in the main chain and is given by the structure in Fig. 2.47. This

polymer can absorb water as much as 100 to 1000 times its mass. Sodium neutralized polyacrylic acids are the most usual form used in industry, there are also other salts available including potassium (K^+), lithium (Li^+) and ammonium (NH_4^+).

Scalia et al. (2011) and Scalia et al. (2014) produced bentonite polymer composite (BPC or BPN, where it is the same material) using sodium polyacrylate. The sodium bentonite (Na-B) was polymerized by sodium polyacrylate. The results showed that swell index (Fig. 2.48) of the BPC was higher than that of the untreated bentonite (Na-B) in different concentration of $CaCl_2$ solution. The values of *k* of the BPC was lower compared with that of the corresponding Na-B as shown in Fig. 2.49 (Scalia et al., 2011).

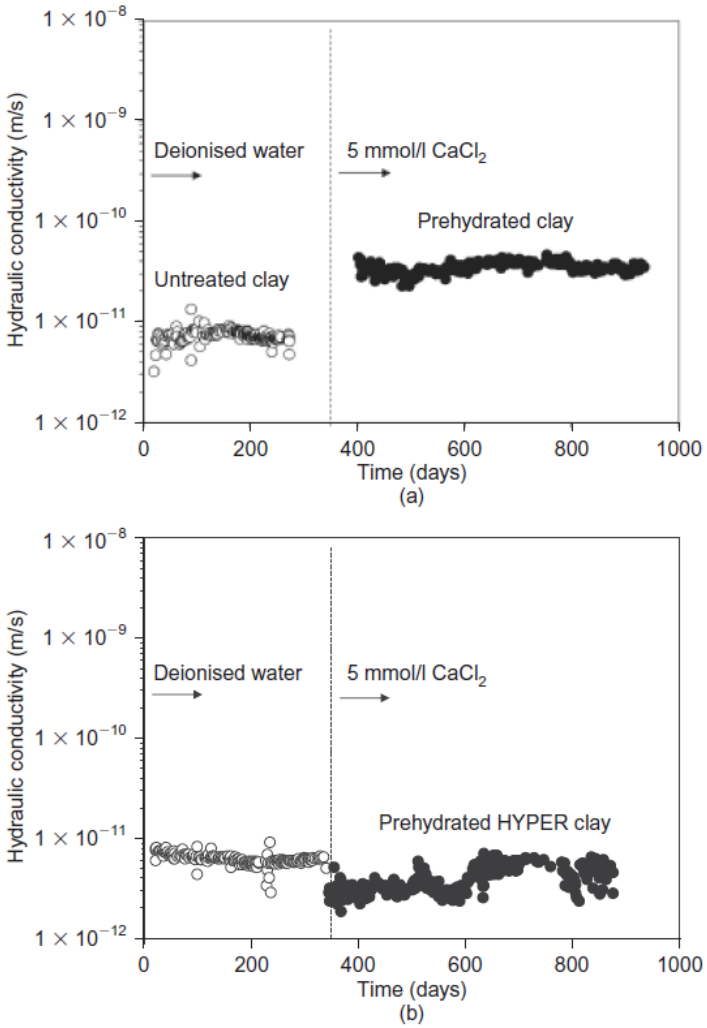

Fig. 2.46 Hydraulic conductivity to 5 mM $CaCl_2$ solution of: (a) untreated clay and (b) the HYPER clay (after Di Edimio et al., 2015)

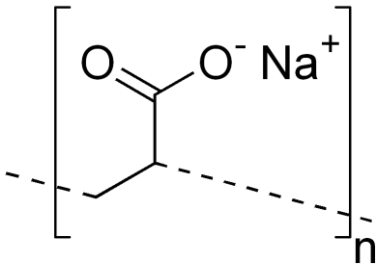

Fig. 2.47 Chemical structure of sodium polyacrylate

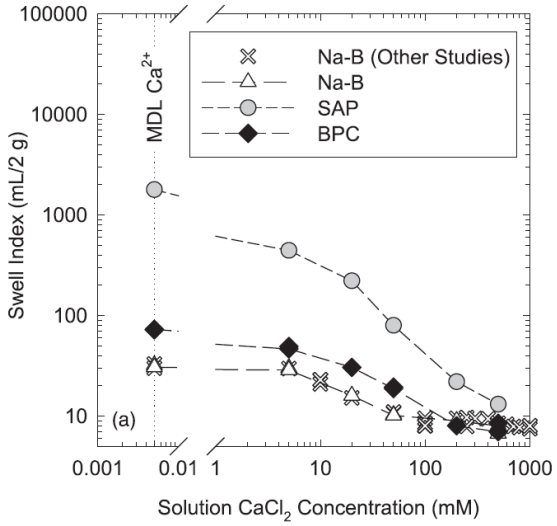

Fig. 2.48 Swelling index versus solution $CaCl_2$ concentration (after Scalia et al., 2014)

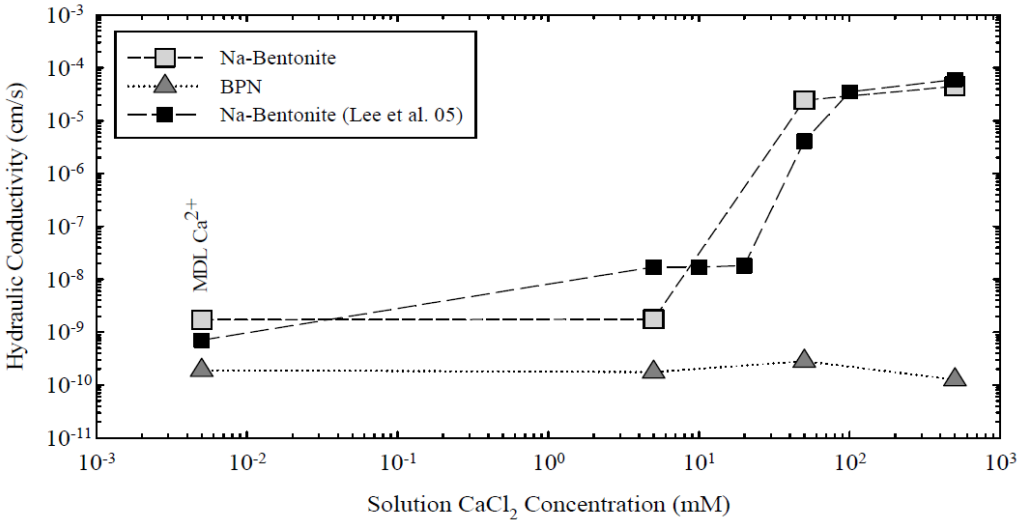

Fig. 2.49 Hydraulic conductivity of Na-bentonite, BPN, and Na-bentonite GCLs tested by Lee et al. (2005) (after Scalia et al., 2011).

2.4.5 Materials and methods for polymerized bentonite (PB) using sodium polyacrylate

(1) Materials

A sodium acrylate ($C_3H_3NaO_2$, Na-AA) monomer were obtained from a mixture of acrylic acid ($C_3H_4O_2$), sodium carbonate (Na_2CO_3) and sodium hydroxide (NaOH). Several initiators can be used such as, azobisisobutyronitrile (AIBN) (Okamoto, 2003; Bogdal et al., 2014; Wang et al., 2011a; Yanovska et al., 2017), 2,2'-azobis(2-methylpropionamidine) dihydrochloride (AAPH) (Wahl et al., 1998; Zdanowicz et al., 2010), potassium persulfate (KPS) (Khulbe et al., 1982; Choi et al., 2003; Wang et al., 2011a; Haraguchi et al., 2015) and sodium persulfate (NaPS) (Ahmed et al, 2012; Bohnhoff and Shackelford, 2013). Choi et al. (2013) have used about 1.0 g/g by weight of the monomer for polymerization. There are many initiator types can be used for polymerization and there is limit number of publications provided enough data about the amount of initiator used as listed above. Therefore, the initiator type and amount of initiator is needed to investigate.

(2) Synthesis of sodium acrylate ($C_3H_3NaO_2$, Na-AA)

The Na-AA are obtained from a mixture of Na_2CO_3 solution and the acrylic acid solution as following Eq. 2.5. Then, NaOH was added until the design pH value such as, pH = 7 (Scalia et al., 2011; Bohnhoff and Shackelford, 2013) or pH =10 (Wang et al., 2011b). Finally, the clear solution of sodium acrylate was obtained by vacuum filtration. There are two different groups using different pH condition. To confirms the pH condition, the study of pH condition is needed.

$$2C_3H_4O_2 + Na_2CO_3 = 2C_3H_3NaO_2 + CO_2 + H_2O \quad (2.5)$$

(3) Schlenk-line system

As discussed in section (3.4), the inhibition of propagation polymerization will occur when an active center oxidation with oxygen (O_2) molecule. To avoid this problem, the Schlenk-line is adopted (Fig. 2.50).

The Schlenk line consists of a dual manifold with several ports. One manifold is connected to a source of purified inert gas (e.g., nitrogen or argon gas), while the other channel is connected to a vacuum pump. The inert-gas line is vented through an oil bubbler, while solvent vapors and gaseous reaction products are prevented from contaminating the vacuum pump by a liquid-nitrogen cold trap.

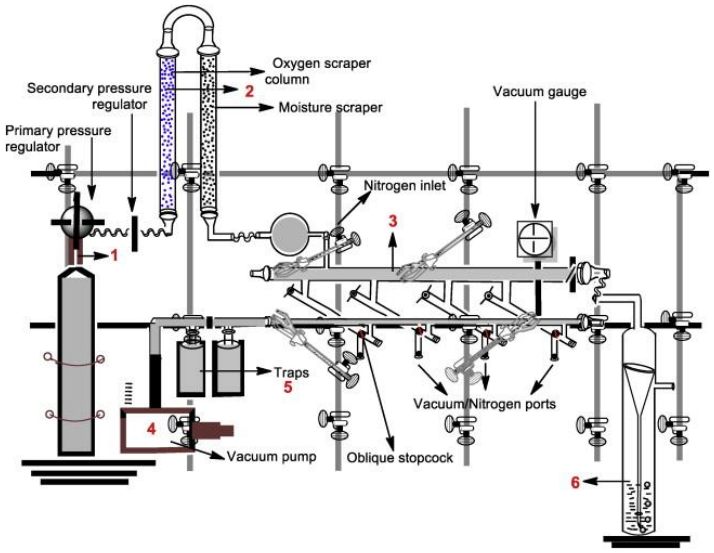

Fig. 2.50 Double manifold Schlenk line equipped with an inert gas system and a bubbler (after Chandra and Zebrowski, 2014).

(4) Polymerization

The free-radical polymerization can be started when the initiator generates the radical part. There are several ways to start initiation as mention in the previous section. There are many researcher (e.g., Bohnhoff and Shackelford, 2013; Wang et al., 2011a) used the thermal decomposition method, while activated by redox reaction (Haraguchi et al., 2015) is also available. However, the redox reaction method needs an additional chemical which can be costly and difficult to be removed. Therefore, this study uses the thermal decomposition for producing the polymerized bentonite (PB). Fig. 2.51 shows the details of simple polymerization chamber.

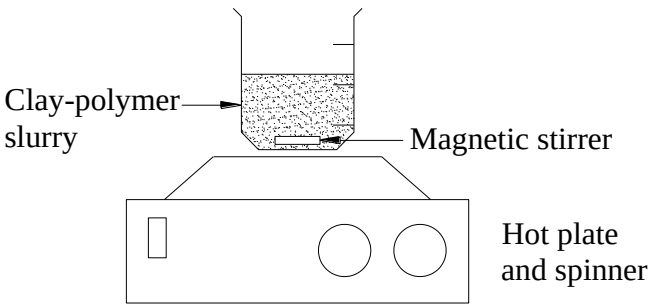

Fig. 2.51 Polymerization chamber (modified from Armstrong, 2015)

Time requirement for polymerization process depends on the material and method used. Mingzhu and Tianhua (2000) reported that the optimum time is 25-min for reaction time to prepare cross-linked sodium polyacrylate. Haraguchi et al. (2015) reported that the free-radical

polymerization is needed for 20 h. To achieve the optimum polymerization time for selecting method, the time for polymerization is needed to be investigation.

(5) Removal of residual substances and powdering method

Usually, residual substances (e.g., monomer, initiator, emulsifier, etc.) will remain in solution after polymerization. This substance can be removed by washing with deionized water and acetone (C_3H_6O) (e.g.., Zhang and Rong, 2011). The schematic of a vacuum washer chamber is shown in Fig. 2.52.

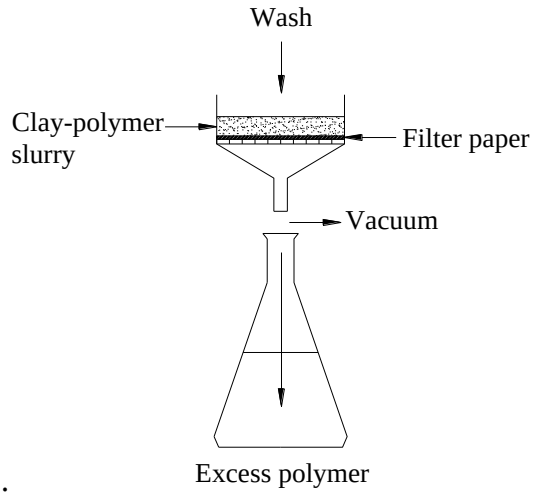

Fig. 2.52 Schematic of vacuum washed (modified from Armstrong, 2015)

After well washed, the soft gel can be dried by several methods. For example, Wang et al. (2011a) dried the swollen hydrogels at room temperature for 2 days, and then dried at 40 °C under vacuum for 48 h. Ning et al. (2013) also used vacuum dried for polymer clay nanocomposite. Due to time consuming process, heat dried method is also available (Scalia et al., 2011; Bohnhoff and Shackelford, 2013). The composite material can be heat-dried at 105 °C. After dried, it was milled and screened by no. 200 sieve (Bohnhoff and Shackelford, 2013). The obtained fine powder is served to be used for further purpose.

2.5 Summary

GCLs are commonly used as a barrier material to prevent the toxic liquids/gases leaked to surrounding environment. It is well known that the barrier capability of the GCLs are controlled by the swelling capacity and permeability (k) of the bentonite layer in the GCLs, but the swelling of the bentonite can be decreased when interacted with chemical liquids due to the

collapse in the thickness of diffuse double layer of the bentonite particles. To protect the weak-bond interlayer from chemical substances, one of the methods is coating bentonite particles by using polymerization technique. The polymer can protect the exchange ion from the bentonite particles, resulting in better swelling capacity in chemical solutions. However, in the literature there is limited source of information on how to efficiently produce the polymerized bentonite (PB). Also, the swelling and permeability of PB need further investigation. While, the self-healing capacity of GCL with the PB (PB-GCL) permeated with chemical solutions has not been investigated.

In summary, there are two main issues need to be investigated, i.e. (1) materials and methods for producing the PB and (2) investigation on self-healing capacity of the PB-GCL in chemical solutions.

CHAPTER THREE
POLYMERIZED BENTONITE

3.1 Introduction

Swelling potential of a natural sodium bentonite (UB) decreases when it interacts with high concentration cation solutions and very low (pH < 3) or very high (pH > 12) pH solutions (Jo et al., 2001). The main reason is that the cations will enter that diffuse double layer around the bentonite particles and reduce the bentonite interlayers. To prevent the cations entered the weak-bond interlayer of bentonite particles, coating bentonite particles by polymer is an effective method (Elhajji et al., 2001; Razakamanantsoa et al., 2008; Bohnhoff and Shackelford, 2013; Di Emidio et al., 2015). An anionic polymer, sodium polyacrylate is a polymer generally used in diaper disposal. Due to its very high expansion in water or some chemical liquids, some researchers have been used this polymer to treat the bentonite and they reported that polymerizing bentonite particles by sodium polyacrylate increased the swelling capacity and decreased the permeability against cationic solutions (Scalia et al., 2011; Scalia et al., 2014). However, to the optimum method for producing the polymerized bentonite (PB) is still not clear because there is insufficient information provided in the literatures. Therefore, this chapter aims to examine effective materials and methods to produce the PB. Then, the physical properties, consolidation properties, swelling properties and permeability (k) of the PB under the proposed condition were evaluated by comparison with the test results of the UB.

3.2 Material and methods for polymerizing sodium bentonite

3.2.1 Materials

(1) Chemicals

A sodium acrylate monomer ($C_3H_3NaO_2$, Na-AA) was used to polymerize sodium bentonite. Four (4) commercial initiators, including azobisisobutyronitrile (AIBN), 2,2'-azobis(2-methylpropionamidine) dihydrochloride (AAPH), potassium persulfate (KPS) and sodium persulfate (NaPS), were used to investigate the effect of initiator type. All initiators used are thermal decomposable with a decomposition temperature about 60 °C (Mingzhu et al., 1996; Wang et al., 2011a). Deionized water was used as a solvent, and an acetone was used for cleaning the produced polymerized bentonite (PB).

(2) Sodium bentonites

Four different sodium bentonites were used in this study. The bentonite-1 namely "Super Clay" is the sodium bentonite which is from Wyoming, USA (Tang et al., 2014) and it was the only one bentonite that had a free swelling index (FSI) value meets the minimum requirement (≥ 24 ml/2g) for geosynthetic clay liners (GCLs) (Bathurst et al., 2007). Other three bentonites are natural sodium bentonites in Japan and their properties are not qualified for GCLs material (their FSI values in deionized water ≤ 24 ml/2g). The chemical compositions of the four types of sodium bentonite are listed in Table 3.1. To investigate the optimum conditions for polymerizing the sodium bentonite, the bentonite-1 (Super Clay) was predominantly used. Subsequently, the proposed condition was applied to other three sodium bentonites to evaluate the efficiency of the proposed optimum conditions. All bentonite used for all the tests was screened passing No. 200 (< 75 μm).

Table 3.1 Chemical compositions of four bentonites (data provided by the manufacturers)

Chemical composition (%)	Bentonite -1 (Super Clay)	Bentonite-2 (Earth Friend)	Bentonite-3 (Kunigel V-1)	Bentonite-4 (Haruna)
SiO_2	73.8	68.4	69.4	68.7
Al_2O_3	13.8	13.5	15.6	12.6
Fe_2O_3	4.3	2.8	2	2.8
MgO	1.6	2.7	2.2	2.1
CaO	1.5	4.0	2.1	5.1
Na_2O	1.7	2.3	2.0	2.6
K_2O	0.5	1.5	0.3	1.5
Loss on ignition	1.6	4.1	5.3	3.3
Total	98.8	99.3	98.9	98.7

3.1.2 *Polymerization method*

Free-radical polymerization method was used in this study.

(1) Synthesis of sodium acrylate monomer (Na-AA)

Na-AA was prepared with the following steps:

(a) The concentration of acrylic acid ($C_3H_4O_2$, AA) was determined from a monomer content (%) by dry weight of the sodium bentonite. For example, the monomer content of 10% by dry weight of the bentonite of 10.0 g requires the concentration of the AA of 0.14 M (volume of the AA used is 1 ml) dissolved in the deionized water of 100 ml). Four different monomer contents of 5%, 10%, 15% and 20% were used in this study. Then, the AA solution (100 ml) was mixed with a sodium carbonate (Na_2CO_3) solution (100 ml), and the amount of Na_2CO_3 was determined by the equilibrium of the chemical reaction as indicated in Eq. (2.5).

(b) Sodium hydroxide (NaOH) solution was added to the solution to adjust the pH value of the solution and then we abbreviated the solution as Na-AA as shown in Fig. 3.1. The values of pH adopted were 7, 10 and 12. Fig. 3.1 shows the pH monitoring during adjusting of pH value by NaOH solution.

(c) The clear Na-AA solution was filtrated and reserved for the polymerization process.

Fig. 3.1 pH level monitors by pH meter

(2) Schlenk line

Free-radical polymerization is sensitive to oxygen molecules (O_2). During polymerization, active chains and/or active initiators can react with O_2, producing an oxygen radical, which reduces polymerization efficiency. To remove O_2 from the reaction process, the Schlenk line is used.

(a) Materials

The key features of a basic Schlenk line includes of dual manifold, inert gas inlet (Nitrogen, N_2), gas bubbler, vacuum pump, cold trap as shown in Fig. 3.2.

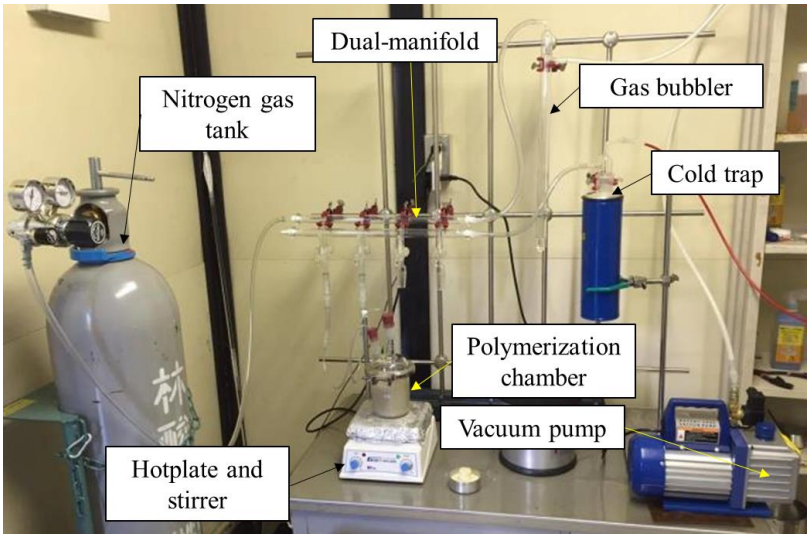

Fig. 3.2 Photo of Schlenk line

The dual manifold is the main body of the Schlenk line as shown in detail in Fig. 3.3. The dual manifold has two parallel glass tubes; one is connected to the inert gas supply (red line) and the other one is connected to the vacuum pump (blue line). Taps or switches are used for manipulating to the gas, and/or the vacuum lines, and/or closed mode.

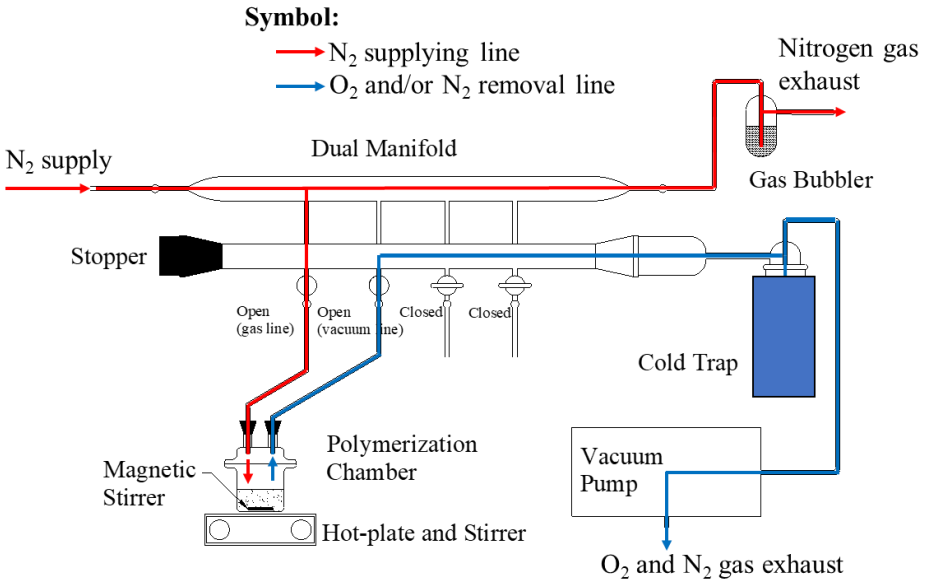

Fig. 3.3 Details schematic of Schlenk line

(b) Methods

The procedures for using Schenk line are explained as following.

(i) Before using, applying a thin layer of grease to all taps. It should be avoided for applying too much grease which can block some necessary holes. Then, connect the polymerization chamber to the Schenk line as shown in Fig. 3.4.

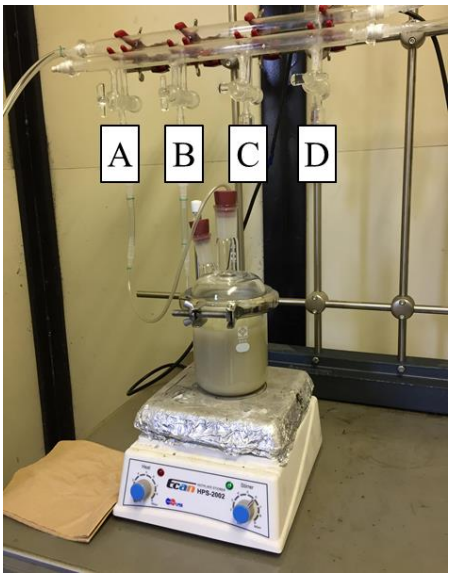

Fig. 3.4 Polymerization chamber connected to the Schenk line

(ii) Open the tap A (gas line) and the tap B (vacuum line) While, tap C and tap D are closed (Fig. 3.5).

(iii) The cold trap was filled with a liquid nitrogen as shown in Fig. 3.6. The liquid nitrogen cools the cold trap and forces vapors and gases from the Schlenk line to condense. The function of the cold trap is used to prevent the vapors and gases destroyed the vacuum pump.

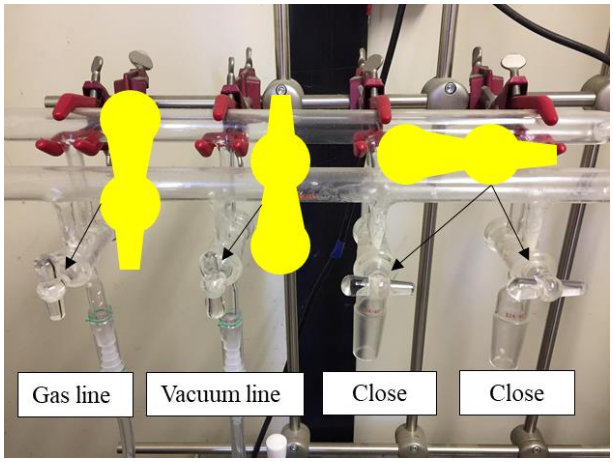

Fig. 3.5 Tap patterns for circulating N_2 and removing O_2 in the chamber

Fig. 3.6 The Dewar flask contained the liquid nitrogen

(iv) Then, gas supply was opened. Fig. 3.7 shows the details of gas regulator and N_2 gas. The function of gas regulator is to adjust the gas supply rate. It is very important to note that the gas supply has to be open slowly to prevent gas bubbler and the taps bumping. The rate of supplying can be monitored by the gas bubbler. The rate of bubbler is controlled about one bubble per second. Then, turn on the vacuum pump and allow it to warm up for 3 to 5 minutes. It is very important to note that when open the vacuum pump, the rate of bubble will be decreased, and it need to increase the gas supply rate to prevent the oil reversely moving to the Schlenk line.

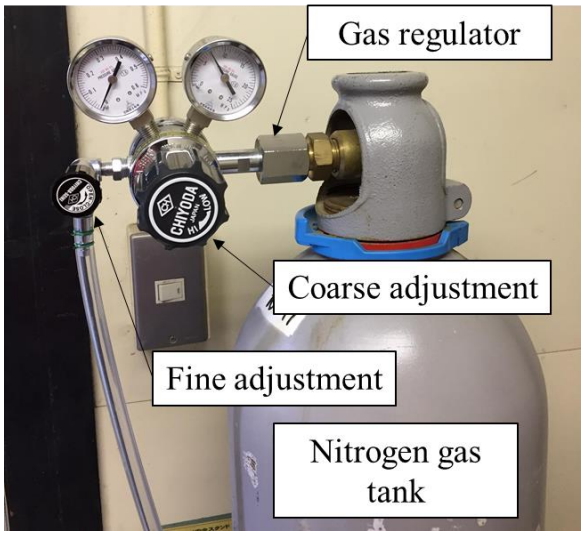

Fig. 3.7 Gas regular installed with N_2 gas tank

(v) The chamber was allowing to circulate with the N_2 for 30 minute (Davis, 2004). Then, all taps were closed to prevent the O_2 enter to the chamber as shown in Fig. 3.8. The

polymerization was started by increasing the temperature by turn on the heat button (left button in Fig. 3.8).

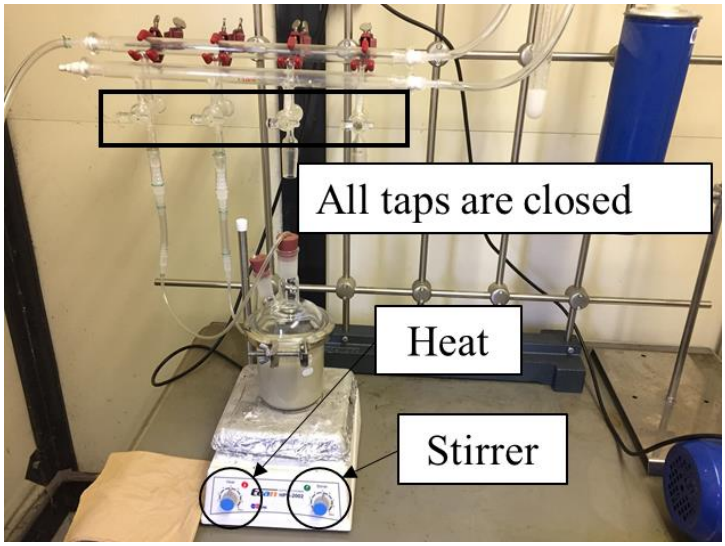

Fig. 3.8 Schenk line condition before polymerization

(3) Polymerization

The polymerization follows the following steps;

(a) A certain amount of initiator was dissolved in the Na-AA solution. The amount of the initiator was determined as the ratios of the weight of the initiator (*I*) to the weight of the monomer (*M*). Four values of *I/M* of 0.1, 0.2, 0.4 and 1.0 were used in this study.

(b) 10.0 g of air-dried bentonite (4%) was dispersed into the 250 ml of the deionized water to make a bentonite slurry.

(c) The slurry was mixed with the pre-prepared mixture solution of Na-AA with the initiator.

(d) The mixture slurry was transferred to a polymerization chamber. Then, the chamber was connected to the Schenk line to remove the O_2 from the mixture solution by circulating with nitrogen gas as describes in the previous section.

(e) After the oxygen was removed, the temperature of the mixture was increased to 65 °C. The obtained PB slurry was washed with deionized water and acetone to remove the residual monomer and the initiator as shown in Fig. 3.9. About the polymerization time, a series tests were conducted by varying polymerization time as 0.5 h, 1 h, 2 h and 4 h. Fig. 3.10 shows the test results of final product mass of the PB prepared under the conditions: KPS used as initiator, *I/M* ratio of 0.2, pH of 7 and monomer content of 10%. In Fig. 3.10, it is found that when polymerization time is more than 1.0 h, the resulting mass of the PB was

not changed much. So, the polymerization time of 2.5 h was selected for further study to ensure the completion of the polymerization process.

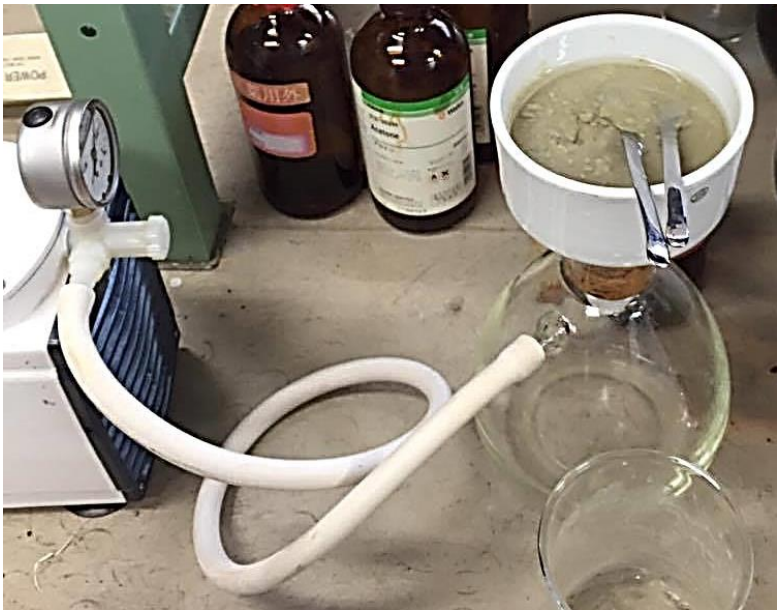

Fig. 3.9 Vacuum washing chamber

(f) The PB was oven dried at 105 °C. Then, the dried PB was milled as demonstrated in Fig. 3.11, and screened by the number 200 sieve (< 75 μm). The passing particle was collected into an airtight storage container for further investigation.

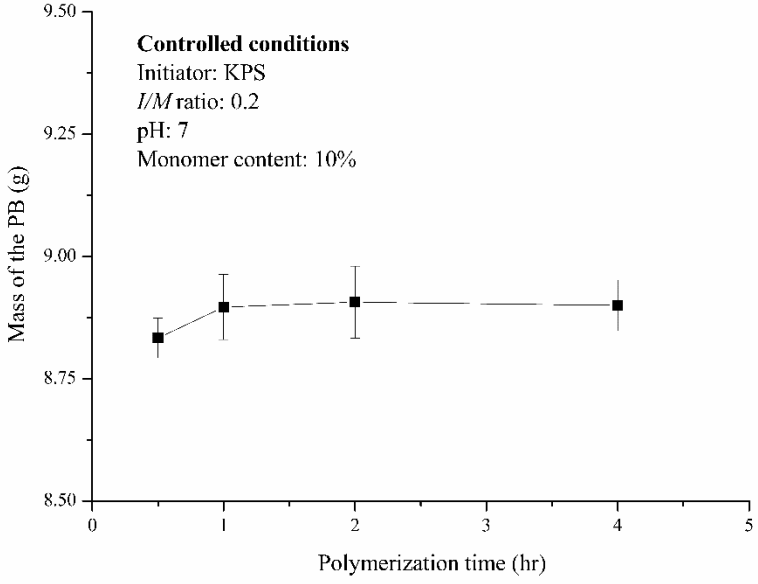

Fig. 3.10 Results of mass of the PB

(a) After drying (b) After powering

Fig. 3.11 The PB (a) after drying, and (b) after powering

3.3 Optimum conditions evaluated using free swelling index (FSI)

3.3.1 Test conditions

FSI tests was performed following the ASTM D5890. Total 2.0 g of dried powder polymerized bentonite (PB) or untreated bentonite (UB) were dropped into 100 ml of the desired liquid as shown in Fig. 3.12. The dropping rate is 0.1 g per 10 min. The final volume of expanded sample was measured after 24 h and each case was repeated for 3 times.

Four different cationic liquids namely, 0.1 M NaCl, 0.6 M NaCl and 0.1 M $CaCl_2$, 0.6 M $CaCl_2$ were used. The 0.6 M NaCl was used to simulate the sea water (Miyahara et al., 2015). The 0.6 M $CaCl_2$ is an aggressive divalent cation solution. These chemical solutions were chosen to evaluate the performance of the PB against aggressive di-valence and mono-valence cation solutions. The different chemical concentrations of 0.1 M and 0.6 M were prepared to investigate the effect of chemical concentration. Table 3.2 reported the results of pH and electro-conductivity (*EC*) of the liquid tested.

Other seven different liquids were used to investigate of effect of pH on properties of the PB. By definition, pH = $-\log_{10}H^+$ concentration: pH lower than 7 is acid and pH gathered than 7 is alkaline. Therefore, 0.001 M HCl, 0.1 M HCl, 0.001 M NaOH, 0.01 M NaOH, 0.03 M NaOH, 0.05 M NaOH, 0.1 M NaOH solution can be considered as the pH value of 1, 3, 11, 13, respectively. The simulation of solution with pH of 7 was used the deionized water. The measured pH value and *EC* value are given in the Table 3.3.

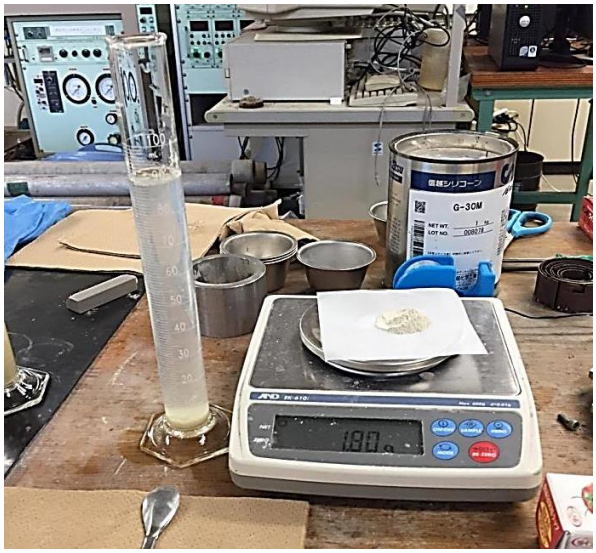

Fig. 3.12 Free swelling index test

Table 3.2 Properties of the deionized water and cationic liquids

Liquids	pH	*EC* (mS/cm)
Deionized water	6.99	0.00
0.1 M NaCl	5.92	4.00
0.6 M NaCl	6.21	11.10
0.1 M $CaCl_2$	7.13	6.30
0.6 M $CaCl_2$	6.94	16.60

Table 3.3 Properties of the various pH level solutions

Liquids	pH	*EC* (μS/cm)
0.1 M HCl	1.02	36.30
0.001 M HCl	3.02	0.32
Deionized water	6.99	0.00
0.001 M NaOH	11.03	0.33
0.01 M NaOH	12.01	2.65
0.03 M NaOH	12.49	7.05
0.05 M NaOH	12.68	11.14
0.1 M NaOH	13.01	20.80

3.3.2 Effect of initiators

Fig. 3.13 shows the test results of the FSI values of four PBs prepared with different initiators as well as the UB with 3 different liquids (deionized water, 0.6 M NaCl and 0.6 M $CaCl_2$). The PBs were produced with a monomer content of 10%, pH of 7 and *I/M* ratio of 0.2. The FSI values of the PBs and the UB show the same tendency that FSI decreases as the cation concentration and valence of the cations increased due to the decreasing of thickness of double layer ($1/\kappa$). It is well known that the $1/\kappa$ value is a function of the concentration of cations and the valence of cation (Bolt, 1956; Mitchell and Soga, 2005).

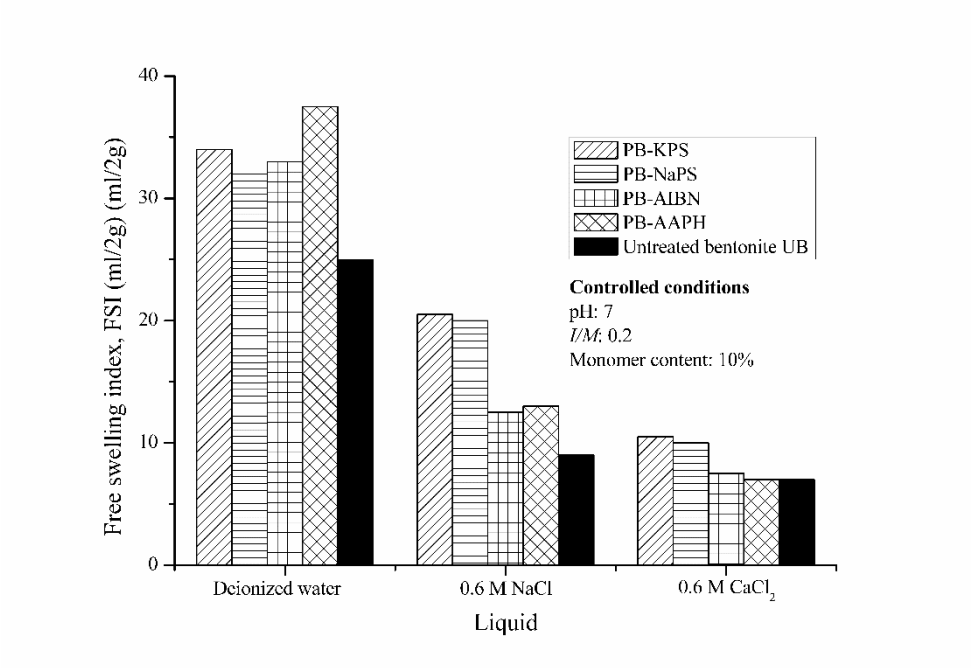

Fig. 3.13 Effect of liquids on FSI with various initiators

In deionized water, PB using any initiator has a FSI value higher than that of the UB. For the 0.6 M NaCl solution, PBs still has higher FSI values compared with that of the UB. It is of interest to note that the FSI value in 0.6 M NaCl for PBs using KPS and NaPS are higher than that using AIBN and AAPH. In the 0.6 M $CaCl_2$ solution, PBs produced using KPS and NaPS has higher FSI values, but PBs using AIBN and AAPH has approximately the same FSI value as the UB. Possible reasons are that the hydrophobic AIBN (Hu et al., 2016) has lower solubility (< 0.1 g/100 g in water at 25 °C) in water, and the AAPH is a cationic initiator (Destarac et al., 2010). The presence of cation in the solution can induce coagulation effect to the negatively charged bentonite particles (Rozainy et al., 2014), which may reduce the

effectiveness of the initiator. In Fig. 3.13, the PB-KPS and the PB-NaPS gave similar FSI values for the liquids tested, but the PB-KPS had slightly higher FSI results, therefore the KPS was selected as the initiator for further investigation.

3.3.3 Effect of pH and the amount of the initiator

Under the condition of 10% monomer content with respect to the bentonite to be polymerized, the relationship between FSI and *I/M* with various values of pH are plotted in Fig. 3.14 for using the 0.6 M NaCl solution.

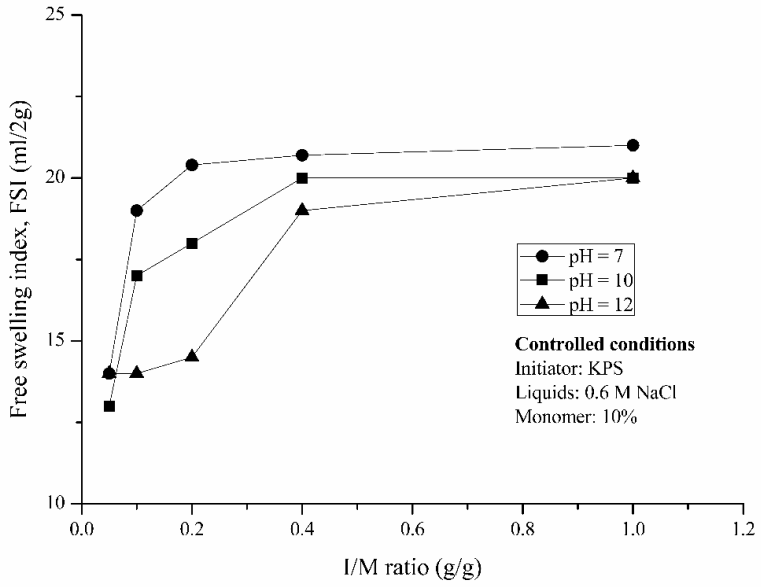

Fig. 3.14 Effect of pH and *I /M* ratio on FSI

In Fig. 3.14, under the same *I/M* ratio, it is observed that an increase in pH value results in a lower FSI value. This results confirms by Mingzhu et al. (1996). The possible reason is increasing the pH value by adding the NaOH solution, which increase the concentration of OH^- in the solution, and the $S_2O_8^{-2}$ ion from the initiator (KPS) can be easily oxidized by OH^-, following Eq. (3.2):

$$S_2O_8^{-2} + OH^- \rightarrow HSO^{-4} + SO_4^{-2} + 1/2O_2 \qquad (3.2)$$

For an oxidized initiator, the ability of generating the active radicals will be weakened. The highest FSI value is obtained at the pH of 7. For pH value of 7, the FSI value increased as the *I/M* ratio increased until it reached to the *I/M* of 0.2. For the *I/M* > 0.2, the FSI values remain

close to a constant for the conditions tested. The function of the initiator is to initiate polymerization process, and it is not a main reaction component. For the case of *I/M* > 0.2, some of the initiator might be remained in the solution and finally removed from the final product by the deionized water and the acetone. Based on the results in Fig. 3.14, it is suggested that the optimum conditions for producing PB using KPS as the initiator should be pH = 7 and *I/M* = 0.2. The tests using 0.6 M $CaCl_2$ were also conducted, but there was no clear trend about the influence of pH and/or *I/M* ratio on the FSI, and the results are not presented.

3.3.4 Effect of monomer content

Under the conditions of pH = 7, *I/M* = 0.2 and using KPS as the initiator, Fig. 3.15 shows the effect of the monomer content on the FSI of the PB. In the 0.6 M NaCl solution, the results indicate that the FSI value increases with increasing monomer content. This is in consistent with the test results reported by Di Emidio et al. (2015). While, the increasing rate reduce for monomer contents over 10%. For the 0.6 M $CaCl_2$ solution, when the monomer content is more than 5%, the FSI values of PBs do not show considerable change. Based on the test results, a monomer content of 10% is suggested.

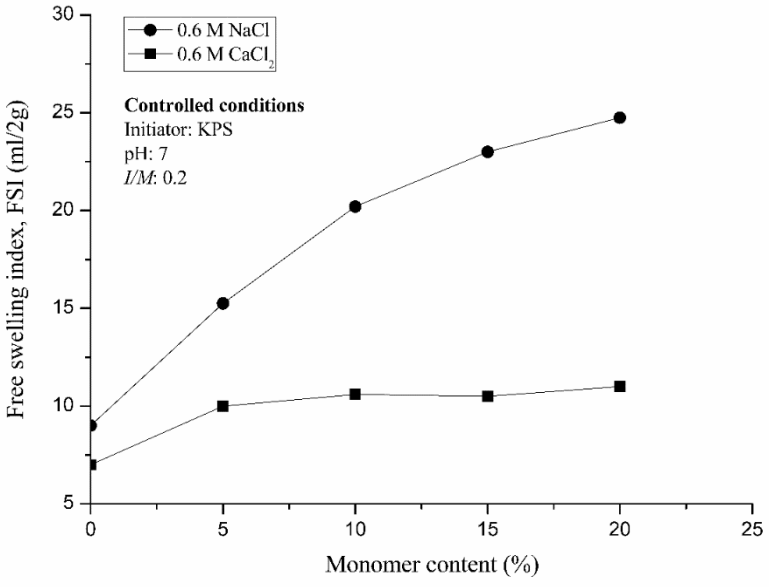

Fig. 3.15 Effect of monomer content on FSI

According to the results of FSI, using the free radical polymerization method and sodium acrylate as the monomer, the optimum condition for producing PB can be summarized as (1) using KPS as the initiator, (2) pH of 7, (3) *I/M* ratio of 0.2 and (4) monomer content of 10%.

3.3.5 FSI of PBs from other bentonites

To check the effectiveness of the proposed conditions for polymerizing bentonites, three other bentonites from Japan, as listed in Table 3.1, were polymerized under the identical conditions. The FSI values in deionized water are compared in Fig. 3.16. The figure clearly shows that for all the bentonites investigated, the FSI values of the PBs are higher than those of the UBs. For bentonite-2 and bentonite-3, after polymerization, the FSI value is reached at 24 ml/2g; i.e., they can be used in a geosynthetic clay liners (GCLs) (Bathurst et al., 2007).

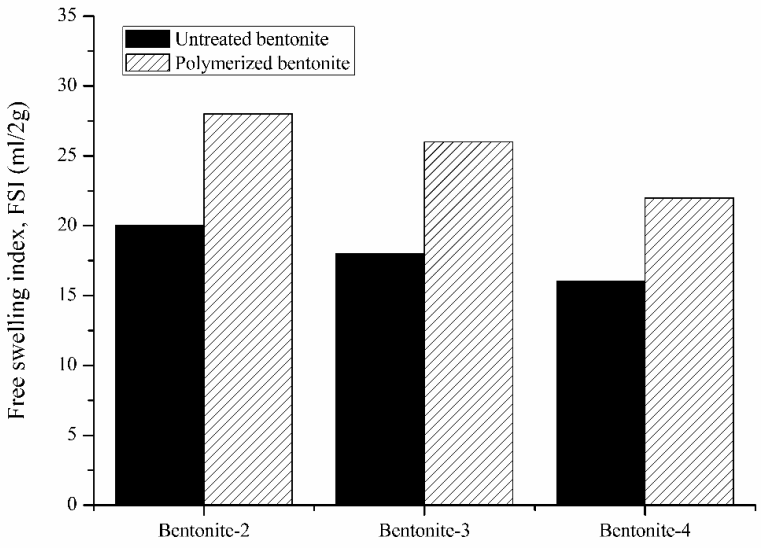

Fig. 3.16 Results of FSI in deionized

3.4 Microstructure analysis

3.4.1 X-ray diffraction (XRD) *analysis*

(1) Test methods

XRD test for the PB from bentonite-1 (Super Clay) and the corresponding UB was conducted using a SHIMADZU XRD-6000 as shown in Fig. 3.17. The oven dried fine powder of the PB or UB was fully packed into the specimen container 20 mm in diameter and 1.25 mm in height as shown in Fig. 3.18. The PB or UB specimen was scanned from 4° to 40° at a rate of 0.02 °/s. The voltage and current of the X-ray tubes used were 40 kV and 30 mA, respectively.

Fig. 3.17 XRD test machine

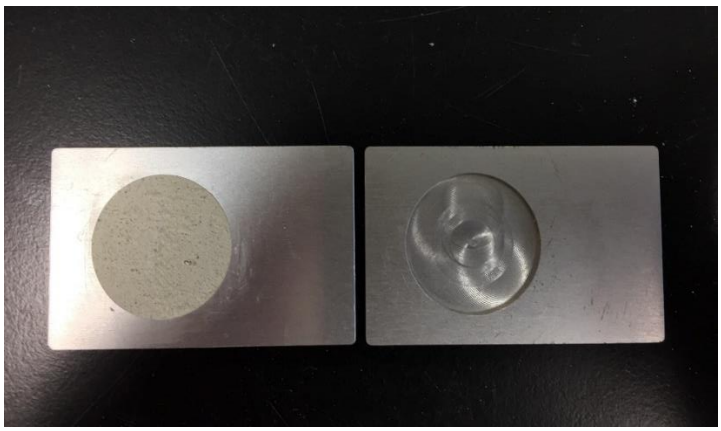

Fig. 3.18 XRD specimen

(2) XRD patterns of the UB and PB

Figs. 3.19(a) and (b) show the results of the peaks indicated {001} plane of the PB and the corresponding UB, respectively. It can be seen that the interlayer spacing (d-spacing) of the bentonite particle was not modified by the polymer because the value of diffraction angle (2θ) of the peaks {001} were remained unchanged, which is the same as reported by Geckeler et

al. (2009). There are some publications indicate the increase of the d-spacing of the polymerized bentonite particles (Gao, 2004; Olad, 2011). However, for the PB reported, more than 90% was polymer and the bentonite content was less than 10%.

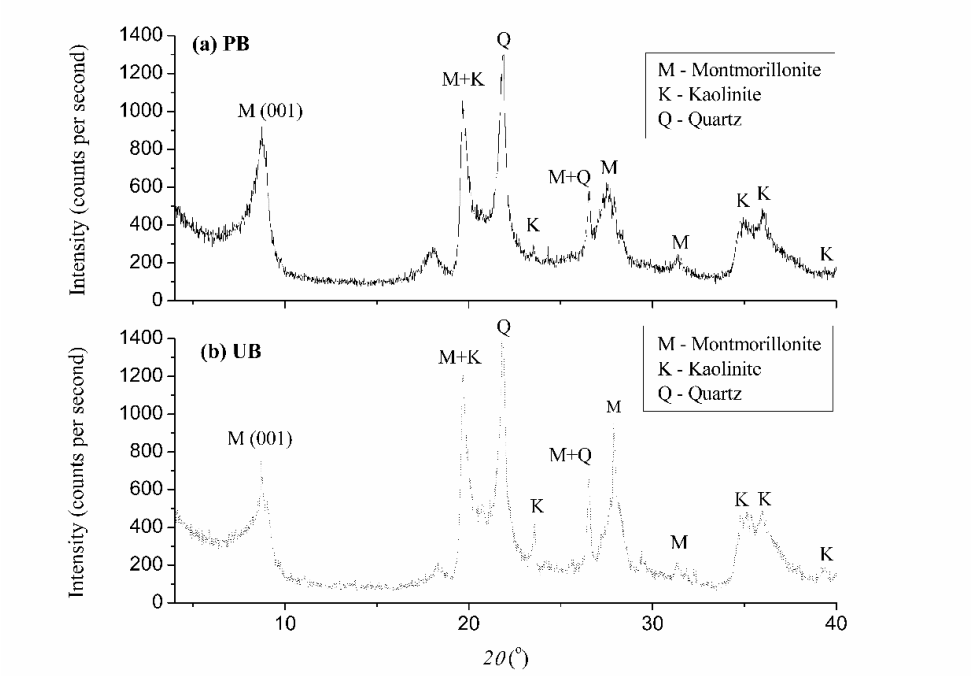

Fig 3.19 XRD patterns of (a) UB and (b) PB under given condition

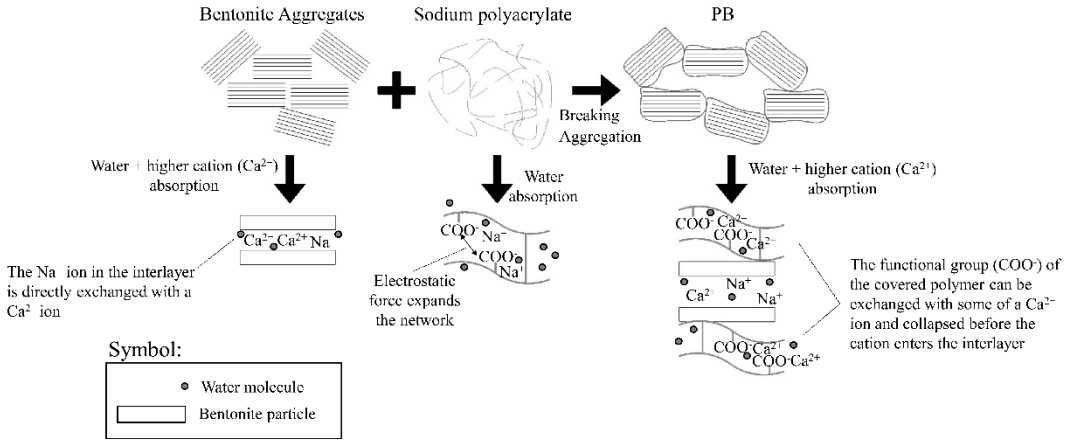

Fig. 3.20 Mechanism of the sodium polyacrylate protected

Then, the main possible function of the polymerization process is that the sodium polyacrylate dispersed and covered the individual bentonite particle as illustrated in Fig. 3.20.

After the PB interacted with the cationic solutions, the functional group (carboxylate salts, COO^-) of the sodium polyacrylate may attracted to some cations in the solutions prior it tried to enter to the interlayer of the bentonite particles as demonstrated in Fig. 3.20.

3.4.2 Scanning Electron Microscopy (SEM)

Scaning Electron Microscopy (SEM) image was used to observe the morphology of the UB and the PB particles. The SEM specimens were prepared as follows. Air-dried powder of the PB or UB was thoroughly mixed with the deionized water at 2.0 times its liquid limit and the slurry was cured for at least 24 h. After that, the slurry was pre-consolidated under a vertical effective stress (σ_v') of 50 kPa in an oedometer ring 60 mm in diameter and 20 mm in height for about 3 days. The pre-consolidated sample of the PB and the UB were taken out from the ring and it was carefully cut to from a cubic specimen with side length 10 mm. Then, the SEM specimen was frozen by immersing it in liquid nitrogen for 5 minutes and evacuated at a pressure of 0.5 Pa at -40 °C for 5 days before taking the SEM images. The photo of freeze dryer machine is shown in Fig. 3.21.

Fig. 3.21 Freeze dryer machine

Figs. 3.22(a) and (b) present the SEM images observed from the vertical planes perpendicular to the plane consolidation pressure was applied. Although, the polymer cannot be clearly seen, but it shows that the PB particle has rounder edges due to the polymer coating (PB in Fig. 3.22(b)) when compared with that of the UB (Fig. 3.22(a)).

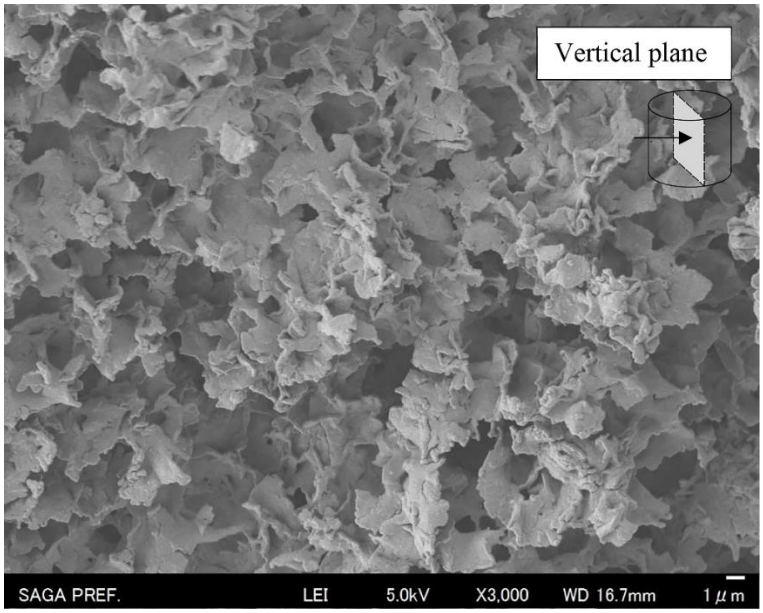

(a) Untreated bentonite (UB)

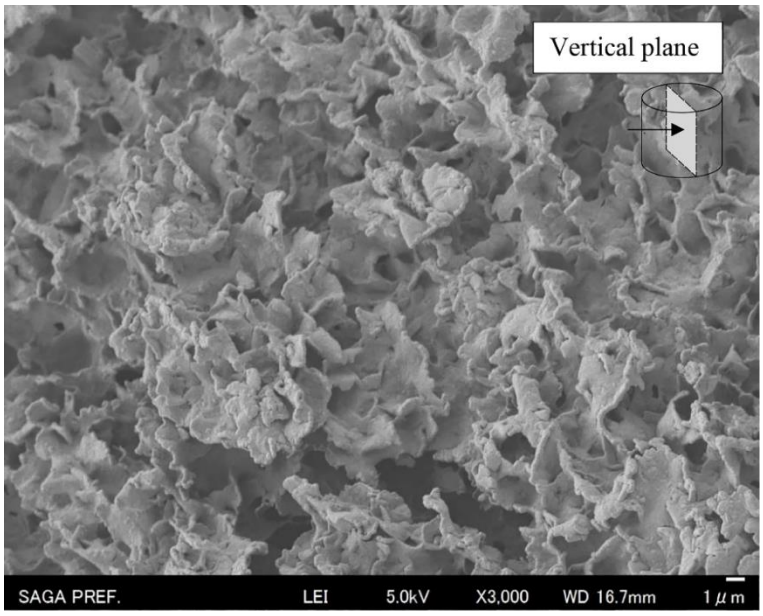

(b) Polymerized bentonite (PB)

Fig. 3.22 Scanning Electron Microscopy (SEM) images

With the SEM image in Fig. 3.22(b), the possible mechanisms considered for the PB had higher FSI value than that of the UB are: (1) polymer "locked" Na^+ ions carried by the bentonite particles and partially prevented it to be replaced by Ca^{2+} ion (Deng et al., 2006), and (2) polymer covering may promote the formation of dispersive micro-structure of the PB. The

anionic polymer can also weaken the effect of positive charge at the edges of a bentonite particle, and edge to face contacts between the bentonite particles may be unlikely to be formed.

3.5 Physical properties

3.5.1 Effect of cationic solutions

(1) Test conditions

Physical properties of the UB and the PB were examined through a series of Atterberg limits and specific gravity (G) test. The liquid limit and plastic limit tests were performed following ASTM D4318 and the specimen gravity test followed ASTM D854.

(2) Test results

The values of liquids limits (w_l), plastic limit (w_p) and G are listed in Table 3.4. The G value of the PB was lower than that of the UB. The G value of the PB is lower than that of the UB. This because the lower density Na-PAA (G = 1.33) coated onto the surface of bentonite particles (Prongmanee et al., 2018) resulting in decrease of G.

Table 3.4 Specific gravity, plastic limit and liquid limits of the bentonites

Test	UB-1	PB
Liquid limit, w_l	621	499
Plastic limit, w_p	47	48
Plasticity index, I_p	584	451
Specific gravity, G	2.86	2.62

The test results of w_l show that the PB had slightly lower w_l value than that of the UB in the deionized water, while in cationic solutions, the PB gave higher w_l value comparted with that of the UB. The w_l of soil is generally controlled by (1) water in diffuse double layer (DDL), and (2) water in micro-pores structure of soil (Sridharan and Prekash, 1999). It is considered that the reduction of liquid limit (w_l) in deionized water of the PB compared with that of the UB is because with the sodium polyacrylate (Na-PAA) wrapped around the particles of bentonite, the PB particles tend to from dispersive micro-structure and reduced amount of water held in the micro-pores (Du et al., 2016). In cationic solutions, the PB provided higher w_l value. It is postulated that the polymer "fixed" more Na^+ on the surface of the bentonite particles and resulted in thicker DDL (Prongmanee et al., 2018).

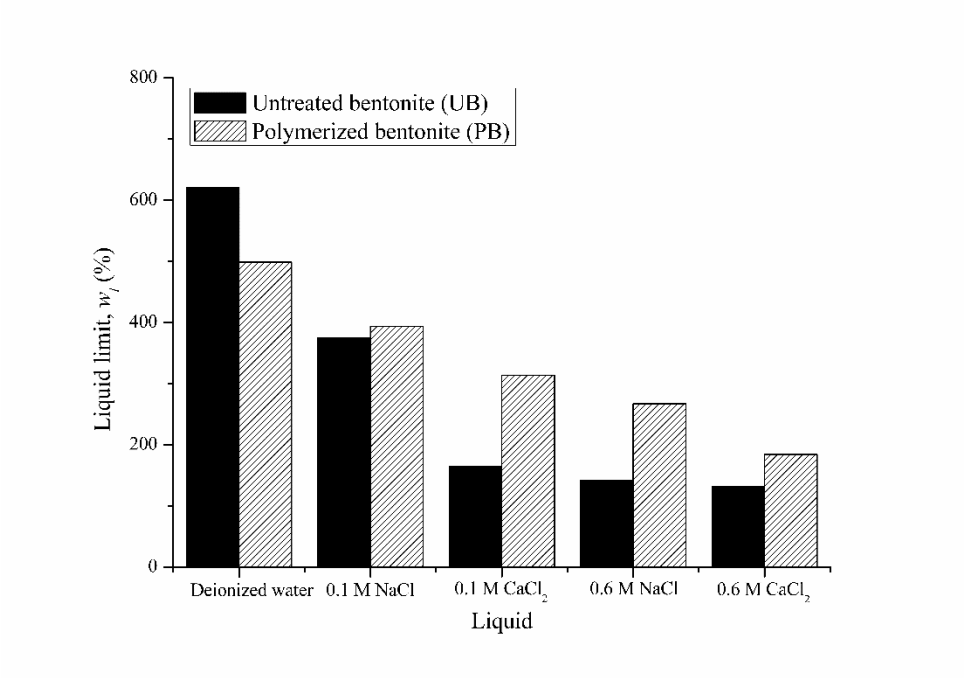

Fig. 3.23 Liquids limit of the PB and the UB with various liquids

3.5.2 Effect of pH solutions

(1) Test conditions

The test methods are the same as the section 3.5.1 except the test liquids. This section uses the liquids as listed in Table 3.3.

(2) Test results

The relationship of FSI values and pH values were plotted in Fig. 3.24. Test results of FSI values show that the PB gave higher FSI value compared with that of the UB for all liquids tested. In acid solutions, the FSI value of both materials decrease with decreasing of the pH value. Especially, for the solution with pH value of 1, the FSI value of the UB is significantly decreased (about 44%) of FSI value in deionized water), while the PB is slightly decreased (about 18%) compared with their FSI value in deionized water. For samples submerged in alkaline solutions, the FSI value of the UB is gradually decreased with increasing of the pH value, while the PB has different behavior that the PB trends to increase with increasing of the pH value comparison with the results in deionized water.

Based on the test results of FSI, it founds that the UB is very sensitive in pH value below 3 and above 11 while, the PB shows excellent pH resistant capacity.

Test results of liquid limit (w_l) with various pH solution were plotted in Fig. 3.25. The test results of w_l of each material show the same general tendency with the test results of the FSI (Fig. 3.24). For pH in the range of 3 to 11, the UB gave higher w_l than that of the PB. Beyond this range, the PB has higher w_l value (pH = 1) and similar value of w_l (pH = 13) compared with that of the UB.

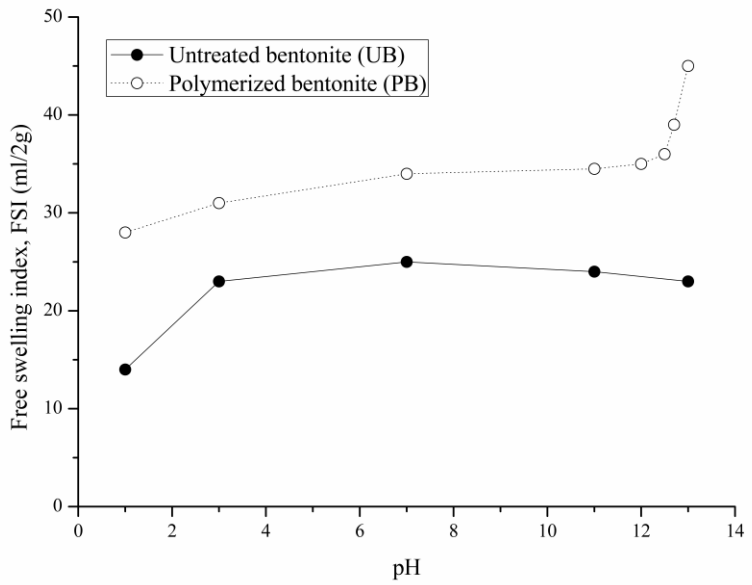

Fig. 3.24 FSI versus pH of the UB and the PB in varies pH solutions

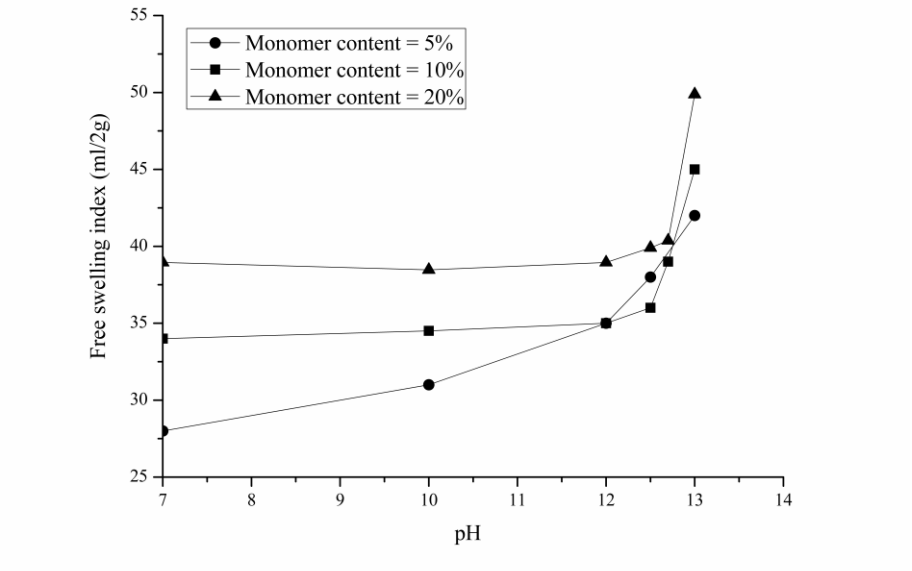

Fig. 3.25 FSI versus pH of the PB with various monomer content

Fig. 3.25 shows the results of FSI of the PBs prepared with various monomer contents of 5%, 10% and 20% in the test solutions with pH varied from 7 to 13. The results are clearly shown that the FSI increase with increasing of the pH value for all PBs. However, the different monomer contents had different rate of the swelling. Fig. 3.25 is indicated that the swelling behavior of the PB in alkaline solution is depended on the monomer content used to produce the PB. The higher monomer content requires the solution with higher pH value to increase the expansion rate of the PBs.

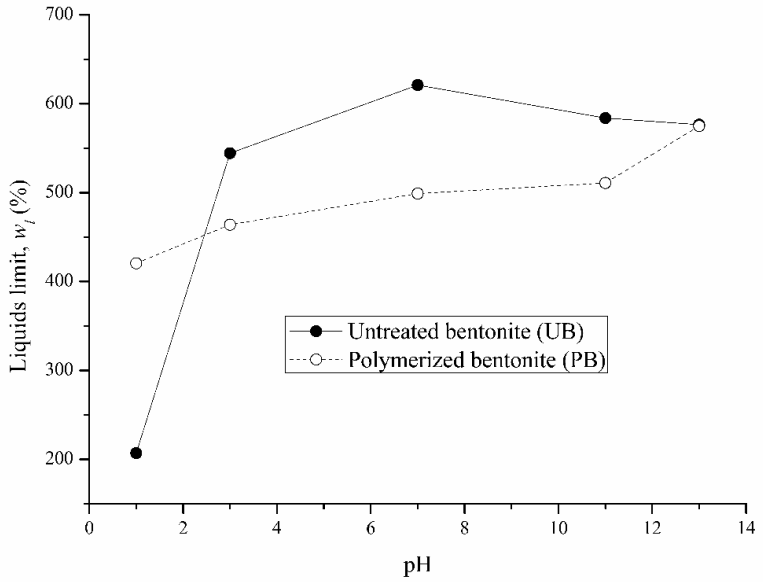

Fig. 3.26 Liquid limit versus pH

3.6 Consolidation tests

3.6.1 Effect of cation

(1) Sample preparation

Dry powder of the PB or UB was thoroughly mixed with 2.0 times its liquid limit and the slurry was cured for at least 24 h. After that, the slurry was pre-consolidated under a vertical effective stress (σ_v') of 50 kPa in an oedometer ring 60 mm in diameter and 20 mm in height for about 3 days. After the pre-consolidation, the specimen had a height approximately 16 mm which is smaller than 20 mm height for the standard oedometer ring test. So, it was decided to trim the specimen to 10 mm in thickness for the oedometer test by pushing the specimen into a 60 mm in diameter and 10 mm in height ring and cutting the extra PB or UB by a wire saw.

The consolidation test was carried out with σ_v' from 10 kPa to 1280 kPa, by doubling the stress for each subsequent step. Initial water content (w_i), initial void ratio (e_i) of the PB and the UB in cationic solutions are given in Table 3.5. Table 3.6 reported the initial water content (w_i), initial void ratio (e_i) of the PB and the UB for pH solutions

Table 3.5 Initial water content (w_i), and initial void ratio (e_i) of the PB and UB

Liquid	UB		PB	
	W_i	e_i	W_i	e_i
Deionized water	332.05	10.17	290.96	7.82
0.1 M NaCl	198.33	7.14	260.16	7.19
0.1 M $CaCl_2$	97.20	3.51	174.09	4.76
0.6 M NaCl	100.06	2.86	155.72	4.37
0.6 M $CaCl_2$	81.89	2.36	112.50	3.19

Table 3.6 Initial water content (w_i), and initial void ratio (e_i) of the PB and UB

Liquid	UB		PB	
	W_i	e_i	W_i	e_i
pH =1 solution	90.00	2.77	249.03	7.15
pH =3 solution	295.55	8.60	275.08	7.78
pH =7 (Deionized water)	322.05	10.17	290.96	7.82
pH =11 solution	278.16	8.48	273.36	8.43
pH =13 solution	214.47	8.58	374.27	10.77

(2) Test results

The consolidation test results of the UB and the PB with different liquids are presented in Figs. 3.26(a) and (b). In Figs. 3.26(a) and (b), compression, i.e. initial void ratio (e_0) decrease as ion valence and concentration increase. Also, swelling behaviors of the materials are clearly affected by the cations charges and concentration.

Fig. 3.27 and Fig. 3.28 represent the results of compression index (C_c) and swelling index (C_s) in various liquids tested, respectively. Fig. 3.27 shows C_c decrease with increasing of cation concentration and valence of cation. The decrease in C_c was found to be more significant for UB in comparison to that of the PB in cationic liquids.

In Fig. 3.28, it is clearly to see that the PB gave higher C_s value than that of the UB for all liquids tested. This is in good agreement with the test results of the FSI value as indicated in Fig. 3.13.

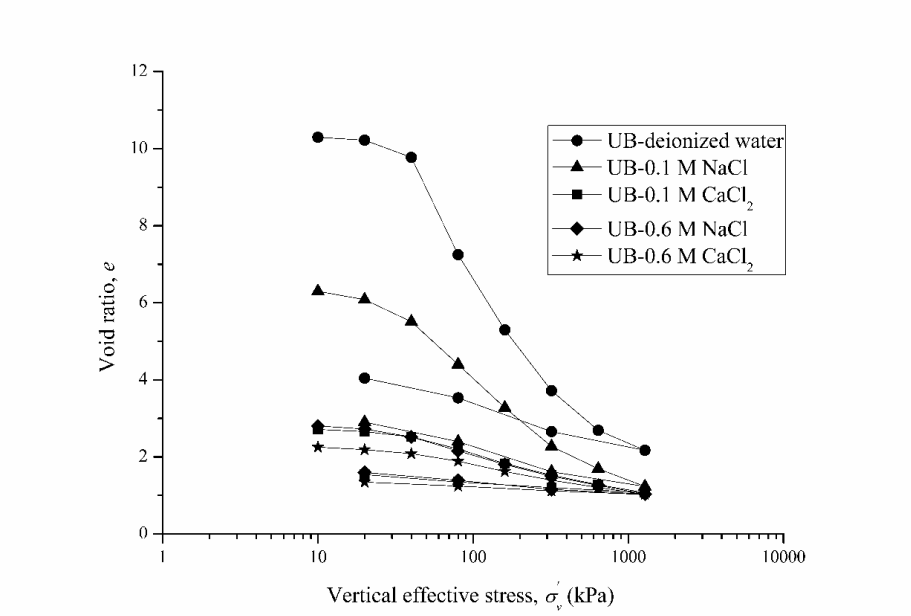

(a) Untreated bentonite (UB)

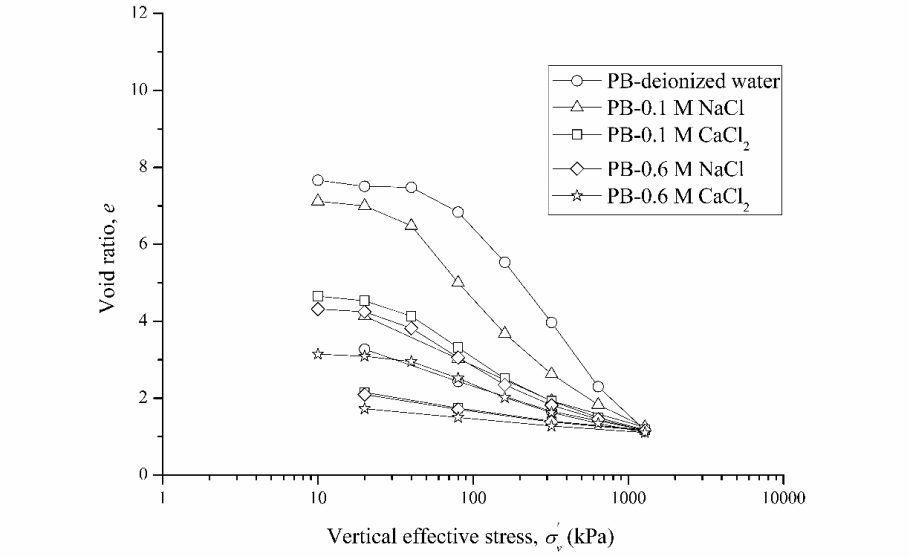

(b) Polymerized bentonite (PB)

Fig. 3.27 Void ratio (e) - σ_v' value of (a) the UB, and (b) the PB

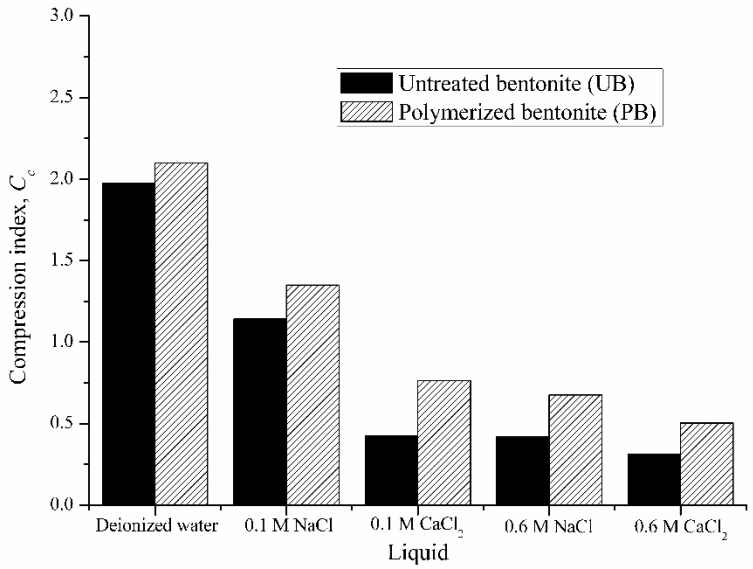

Fig. 3.28 Results of C_c with different liquids

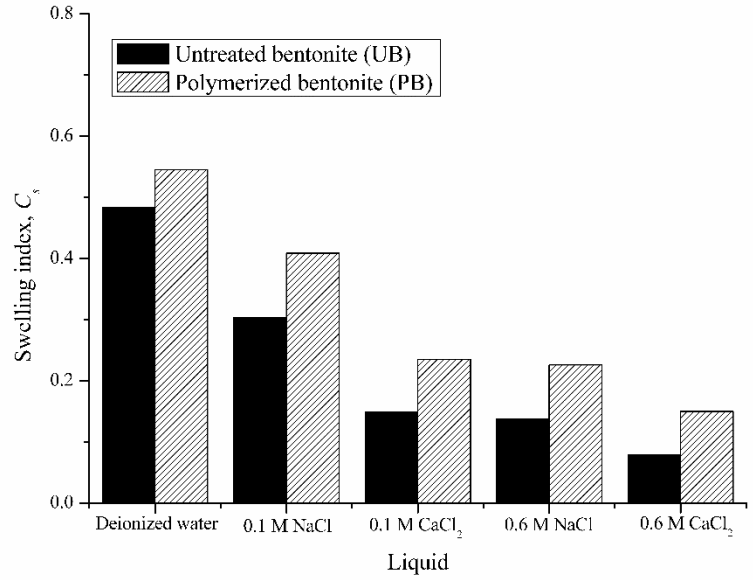

Fig. 3.29 Results of C_s with different liquids

The results of coefficient of volume change (m_v) are plotted with vertical effective stress (σ_v') as shown in Figs. 3.29(a) and (b). The value of m_v initially tends to increase and then decreased with an increase of σ_v'. The m_v of both materials decrease with increase in the cation concentration and valence of cation. Under the same σ_v' value, the PB gave higher m_v value

compared with that of the UB. The reason considered is that the polymer coating bentonite particle protected the interlayer cation exchanged, resulting in higher absorbed liquids, and higher compressibility.

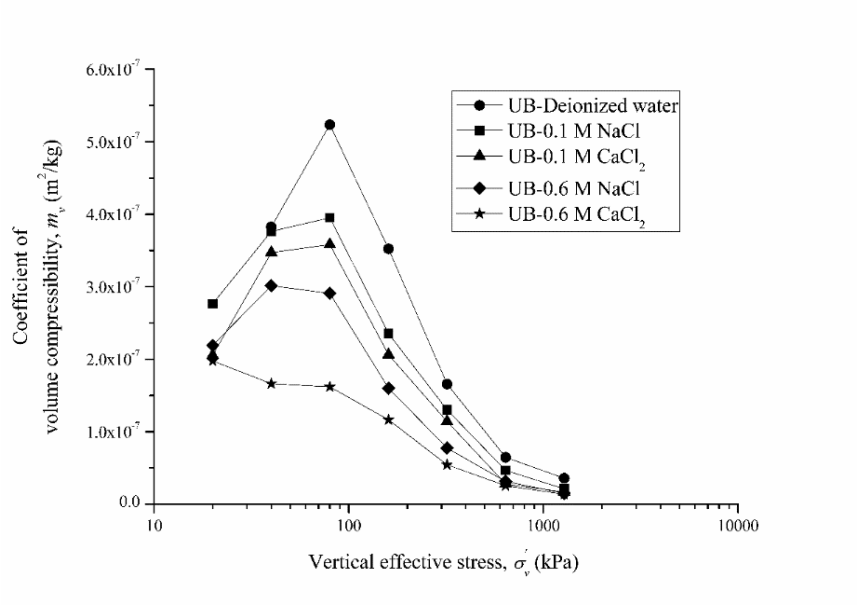

(a) Untreated bentonite (UB)

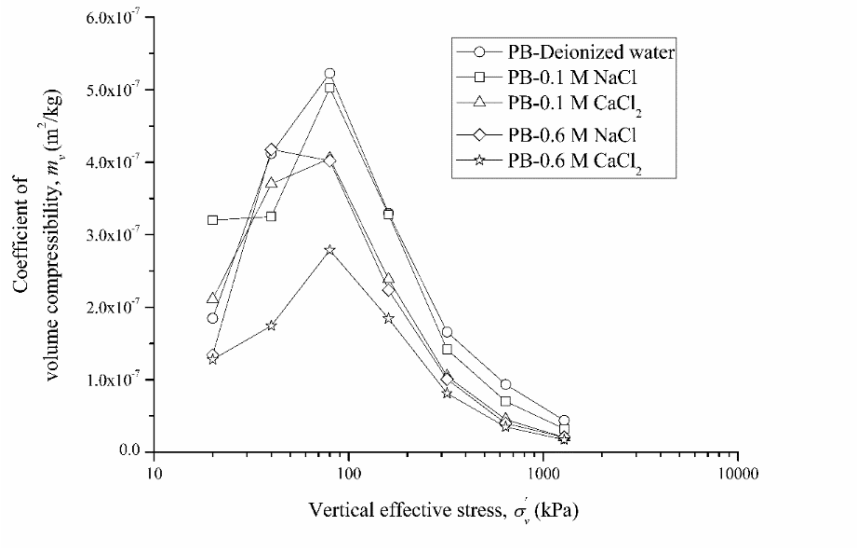

(b) Polymerized bentonite (PB)

Fig. 3.30 Relationship between m_v value versus σ_v' values; (a) the UB, (b) the PB

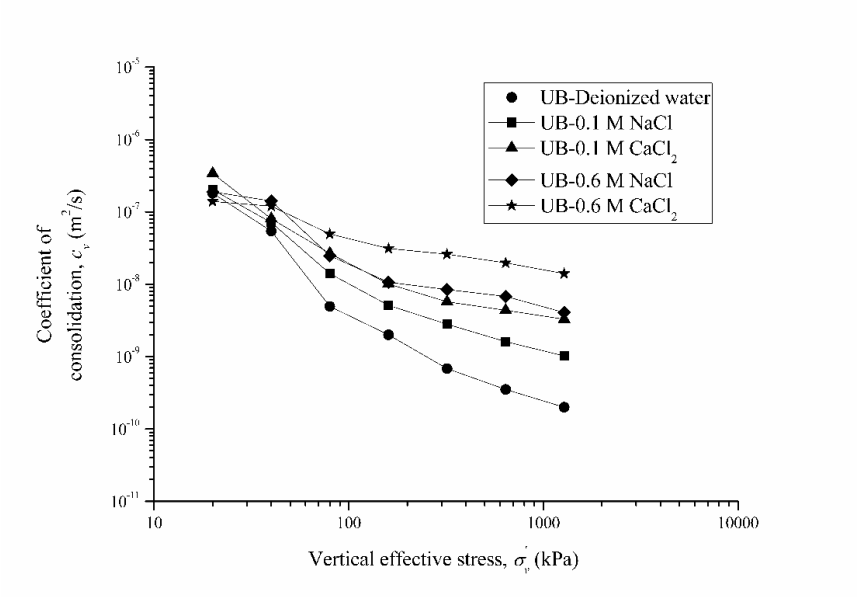

(a) Untreated bentonite (UB)

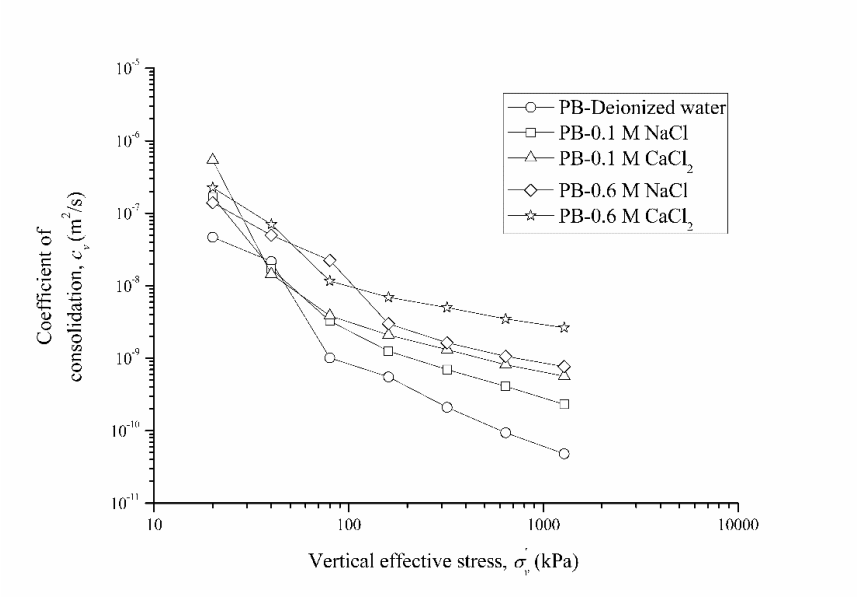

(b) Polymerized bentonite (PB)

Fig. 3.31 Results of value of c_v versus σ_v' values; (a) the UB, (b) the PB

The relationships between the coefficients of consolidation (c_v) and σ_v' are plotted in Figs. 3.30(a) and (b). The c_v values were determined using the square root of time (Taylor) methods for each loading stage of consolidation test. Generally, the c_v value decreased with increasing of vertical effective stress (σ_v'). For a given σ_v', c_v increased with the increase in the cation concentration and valence of cation, and the primary reason considered is the increase

in permeability. Under the same σ_v' values in cationic liquids indicates that the PB which has a higher FSI value and w_l value, had a lower c_v value compared with that of the UB.

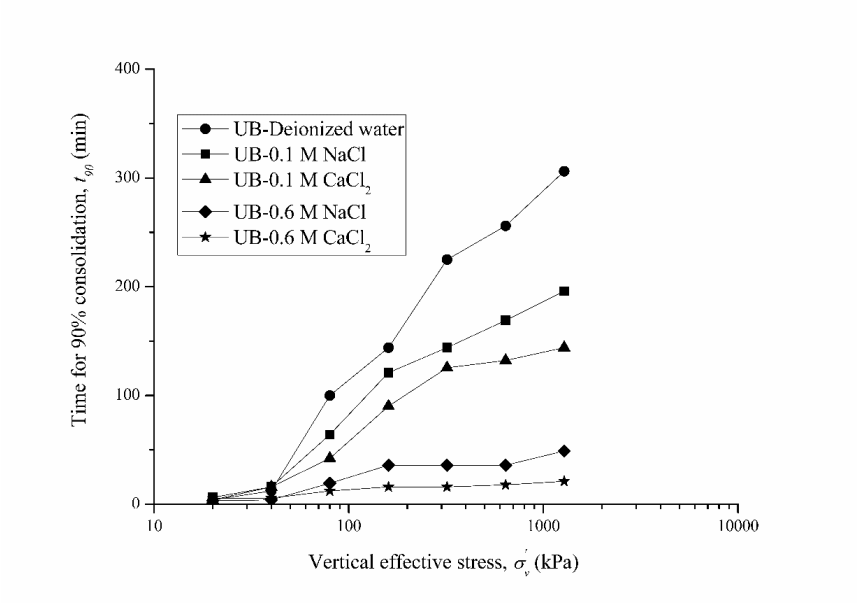

(a) Untreated bentonite (UB)

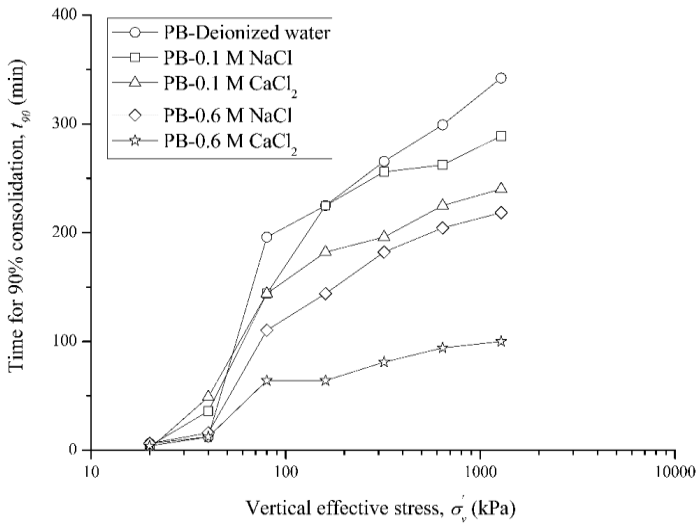

(b) Polymerized bentonite (PB)

Fig. 3.32 Time for 90% of consolidation versus σ_v' values; (a) the UB, (b) the PB

For further investigation, a time at 90% of consolidation (t_{90}), were plotted with the σ_v' as shown in Figs. 3.31(a) and (b) for the UB and the PB, respectively. Fig. 3.29(a) and (b)

indicate that the t_{90} increase with increasing of σ_v' values. For effects of cations, t_{90} decreases with the increase in cation concentration and valence of cation, i.e. increase in rate of consolidation. For a given σ_v' values, the PB gave higher t_{90} than that of the UB.

3.6.2 Effect of pH

(1) Test methods

The test methods performed the same procedures as reported in the section 3.6.1.

(2) Test results

The relationship between void ratio (e) and vertical effective stress (σ'_v) of the UB and the PB with various pH solution are demonstrated in Figs. 3.32(a) and (b). In Figs. 3.24(a) and (b), it is clearly seen that the consolidation behavior affected by the effect of pH value.

Fig. 3.33 and Fig. 3.34 represent the results of compression index (C_c) and swelling index (C_s) in various pH solutions, respectively. In Fig. 3.33, the PB had higher C_c values for all liquids tested compared with that of the UB. With the range of pH from 3 to 11, the results of C_c for both the PB and the UB slightly changes, while decreasing or increasing pH value to pH = 1 and pH = 13, the C_c of both materials are obviously changed. In pH =1 solution, C_c of the UB and the PB had significantly decrease compared with the results of deionized water (pH =7). For pH =13 solution, the C_c value of the UB decreases, while the C_c value of the PB had slightly increases when compared with their results in the deionized water.

In Fig. 3.34, it shows the same behavior as reported in Fig. 3.33 that the C_s value decrease in acid solutions, while C_s value of the PB tends to increase in alkaline solutions, while the UB gave decreasing in C_s value for both acid and alkaline solutions. The results in Fig. 3.33 and 3.34 are in good agreement with the test results of the FSI value as indicated in Fig. 3.24.

The results of coefficient of volume change (m_v) are plotted with vertical effective stress (σ_v') as shown in Figs. 3.35 (a) and (b). The m_v of both materials decrease in acid solutions. For alkaline solutions, the m_v of the UB decreases with increasing in the pH value, whereas the PB show same value of m_v for pH = 11 solution and it have higher m_v value in pH = 13 solution compared with that of the deionized water. Under the same σ_v' value, the PB had higher m_v value compared with that of the UB in various pH solutions.

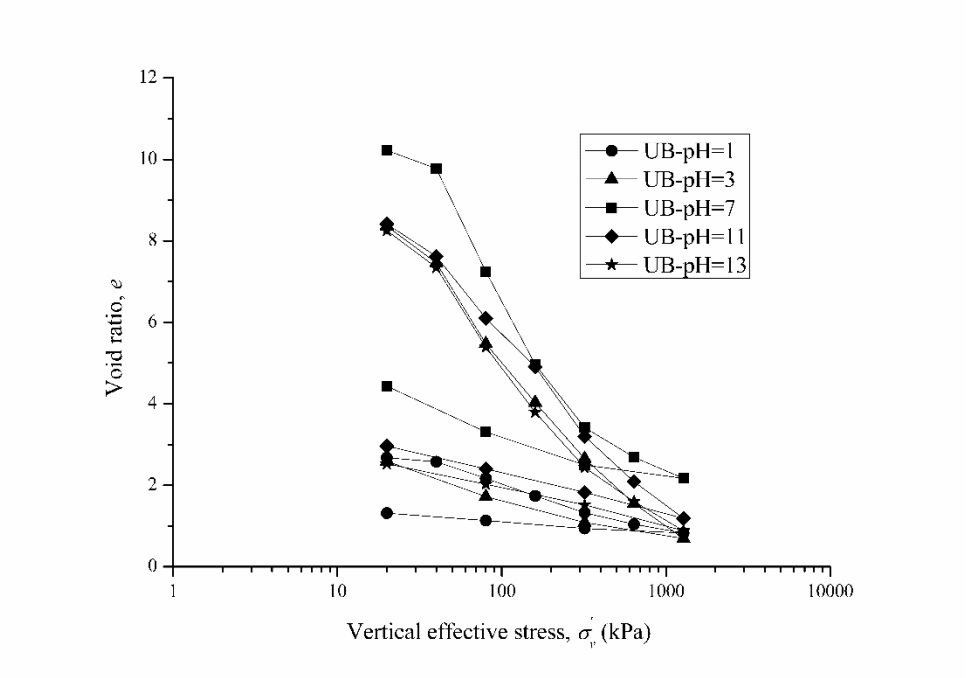

(a) Untreated bentonite (UB)

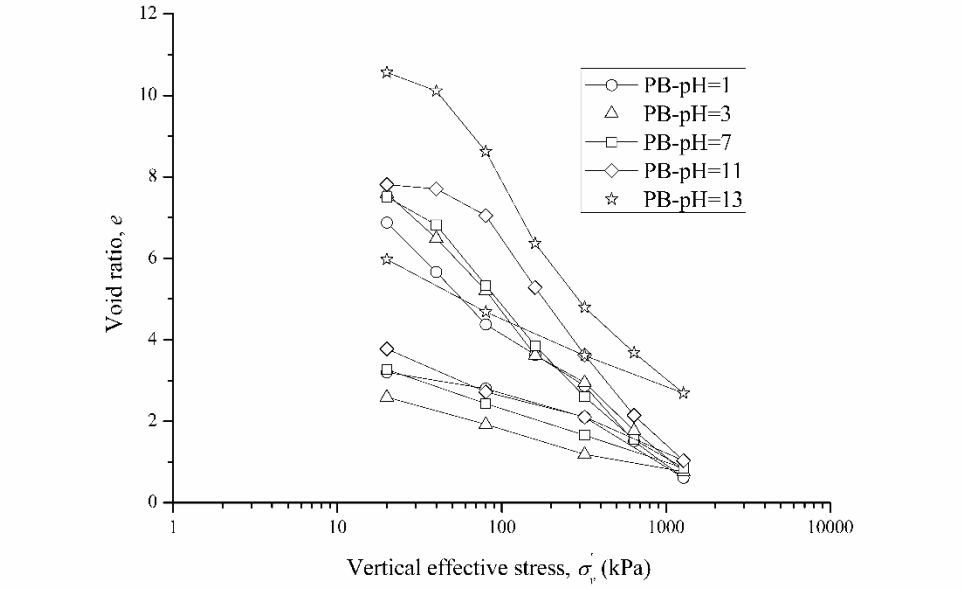

(b) Polymerized bentonite (PB)

Fig. 3.33 Void ratio (e) - σ_v' value of (a) the UB, (b) the PB in various pH solutions

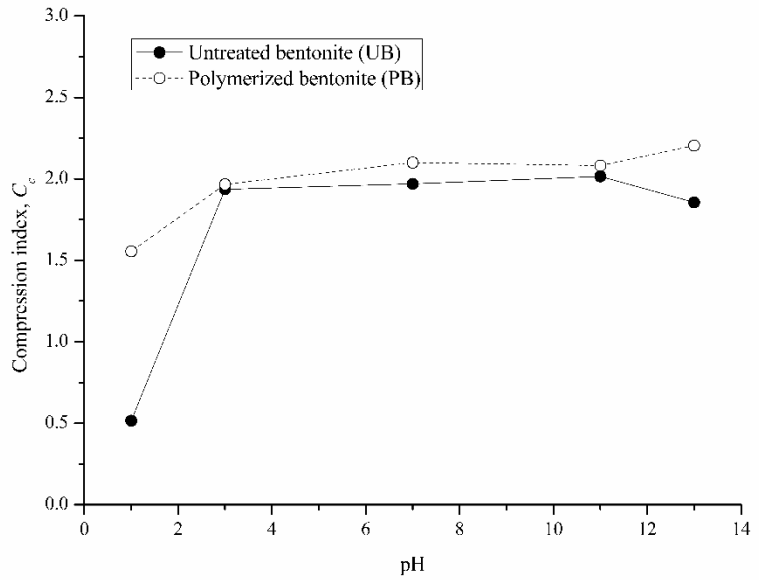

Fig. 3.34 C_c versus pH values

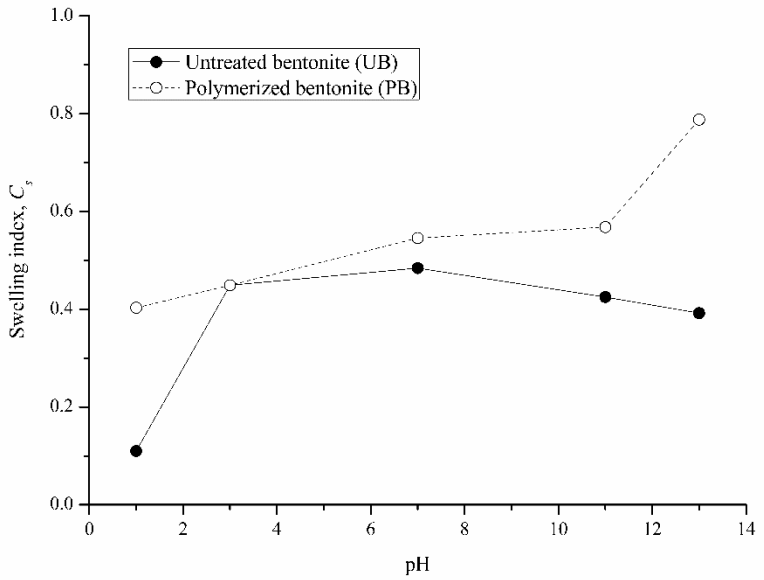

Fig. 3.35 C_s versus pH values

Figs. 3.36(a) and (b) show the relationships between the coefficients of consolidation (c_v) with different σ_v' value. Generally, the c_v value decreased when interacted with acid solutions with pH lower than 7 for both the PB and the UB. For alkaline solution, both material

had the same general tendency as reported before, i.e. the PB in pH = 13 solutions gave lowest c_v value, while the c_v values of the UB decreases in the alkaline solutions.

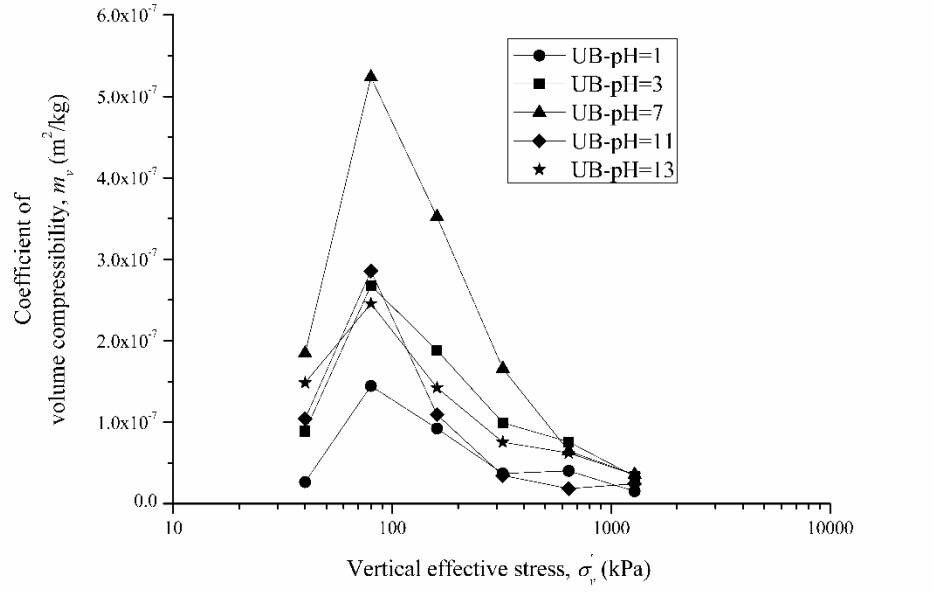

(a) Untreated bentonite (UB)

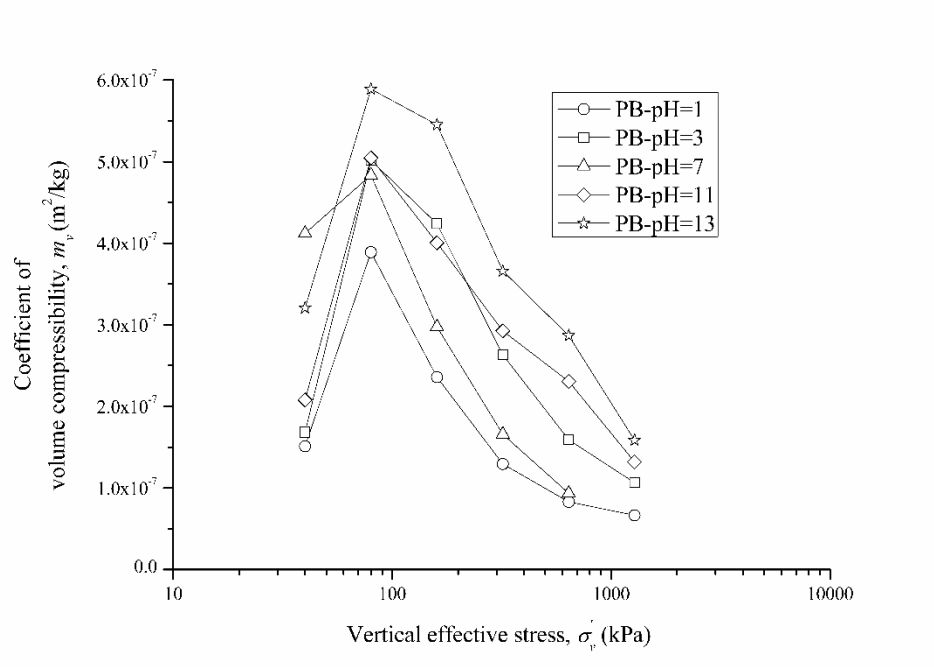

(b) Polymerized bentonite (PB)

Fig. 3.36 m_v versus σ_v' values; (a) the UB, (b) the PB

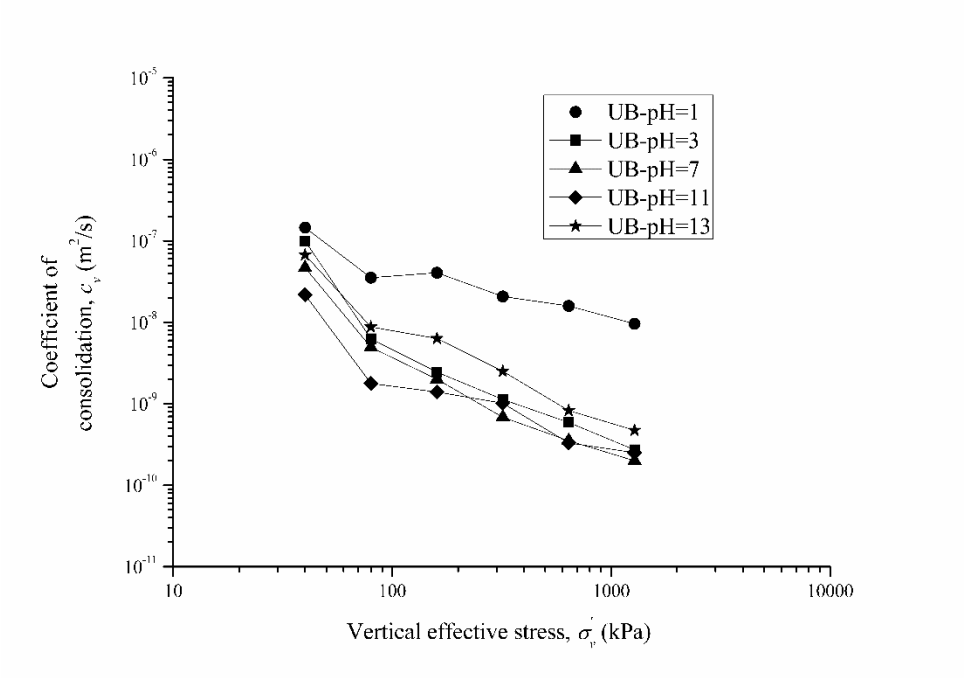

(a) Untreated bentonite (UB)

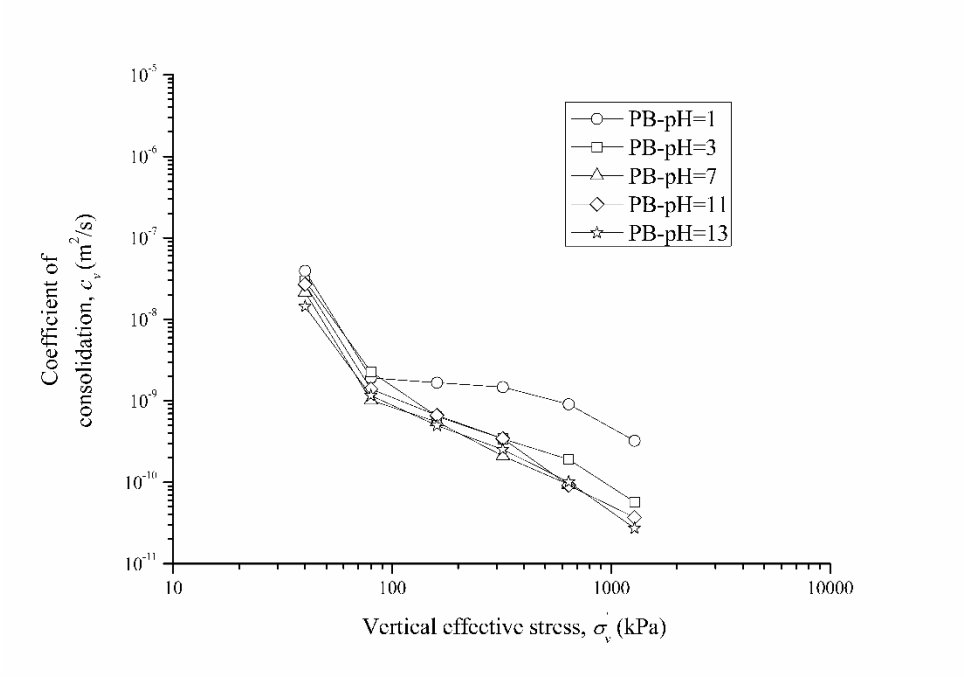

(b) Polymerized bentonite (PB)

Fig. 3.37 c_v versus σ_v' values; (a) the UB, (b) the PB in various pH solutions

3.7 Swelling pressure tests

3.7.1 Test methods

Approximately 43.0 g of air-dried powder of the PB or the UB was statically compressed into a cylindrical rigid ring with a diameter of 60 mm and thickness of 20 mm to form a cylindrical specimen using a CBR (California Bearing Ratio) test device (Marui Compression Testing Apparatus with the maximum capacity of 100 kN). Considering the application of PB in GCL, its dry unit weight of the PB or the UB is normally low (about 11.5 kN/m^3) (Seiphoori et al., 2016). However, to form a swelling pressure test specimen at air-dried moisture content, if the density is too low, it will collapse. By trial and error, it was found that with a dry unit weight of about 12.7 kN/m^3, a sample can be successfully formed by static compression with a thickness of 12.0 mm, and the compression pressure adopted was 10 to 20 MPa. The cylindrical specimens are shown in Fig. 3.37.

Fig. 3.38 Swelling pressure specimens

Then, the compressed specimen was installed into the swelling pressure test equipment as shown in Fig. 3.38. The swelling pressure test was conducted under isochoric condition (Schanz and Tripathy, 2009) which is almost the same as ASTM D4546 Method C. For the equipment used, the total height of the specimen and the load cell system was fixed. While during the test, the swelling pressure will cause compression of the load cell, and then the expansion of the specimen. So, the initial density and the final density of the specimen were different.

The test follows the following steps:

1) The saturated filter paper was placed on top of the saturated porous stone on the bottom pedestal. Then, the lower rigid ring with the specimen inside was carefully placed on the filter paper. After that, the lower rigid ring was fixed by the bolts.

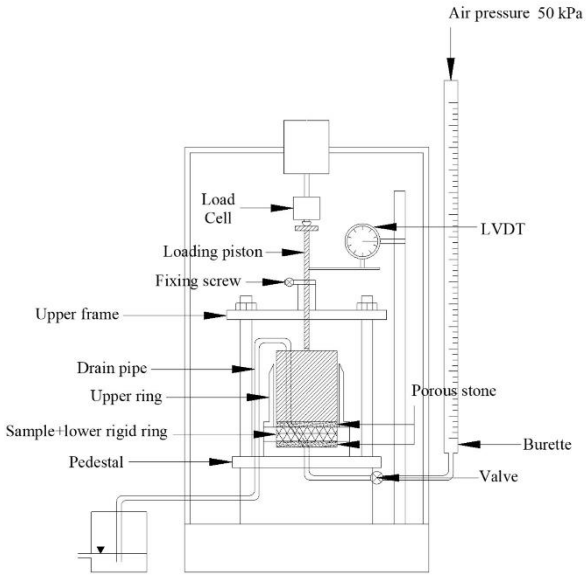

Fig. 3.39 Swelling pressure apparatus

2) Another rigid ring, the upper ring, was installed on the top of the lower ring. Then, another saturated filter paper was placed on the top of the specimen. The saturated filter papers and the saturated porous stones were used to reduce the equilibrium time. The drawback is that during the set-up process, the specimen may suck some water from the filter paper and/or the porous stone and it may influence the initial density of the specimen. Considering this and the fact that density of the specimen changed slightly during the test, the final unit weights are included in the discussion.
3) The piston with a saturated porous stone was put into the upper ring and fixed by tightening the fixing screws.
4) The drainage pipe was connected from the piston to the bottom pedestal. Then, the load cell and linear variable differential transducer (LVDT) were installed.
5) The fixing screws were released, and the liquid was supplied to the specimen. During the test, the expansion of the specimen due to the compression of the load cell was allowed. The swelling pressure was recorded until it reached a steady value. The change in height of the specimen was recorded using the LVDT. The final dry unit weight of the specimen was calculated using the dry mass of the PB and the final thickness of the specimen.

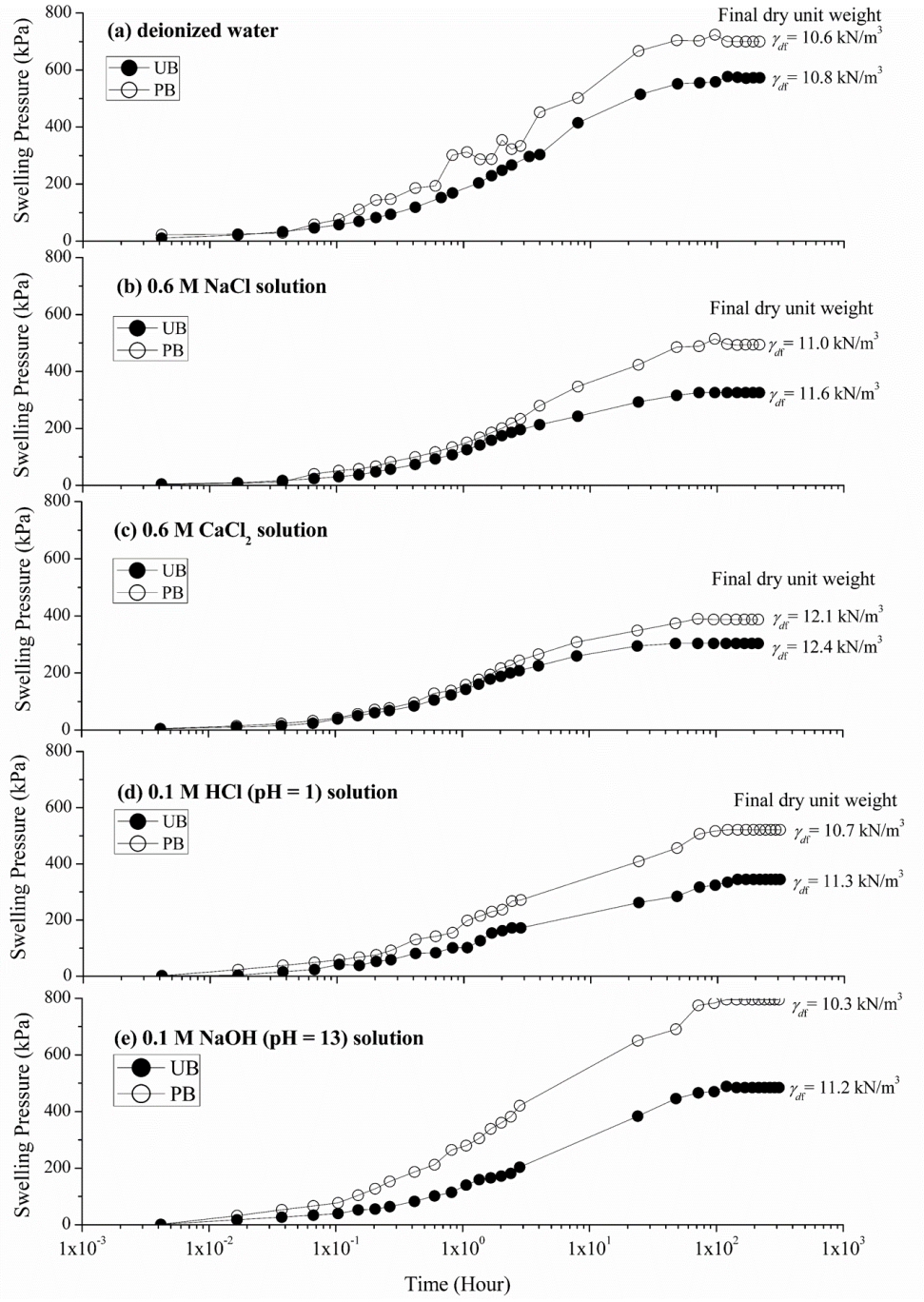

Fig. 3.40(a) to (c) Results of swelling pressure test

3.7.1 Results

The results of swelling pressure of the PB and the UB are shown in Fig. 3.39(a) to (e) for using deionized water, 0.6 M NaCl solution, 0.6 M CaCl2 solution, pH = 1 solution and pH = 13 solution respectively. Initial dry density of the specimens was controlled almost the same, but the final dry density of the PB was less than that of the corresponding UB due to the higher swelling pressure induced more compression of the load cell (more expansion of the specimen).

The PB shows the higher swelling pressure compared with the UB for the three liquids, even 1341 though the final density of the PB was lower than the UB. For using pH = 1 solution and pH = 13 solution, the results of swelling pressure are clearly shown that the PB had higher swelling pressure compared with the UB. The PB in the pH = 13 solution shows higher swelling pressure compared to its swelling pressure in deionized water. This confirms that the produced PB gave the positive swelling capacity in the corrosive alkaline solution.

3.8 Permeability (*k*) tests

Three methods for evaluating of the values of *k* were adopted; the first one was the flexible wall permeameter test; the second method was one-dimensional consolidation test; and the last method used was filter press test.

3.8.1 Flexible wall permeameter test

(1) Test methods

The falling-head, flexible wall permeameter is shown in Fig. 3.40 and the maximum water head can be applied 1315 mm. The confining pressure is applied with air pressure and vertical pressure is applied by a bellofram system. The specimen is 60 mm in diameter, with a nominal height of 10 mm. Sample preparation procedures for the *k* test are same as the preparing method for consolidation test as reported in the section 3.6. Then, for each given vertical pressure, the UB or the PB specimen was consolidated under K_0 conditions (no-horizontal strain) before the permeability test. The value of K_0 adopted was 0.5.

The details of test procedures are as follows;

(a) The specimen was firstly placed into a rubber membrane and it was fixed to the top and the bottom pedestal by O-rings as shown in Fig. 3.41.
(b) An acrylic chamber was installed on the base of cell and completely filled with distilled water from the inlet water tank as shown in Fig. 3.42. Then, the test chamber was moved to the loading piston. The linear variable differential transformer (LVDT) and the load cell were installed.
(c) After that, the specimen was pre-consolidated under approximate at-rest earth pressure (K_0) conditions. Then, the drainage valve was opened to consolidate the specimen under two-way drainage condition. The pre-consolidation was maintained for 24 h. The pre-consolidation pressure adopted in this study were listed in Table 3.7.

(d) After pre-consolidation, the upper pedestal was locked to prevent any vertical movement and maintain the confining cell pressure. Then, the desired liquids were supplied by opening the inlet valve. After that, the outlet valve was opened and the water level change in the burette was recorded periodically until the measured flow rate become steady (about 3 days).

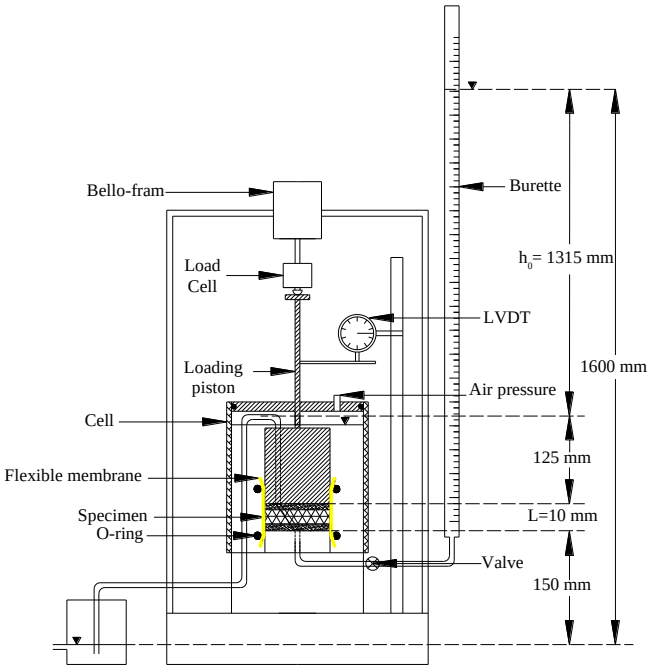

Fig. 3.41 Flexible wall permeameter apparatus

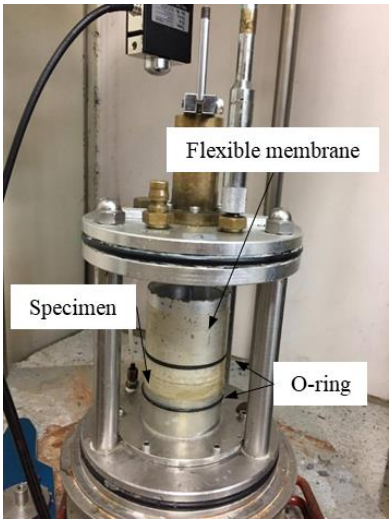

Fig. 3.42 Photo of a specimen encapsulated by the flexible membrane

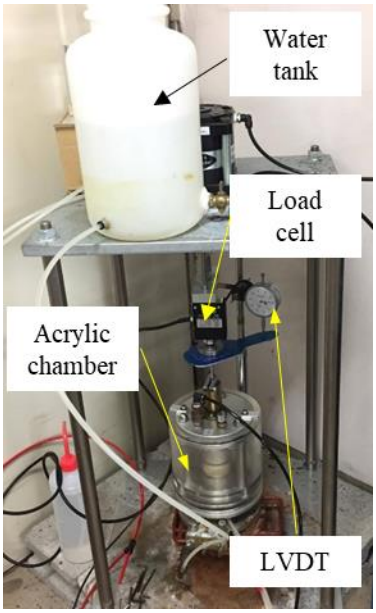

Fig. 3.43 Photo of water supplied into the acrylic chamber

(e) After the permeability test, the current specimen was consolidated under a higher pressure, and a new permeability test was carried out by repeating the procedures. In this way, the relationship between the void ratio (*e*) and permeability (*k*) cloud be determined using a single specimen.

Table 3.7. Lists of pre-consolidation pressure

Vertical pressure kPa	Cell Pressure kPa
50	25
100	50
150	75
200	100

(2) Results

The direct measured values of *k* are presented in a relationship between void ratio (*e*) and permeability (*k*), as shown in Fig. 3.43.

The test results of *k* show that the type of permeated liquid had a significant effect on the value of *k*. Generally, for both the PB and the UB, permeant with deionized water had lowest *k* value, while *k* value for 0.6 M $CaCl_2$ solution was highest. At identical values of *e*, the PB and the UB had similar values of *k* when using deionized water. When using salt solutions, the PB samples had obviously lower *k* value than that of the UB. Although initially

the chemical equilibrium was achieved in the sample, the test condition is different from the long-term direct permeability test, in which some ions the UB or PB carried might be leaked out due to long-term permeation of a liquid and influencing the final permeability. As a tendency using a flexible wall permeable test, for a chemical tends to reduce the value of *k*, *k* value may be over estimates, and for a chemical tends to increase the value of *k*, *k* may be under-estimated. It is considered that under the same test condition, the relative performance of the UB and the PB can be evaluated. From the results in Fig. 3.43, it can be said that the PB gave lower value of *k* than that of the UB in cationic solutions.

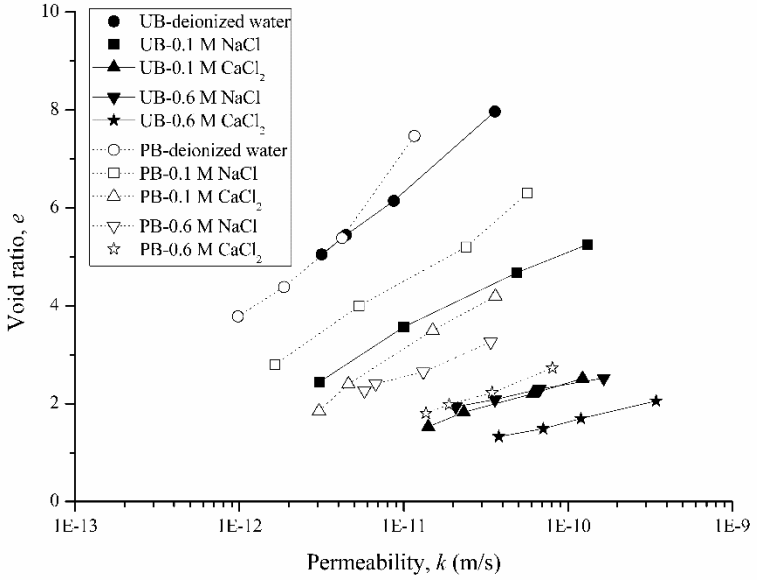

Fig. 3.44 The relationship between the *e* value and *k* value from the permeability test

3.8.2 Permeability interpleaded from consolidation test results

(1) Method of interpretation

The value of permeability (*k*) were calculated from the results of multiple stage loading (MSL) oedometer test results using Taylor's (1984) method. The value of *k* is calculated by Eq. (3.3).

$$k = c_v m_v \gamma_w \tag{3.3}$$

where γ_w is unit weight of water, c_v is coefficients of consolidation and m_v is coefficient of volume change.

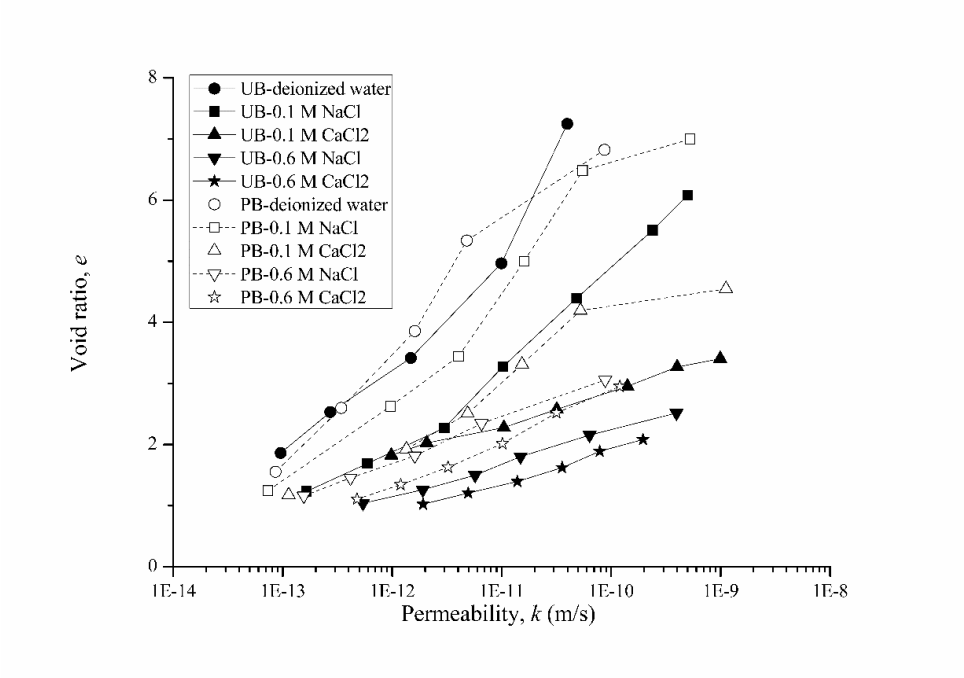

Fig. 3.45 Result of *k*-value from the consolidation test

(2) Test results

The results of the calculated *k* value are presented in a relationship of the void ratio (*e*) versus permeability (*k*) in Fig. 3.44. Results of *k* are consistent with the results from the permeability test as reported in Fig. 3.36. The use of deionized water resulted in lowest *k* value, and the use of a 0.6 M $CaCl_2$ solution yielded the highest *k* values for both the UB and PB. It can be seen that at identical values of *e* for all the liquid tested, the PB exhibited approximately an equal (in case of the deionized water) or lower value of *k* (cation solutions).

3.8.3 Filter press test

An alternative method to determine the value of *k* is from the test result of filter press test (Rosin-Paumier et al., 2010; Rosin-Paumier and Touze-Foltz, 2012). This method provides quick evaluation of the value of *k* compared with those of permeability and consolidation tests.

(1) Test methods

The procedures of the filter press test are almost the same as the fluid loss test (ASTM D 5891) except that in filter press test, the volume of out-flow liquids need to be recorded all over the test, while the fluid loss test only needs to be collected the out-flow volumes from 7.5

± 0.1 min to 30 ± 0.1 min (Totally 22.5 min) period. Fig. 3.45 shows the filter press apparatus ((a) schematic picture, and (b) photo view).

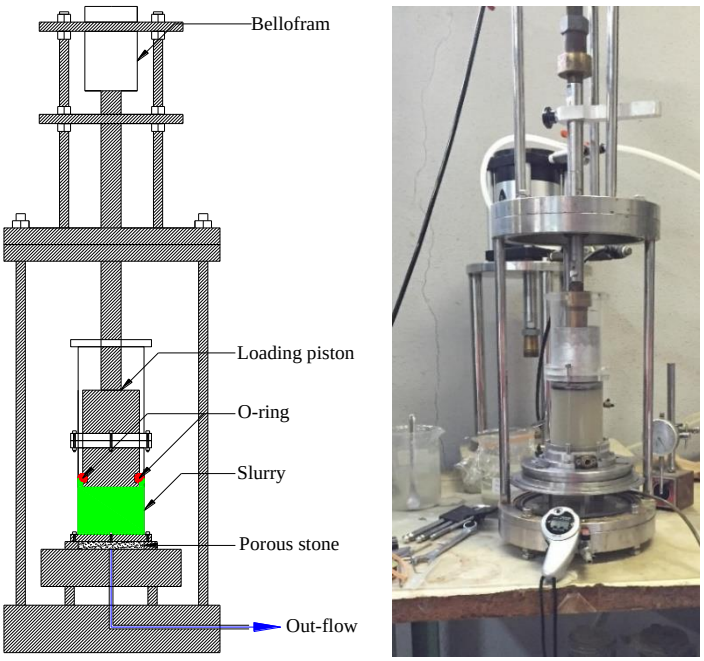

(a) Schematic view (b) Photo view

Fig. 3.46(a) and (b) Fluid loss test apparatus

The test procedures are as follows;

a. Oven dried untreated bentonite (UB) or the polymerized bentonite (PB) of 18.0 g was dispersed into a 300 ml of a desired liquid, i.e. deionized water, or 0.6 M NaCl, or 0.6 M $CaCl_2$ by a mechanical mixer.
b. The filter paper of 60 mm in diameter was firstly placed on the porous stone. Then, the mixture slurry was poured into the filtration cell (cylinder with 60 mm in diameter and 120 mm in height).
c. The vertical pressure of 700 kPa was directly applied on the top of the loading piston. The O-ring was attracted to the piston to prevent the liquid leaked during the filter press test.
d. The volume of the out-flow liquid was recorded with elapsed time. The volume of the out-flow liquid was recorded by a graduated cylinder of 10 ± 0.1 ml. The test duration was 1 hour (Rosin-Paumier et al., 2010).
e. After test, the slurry was drained out and left a thin film layer called “filter cake”. The thickness of the filter cake was measured by a digital caliper Vernier. The water content

and dry mass was measured to determine the initial void ratio (e_0). The results of thickness, water content and initial void ratio (e_0) are listed in Table 3.8.

Table 3.8 Results of thickness, water content and initial void ratio (e_0) of filter cake

Materials	Liquids	Thickness (mm)	Dry mass (g)	Water content (%)	Initial void ratio e_0
UB	Deionized water	0.6	1.3	2890	36.3
UB	0.6 M NaCl	1.0	13.3	377	12.2
UB	0.6 M $CaCl_2$	1.2	18.6	284	11.8
PB	Deionized water	0.3	0.9	3830	31.2
PB	0.6 M NaCl	0.2	2.2	3590	21.2
PB	0.6 M $CaCl_2$	1.1	17.0	380	17.1

(2) Calculation methods

The fluid loss volume (V_f) in milliliters is calculated by Eq. (3.4).

$$V_f = 2 \times V \tag{3.4}$$

where V_f is fluid loss volume, V is the filtrated volume for last 22.5 min interval (collected filtrate volume from 7.5 to 30.0 min)

Permeability from filter press test (k_{filter}) is determined by the Eq. (3.5) and Eq. (3.6). The k_{filter} determines by assuming that the viscosity of filtrate was the same as the water. The value of ψ_{filter} can be obtained from Eq. (3.5).

$$\omega = \left[\psi_{filter} \frac{2\Delta P A \omega_t}{\rho g} \right]^{0.5} t^{0.5} \tag{3.5}$$

$$k_{filter} = \psi_{filter} \cdot c \tag{3.6}$$

where ω is the total filtrate volume, ΔP is the pressure gradient, A_c is the cross-section area, μ is the viscosity of filtrated liquids, t is time, c is the thickness of the filter cake, and g is the gravity acceleration. According to the relationship of ω and $t^{0.5}$ is linear relationship, the permittivity of filter cake (ψ_{filter})(Eq. (3.5)) can be directly calculated from the constant value of the linear regression analysis (zero interception) (Rosin-Paumier et al., 2010).

(3) Test results

The relationship of filtrate volume (ω) and square root time ($t^{0.5}$) are presented in Fig. 3.46. At a given elapse time, it is clearly seen that the UB had higher value of ω than that of the PB in the cationic solutions. While, in the deionize water both materials gave the similar ω value. From test results in Fig. 3.46, the fluid loss volume (V_f) and permeability (k_{filter}) can be calculated by Eq. (3.4) and Eq. (3.6), respectively.

In Fig. 3.47, the results of V_f show that the values of V_f increase with increasing of cation concentration and valence of cation in the solutions. In case of deionize water, both the PB and the UB had the similar V_f value. According to the requirement for the GCL material, the current industry standard is required the V_f must be less than 18.0 ml in deionized water (Von Maubeuge, 2002) and both materials gave the value lower than that of the minimum requirement value (Fig. 3.47). In salt solutions, the PB provided the lower V_f compared to that of the UB.

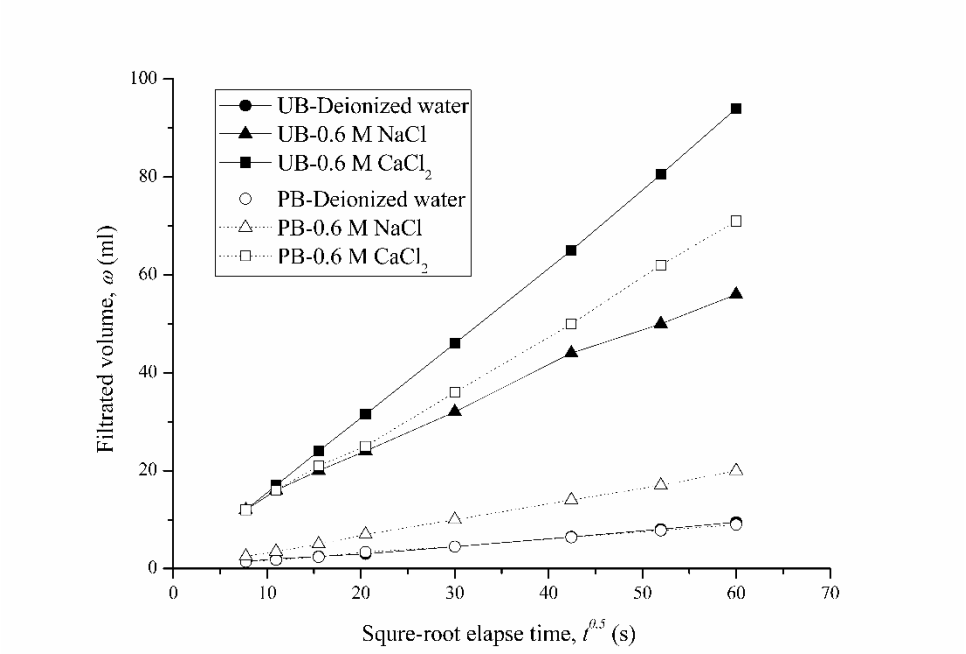

Fig. 3.47 Results of the filtrate volume versus square root of elapse time

In the similar way, Fig. 3.48 shows the k_{filter} value of the PB and the UB with three permeated liquids. The tendency of k_{filter} is consistent with the results of the permeability test and the consolidation test as reported in Fig. 3.43 and Fig. 3.44, i.e. the UB gave higher k value than that of the PB in cationic solutions, while both materials provided similar k value in

deionized water. Based on the *k* value from the three different test methods, they confirm that the PB had lower permeability (*k*) when compared with that of the UB in cationic solutions.

The *k* values from three methods were plotted in Fig. 3.49. It is obvious seen that the results from the filter press test are only qualitatively useful, i.e. only correct in tendency.

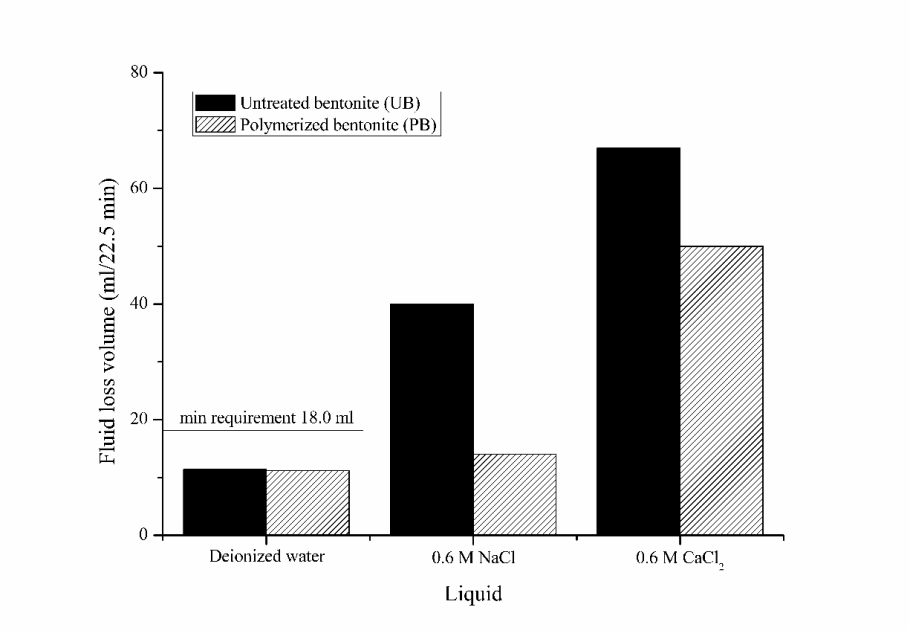

Fig. 3.48 Results of fluid loss volume with different liquids

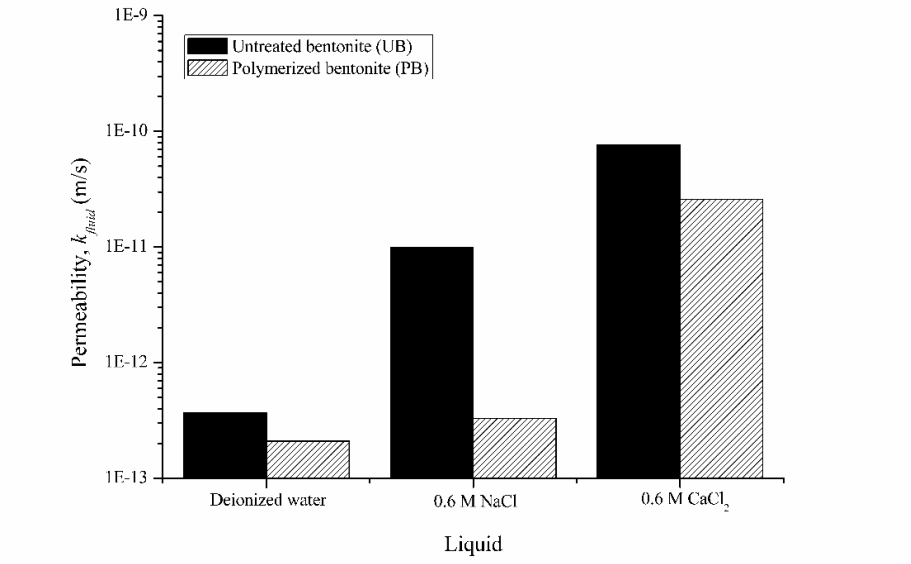

Fig. 3.49 Results of permeability (*k*) in various of liquid types

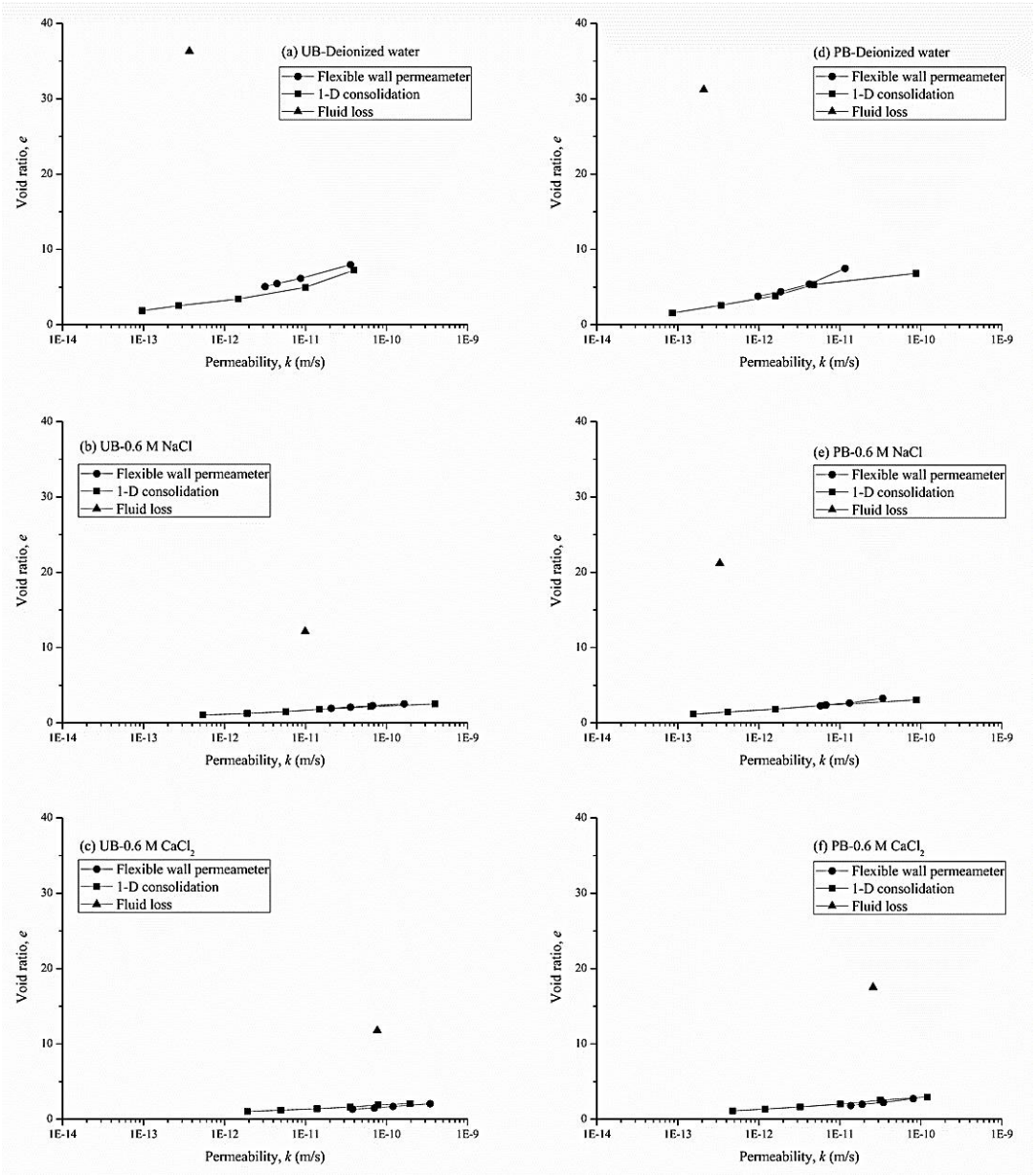

Fig. 3.50 Comparison *k* value from three different test methods

3.8.4 Permeability (k) in corrosive pH solutions

The performance of the PB under various pH conditions was further investigated and reported in this section.

(1) Test methods

The effect of pH value on permeability (*k*) was performed by one dimensional consolidation test.

(2) Results

The results of the calculated *k* value from one dimensional consolidation are presented in a relationship of the void ratio (*e*) versus permeability (*k*) in Figs. 3.50(a) and (b). Under the same void ratio (*e*) conditions, the PB gave the similar or lower *k* value in acid or alkaline solutions compared with that of the UB.

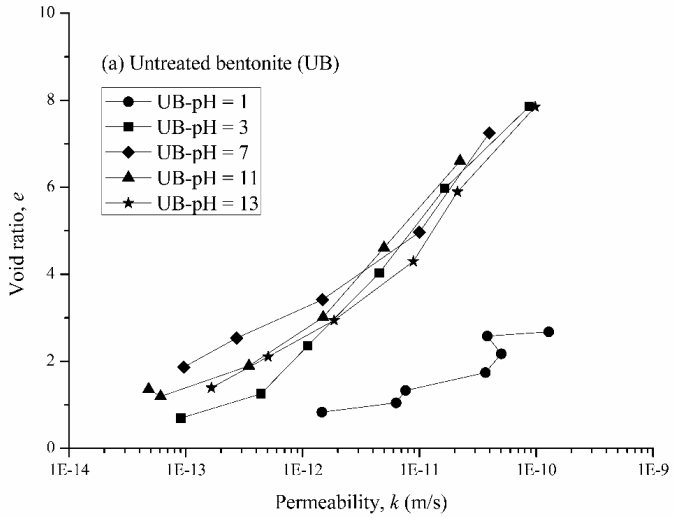

(a) Untreated bentonite (UB)

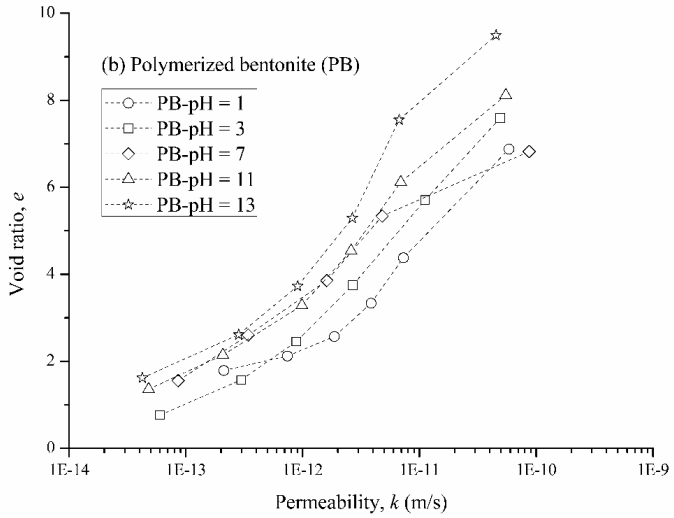

(b) Polymerized bentonite (PB)

Fig. 3.51 Relationships of *e* – log*k*

For the UB, the *k* values increase when permeated with both acid and alkaline solutions. For UB-pH=1 case, it is clearly seen that the value of *k* sharply decreases in the hyper acid (pH=1) solution, and this is possibly because the Al^{3+} ions in the octahedral layer of the montmorillonite were dissolved resulting in decreasing of thickness of the diffuse double layer (DDL) and replaced the Na^{+} ion carried by the bentonite particles. The test results of *k* value for the UB follows the general tendency of results of *k* value of GCL using UB reported by Jo et al., 2001.

For the PB, it gave increasing in *k* values in acid solutions. However, when the PB permeated with alkaline solutions, the PB gave the similar (pH of 11) or lower value of *k* (pH of 13) compared with the value of *k* in deionized water. The possible reason is that the increasing in OH^{-} from the NaOH solution increases the repulsive force between the chained anionic polymer, resulting in increase in swelling capacity of the PB.

3.9 Conclusions

The optimum conditions for polymerizing bentonite using the free radical polymerization method were investigated through a series of laboratory tests. Then, the microstructure analyses, the swelling pressure tests and the consolidation tests of the polymerized bentonite (PB) produced using the proposed conditions were performed and compared with those of the untreated bentonite (UB). Based on the test results, the conclusions can be drawn are as follows.

1. Using the free swelling index (FSI), the optimum conditions for polymerizing the bentonite using the free radical polymerization method are proposed as: using sodium acrylate as the monomer and KPS as the initiator, pH of 7.0, the initiator (*I*) to monomer (*M*) ratio, *I/M*, of 0.2 and the monomer content of 10% with respect to the mass of a bentonite to be polymerized.
2. The results of the X-ray diffraction (XRD) analysis show that the interlayer of the bentonite particles was not modified by the polymerization process. The Scanning electron microscope (SEM) images indicate that the PB particles have rounder edge compared with that of the UB particles. It is postulated that the function of the polymer is coating the bentonite particles.
3. For the four sodium bentonites tested, the PBs produced by the proposed conditions had much higher FSI values compared with those of the corresponding UBs.

4. The produced PBs yielded higher compression index (C_c) and swelling index (C_s) compared with that of the UB. This confirms that the PB had higher compressibility and swelling potential in cationic solutions. The results of coefficient of consolidation (c_v) shows that the PB has lower c_v value compared with that of the UB.
5. The PB produced from the bentontie-1 (Super Clay) yielded higher swelling pressure compared with that of the UB for three liquids tested (deionized water, 0.6 M NaCl solution and 0.6 M $CaCl_2$ solution).
6. Results from permeability tests, indicate that the *k* value increases with increasing of the cation concentration and valence of cation. Under the same void ratio (*e*) conditions, the PB gave the similar (deionized water) or lower (cationic solutions) *k* value compared with that of the UB. For the UB, the *k* value increased when permeated with both acid (pH < 7) and alkaline (pH > 7) solutions, while for the PB, *k* increased with acid solutions, and with alkaline solutions, it resulted in the similar *k* in solution with pH of 11 and lower *k* for solution of pH of 13 compared with the solution of pH = 7.

CHAPTER FOUR
SELF-HEALING CAPACITY OF GEOSYNTHETIC CLAY LINER USING POLYMERIZED BENTONITE

4.1 Introduction

In this chapter, the self-healing capacity of the GCLs using polymerized bentonite (PB) as core material (PB-GCL) and using untreated bentonite (UB) as core material (UB-GCL) when permeated with deionized water, cationic solutions and corrosive solutions was examined and the results are reported. The self-healing capacity of the GCLs in cationic solutions was investigated by a small-scale leakage rate test, while, the self-healing capacity of the GCLs with corrosive solutions was investigated by a series of large-scale leakage rate test. The effect of the pH levels on swelling capacity of the PB and the UB has weaker than that of the effect of cation as shown in Fig 3.13 (effect of cation) and Fig. 3.24 (effect of pH). To investigate the effect of the pH levels on the self-healing capacity, the damage hole larger than 20 mm in diameter is required. Therefore, the large scale leakage rate test apparatus was used because the capacity of the small scale leakage rate test is not suitable to investigate the self-healing capacity of the damage specimen with damage hole larger than 20 mm in diameter.

4.4 Self-healing capacity by small scale leakage rate test

4.2.1 Leakage rate test

To evaluate the self-healing capacity of GCL specimens with both the untreated bentonite (UB) and the polymerized bentonite (PB) in cationic solutions, a series of the leakage rate tests were conducted using a modified rigid-wall permeability test device.

(1) Calibration of the device

For GCL specimen with a damage hole, the flow rate will be basically controlled by the hydraulic resistance of the device itself. A flow test without a GCL specimen was conducted. From the test result, the permeability of the porous stone used in the device of approximately 10^{-5} m/s was obtained.

(2) GCL specimen

The geotextiles used were from a commercial geotextile encased GCL (GT-GCL) by removing the bentonite inside. The cover geotextile is a nonwoven one, and the carrier geotextile has a slit film woven layer. The GCL specimens were manually made by placing the UB (UB-GCL) or the PB (PB-GCL) uniformly between the two geotextiles. The detailed procedures are as follows:

(a) A 70-mm-diameter disk of the GCL specimen was cut from a sheet of a commercial GCL. Then, the original bentonite was removed.

(b) About half of the periphery of the cut GCL specimen without bentonite was sealed by a silyl-modified polymer (SMP) glue as shown in Fig. 4.1. Then, the two layers of geotextile were separated (except the glued part of the periphery), and approximately 4.0 kg/m^2 the UB or PB was filled between the geotextiles.

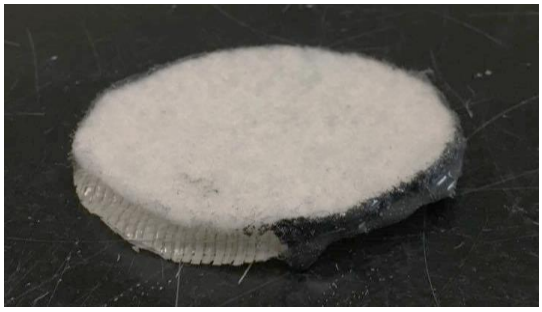

Fig. 4.1 GCL specimen with half of periphery glued

(c) The remaining part of the periphery was glued. The sample was carefully shaken to ensure a uniform distribution of the UB or PB within the specimen.

(d) The sample was oven dried at 105 °C for 24 h before being used to create the specimen for the leakage rate test.

(3) Modified rigid-wall permeameter

The modified rigid-wall falling head permeameter apparatus is shown in Fig. 4.2. The GCL specimen had a diameter of 60 mm. The vertical pressure to the specimen was applied using a mechanical screw system and read by a calibrated loading ring. During the tests, the vertical displacement of a GCL specimen was measured by a dial gauge. The water flows from the bottom to the top of the specimen, and the flow rate was calculated from the change in the water level in the burette (amount of water inflow).

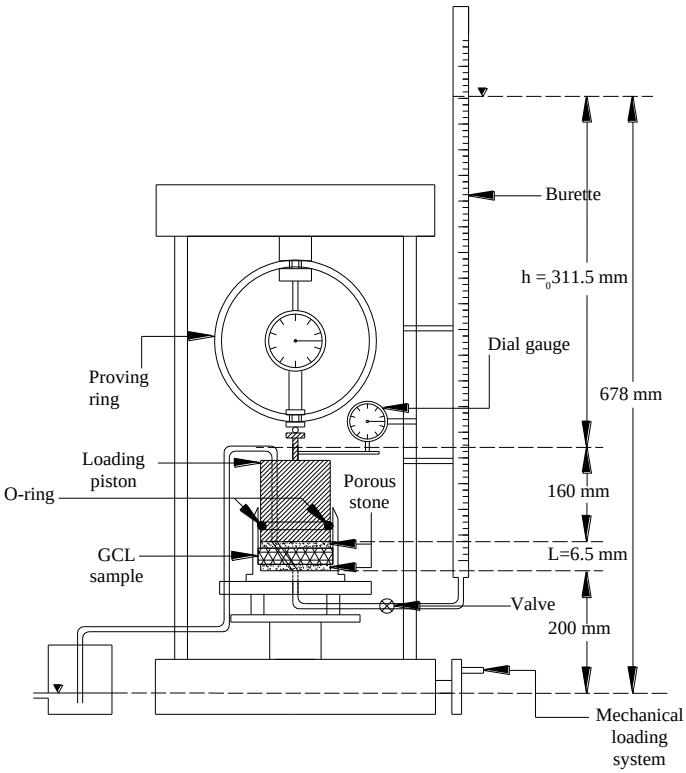

Fig. 4.2 Modified rigid-wall permeameter apparatus

(4) Liquid tested

Five different liquids namely, deionized water, 0.1 M NaCl, 0.6 M NaCl and 0.1 M $CaCl_2$, 0.6 M $CaCl_2$ were used. The properties of the liquids can be referred from Table 3.2.

(5) Test procedures

The small-scale leakage rate test was conducted with the following steps:

(a) On the 70 mm in diameter GCL sample, a specimen of 60 mm in diameter and a 20 mm in diameter circular damage hole was masked as shown in Fig. 4.3.

Fig. 4.3 Marked GCL specimen before trimming

(b) The specimen was cut/trimmed following the marked line using a sharp cutter. Afterwards, the specimen was weighed, and the initial thickness was recorded under a 50 kPa confining

pressure. A summary of the weights and thicknesses (initial and final) of the GCL specimens are listed in Table 4.1.

Table 4.1. Summary of the thickness and weight of the GCL specimens

Case	Specimen	(o)Damaged (-) Undamaged	Liquid	Initial thickness mm	Final thickness mm	Initial weight g
1	UB-GCL	O	deionized water	6.25	6.80	10.01
2	PB-GCL	O	deionized water	6.00	6.67	9.62
3	UB-GCL	O	0.1 M NaCl	4.96	5.13	9.27
4	PB-GCL	O	0.1 M NaCl	5.58	6.02	9.38
5	UB-GCL	O	0.1 M $CaCl_2$	5.61	5.73	9.77
6	PB-GCL	O	0.1 M $CaCl_2$	6.25	6.41	9.59
7	UB-GCL	O	0.6 M NaCl	5.80	5.85	9.97
8	PB-GCL	O	0.6 M NaCl	6.50	6.64	9.48
9	UB-GCL	O	0.6 M $CaCl_2$	6.55	6.64	9.56
10	PB-GCL	O	0.6 M $CaCl_2$	6.02	6.12	9.80
11	UB-GCL	-	deionized water	6.00	6.60	11.27
12	PB-GCL	-	deionized water	5.80	6.39	10.23
13	UB-GCL	-	0.1 M NaCl	6.40	6.52	11.36
14	PB-GCL	-	0.1 M NaCl	6.75	6.97	11.09
15	UB-GCL	-	0.1 M $CaCl_2$	6.42	6.51	11.13
16	PB-GCL	-	0.1 M $CaCl_2$	5.32	5.46	11.52
17	UB-GCL	-	0.6 M NaCl	5.66	5.72	11.39
18	PB-GCL	-	0.6 M NaCl	6.30	6.42	11.00
19	UB-GCL	-	0.6 M $CaCl_2$	5.48	5.56	11.23
20	PB-GCL	-	0.6 M $CaCl_2$	5.97	6.08	11.09

(c) The specimen was placed carefully into the apparatus, and a small amount of bentonite was placed along the periphery between the specimen and the wall of the container to prevent water leakage through the possible micro-gaps between the specimen and the chamber as shown in Fig. 4.4.

(d) The piston was installed. A pressure of 50 kPa was applied, and the settlements were recorded for 30 min (the settlement was almost stable).

(e) The drainage valve was opened, and leakage rate test was started. The water level and the settlement of the specimen were recorded periodically.

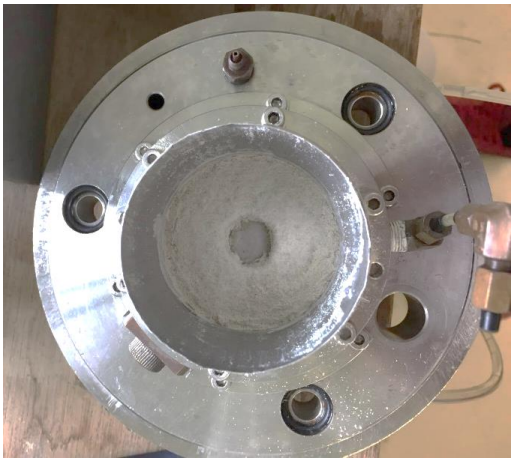

Fig. 4.4 Installation of GCL specimen into the apparatus

(f) After the leakage rate became steady (approximately with an elapsed time of 1 week), the test was terminated, the specimen was photographed, and the amount of the PB or UB that entered into the damage hole and its water content were measured.

The thickness and the density of the PB or UB entered the damage hole is also affecting to the permeability of the damage hole. However, it is difficult to measure the varieties of the thickness and the density of the UB or PB in the hole. To simplify the problem, the self-healing ratio is defined using the area only (2D), and the self-healing ratio (α) was calculated as:

$$\alpha = \frac{A_1}{A_{hole}} \tag{4.1}$$

where A_{hole} is the total damage area and A_1 is the healed area. In Fig. 4.5, A_1 was measured using a scaled photo by an AutoCAD program.

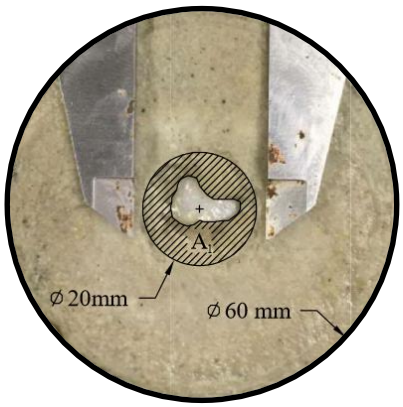

Fig. 4.5 Example to determine the healed area

The permeability of the damage hole (k_{hole}) is calculated as;

$$k_{hole} = \frac{k_d \cdot A_{total} - \lfloor k_{ud} \cdot (A_{total} - A_{hole}) \rfloor}{A_{hole}} \tag{4.2}$$

where k_d is the average permeability of the damaged sample, k_{ud} is the permeability of the sample without damage, A_{total} is the total area of the specimen and A_{hole} is the area of the damage hole.

4.2.2 Test results

The measured final average permeability of the GCL specimens with and without a damage hole are shown in Figs. 4.6(a) to (e) for the specimens permeated with 5 different liquids. For some of the tests, the initial flow rates were scattered, and for clarity, those data are excluded. As shown in Fig. 4.6(a), in the case of permeation with deionized water, both the UB-GCL and PB-GCL specimens yielded the similar steady value of *k*. This result agrees with the permeability test result of the UB and the PB given in the previous chapter. For all the cases, the value of *k* reduced with the elapsed time, which indicates a gradual self-healing of the damage hole, and at steady-state conditions, the value of *k* for the damage specimens is slightly higher than that of the undamaged specimens (Fig. 4.6(a)).

With 0.1 M NaCl and 0.1 M $CaCl_2$ solutions, the PB-GCL specimen yielded a lower value of *k* compared with that of the UB-GCL specimen for both the damaged and undamaged cases (Fig. 4.6(b) and (c)). When using 0.6 M $CaCl_2$ solution, it is evident that the UB-GCL specimen shows almost no self-healing of the damage hole. While for the PB-GCL specimen, *k* gradually decreased with time until steady-state conditions were reduced (Fig. 4.6(e)). Using the results in Figs. 4.7(a) to (c), the permeability of the damage hole (k_{hole}) can be evaluated by Eq. (4.2). The results of the value of k_{hole} are summarized in Fig. 4.7.

Generally, k_{hole} increases with the increase in the cation concentrations and valence of the cations. It can be seen that with the deionized water for both the UB-GCL and the PB-GCL specimens, k_{hole} is approximately in the same order of 10^{-10} m/s, whereas with NaCl solutions, the values of k_{hole} for the PB-GCL specimen is approximately one order of magnitude lower than that of the UB-GCL specimen. When using the $CaCl_2$ solutions, k_{hole} of the PB-GCL specimen is approximately 2 orders of magnitude lower than that of the UB-GCL specimen.

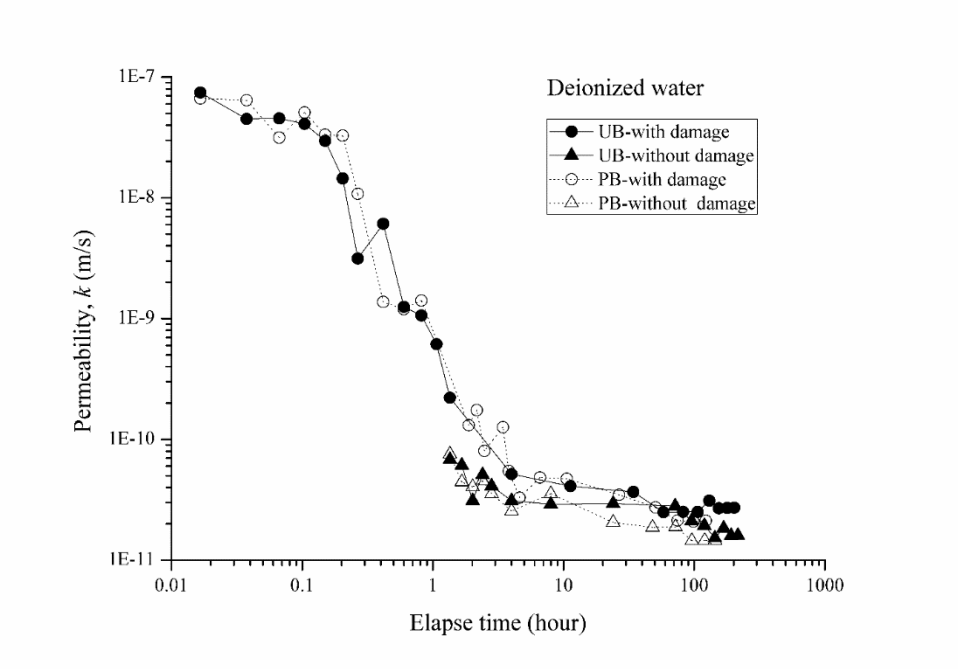

(a) Permeability with deionized water

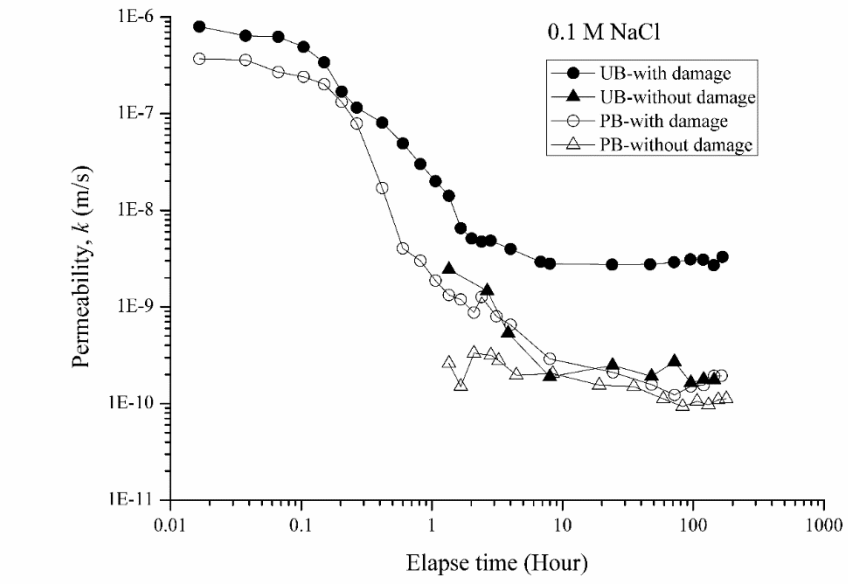

(b) Permeability with 0.1 M NaCl

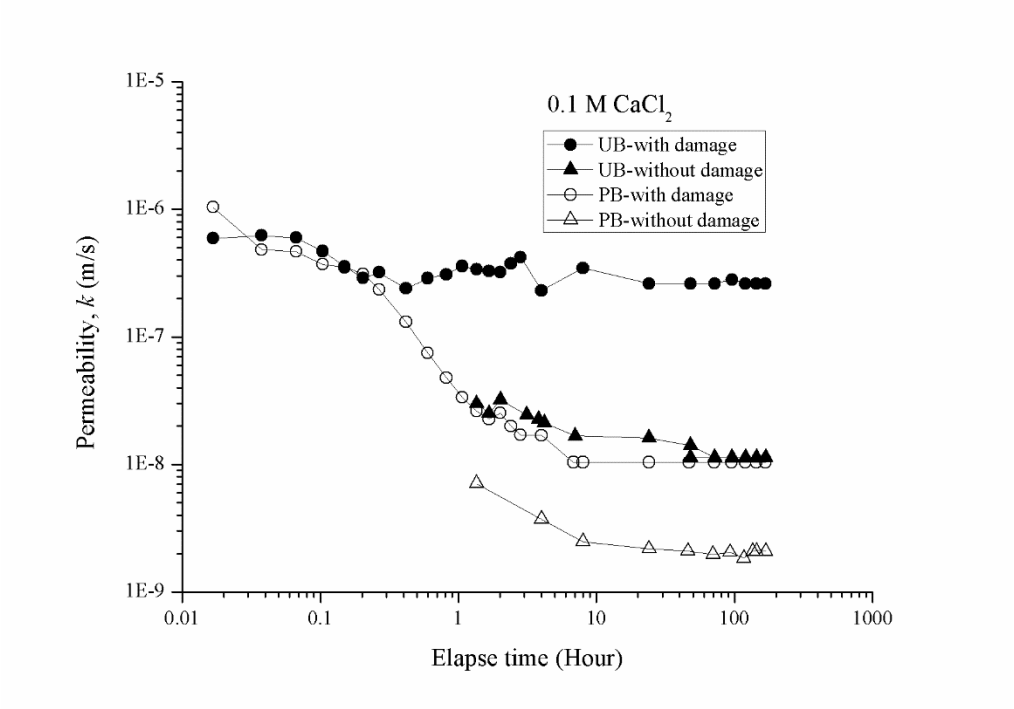

(c) Permeability with 0.1 M $CaCl_2$

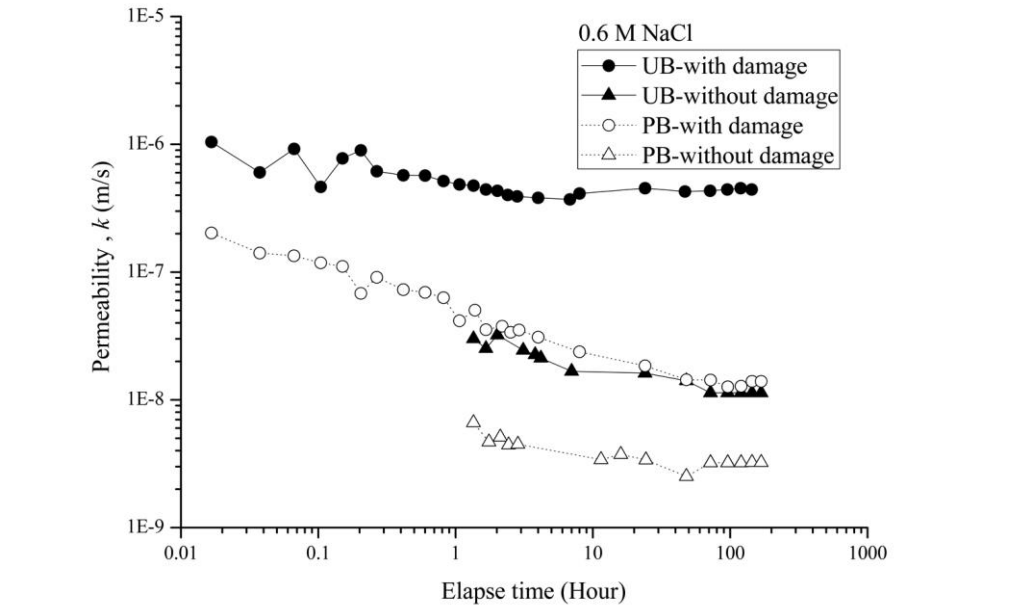

(d) Permeability with 0.6 M NaCl

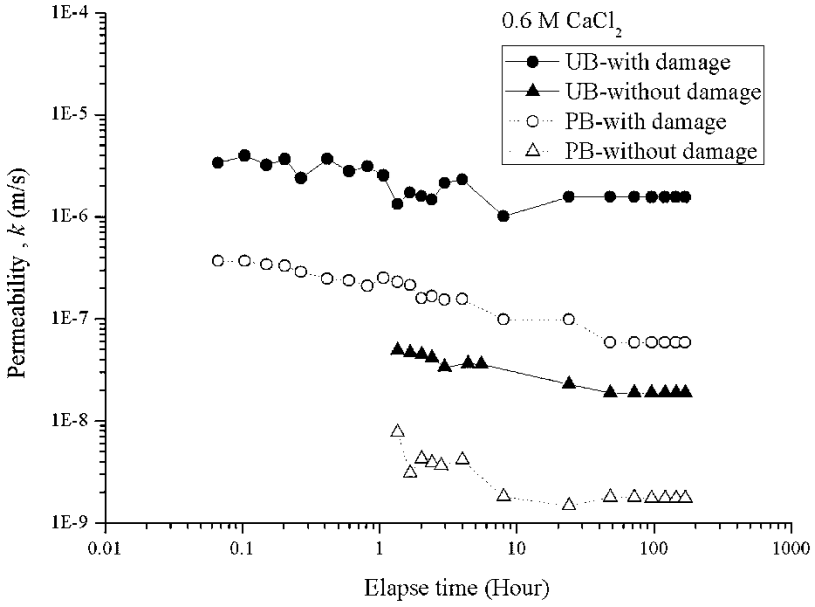

(e) Permeability with 0.6 M $CaCl_2$

Fig. 4.6(a) to (e) Permeability versus time results

As reported in the chapter 3, the PB demonstrated a higher FSI value in all the cationic solutions tested. The lower values of k_{hole} for PB-GCL are because more hydrated PB entered the damage hole and healed more of the hole area.

The photos of the specimens after the leakage rate tests are shown in Figs. 4.8(a) and (b) for the PB-GCL and UB-GCL specimens, respectively. The self-healing ratios (α) were calculated using Eq. (4.1), and the results are shown in Fig. 4.9.

With deionized water and a damage hole of 20 mm in diameter, the damage hole was fully self-healed for both the UB-GCL and PB-GCL specimens. However, with increasing cation concentrations and valence of the cations in the liquids, the self-healing capacity of both the UB-GCL and PB-GCL specimens decreased. By comparison, it can be clearly seen that the PB-GCL specimen had a higher self-healing capacity compared with that of the UB-GCL specimen for all the cationic solutions used. In the case of the 0.6 M $CaCl_2$ solution, the UB-GCL specimen was not healed at all, but the hole of the PB-GCL specimen was healed approximately 76%.

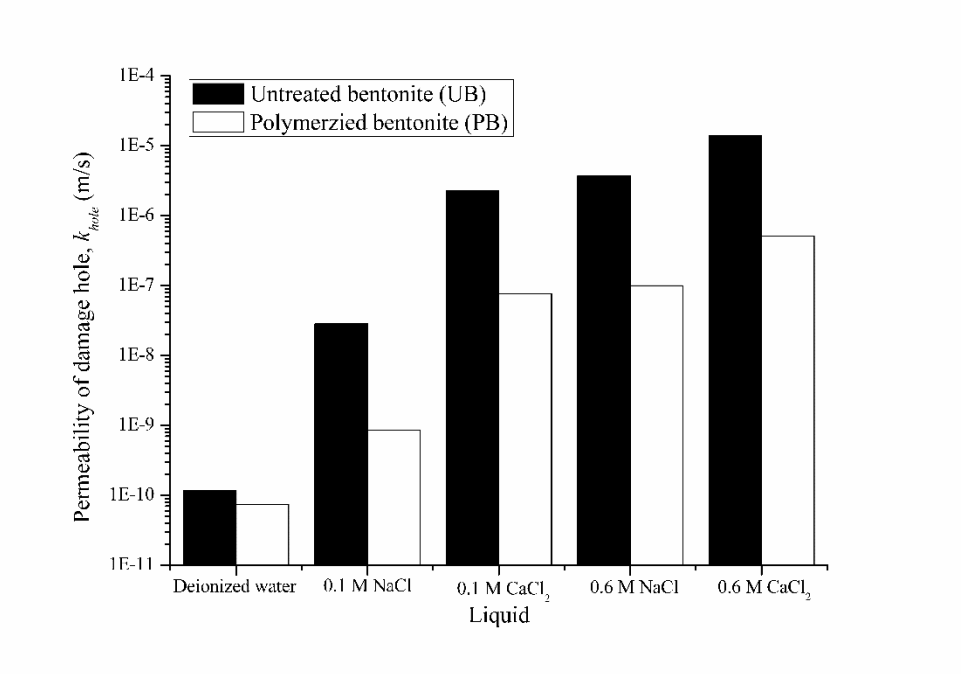

Fig. 4.7 The results of permeability of damage hole with different liquids

The amount of the UB or the PB entered the damage hole and their water contents were measured, and the results are shown in Figs. 4.10 and 4.11, respectively. It can be clearly seen that the PB-GCL specimens had more PB entered into the hole and the PB had higher water content, which is consistent with the value of α presented in Fig. 4.9.

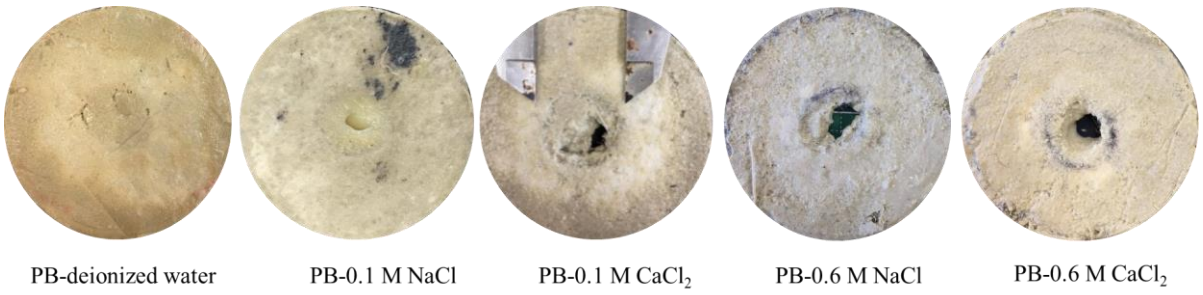

(a) Polymerized bentonite (PB)

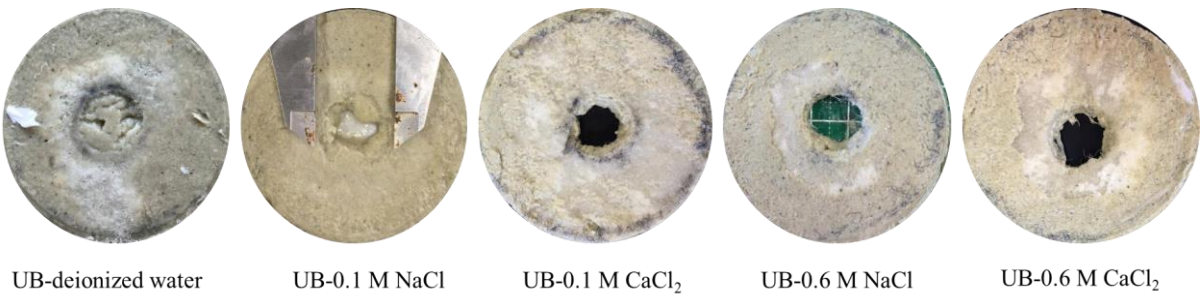

(b) Untreated bentonite (UB)

Fig. 4.8 The healing samples of GCL after the leakage rate test for the PB and the UB

The polymer used to produce the PB is an anionic type with a negatively charged carboxylic group in the backbone. Therefore, the PB can balance more cations than the UB, and even with 0.6 M $CaCl_2$ solution, the PB can still expand.

The relationship of self-healing ratio (α) and permeability of damage hole (k_{hole}) are plotted in semi-log scale as shown in Fig 4.12. For the GCL specimens with $\alpha < 0.7$, the values of k_{hole} had to the approximately the same order of the measured k of the porous stone, while for GCL specimens with $\alpha > 0.7$, the k_{hole} is approximately reversely linearly related with the values of α. This indicates that the α defined by area can be used as an indicator of degree of self-healing of the GCL specimen.

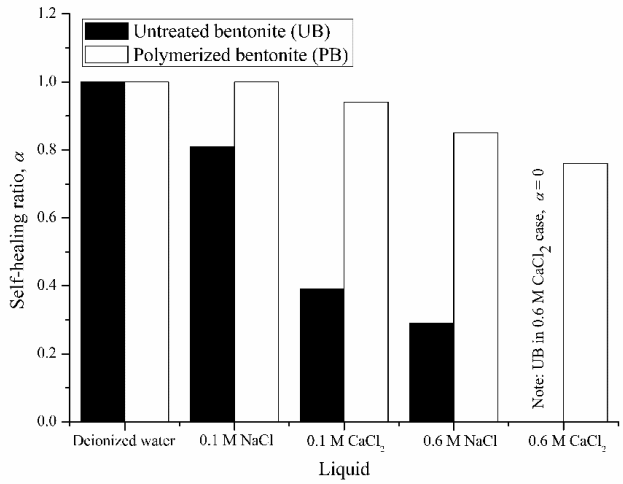

Fig. 4.9 The results of the healing ratio with different liquids

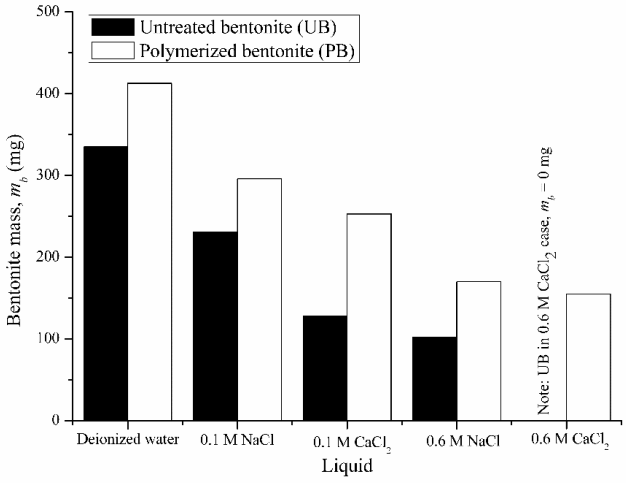

Fig. 4.10 The result of m_b with different liquids

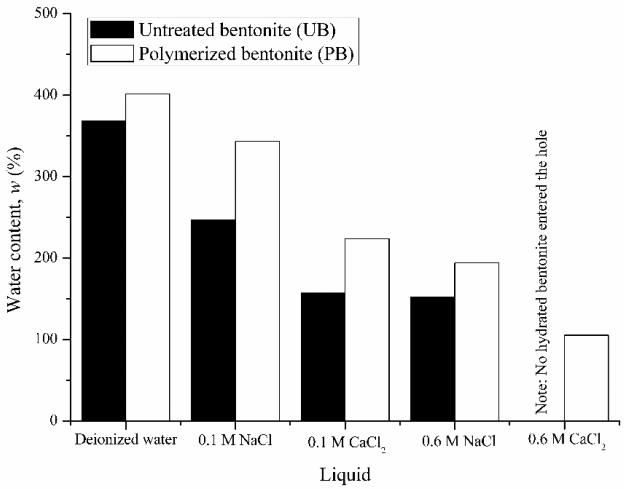

Fig. 4.11 The result of *w* with different liquid types

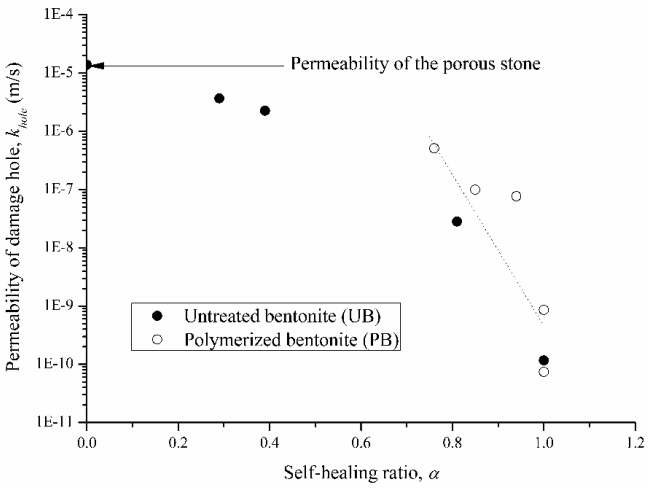

Fig. 4.12 The relationships between self-healing ratio (α) and permeability of damage hole (k_{hole})

4.3 Self-healing capacity by large scale leakage rate tests

4.3.1 Material and methods

(1) Large scale leakage rate test

A rigid-wall constant head permeability cell was used to measure the leakage rate of GCLs with a damage hole. The equipment is mainly composed of a piston loading system, and an acrylic cell with an inner diameter of 150 mm. The overburden pressure was applied using

compressed air through a bellofram cylinder system. A porous stone was inserted into the piston and the piston was perforated. The vertical displacement was measured by a dial gauge. The schematic view of the equipment is shown in Fig. 4.13(a) and the picture is given in Fig. 4.13(b). The water head of 320 mm were used in this study.

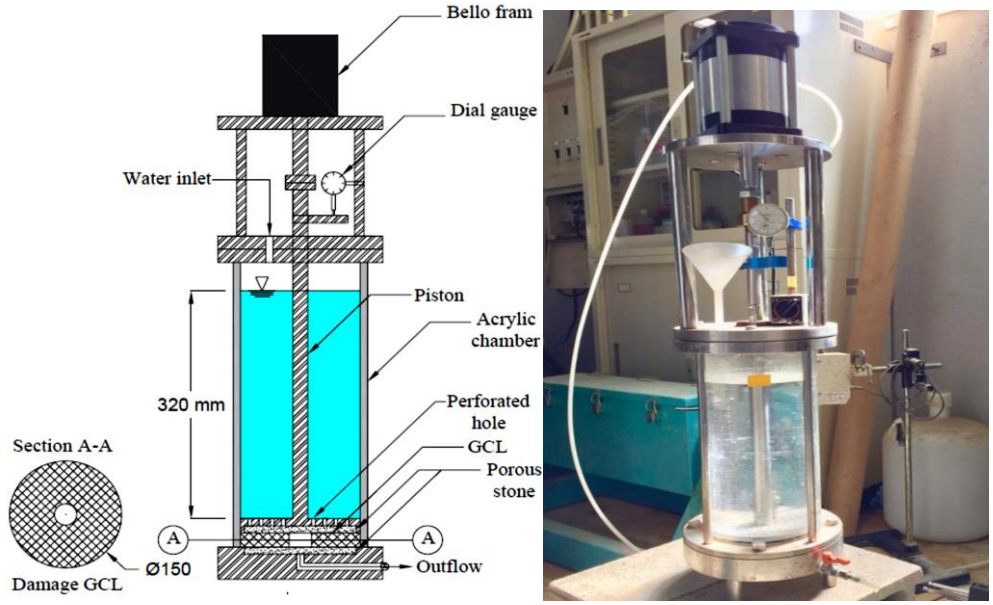

(a) Schematic view (b) Photo view

Fig. 4.13(a) and (b) Large scale leakage rate test apparatus

(2) GCL specimen

The geotextiles used were the same as reported in the section 4.2, whereas the size of specimen and methods to make the GCL in this section are different. The detailed procedures for making the GCL specimens for large scale leakage rate test are as follows:

(a) A square sheet of the GCL specimen with dimension of 200 × 200 mm was cut from a sheet of a commercial GCL. Then, the original bentonite was removed. After that, the GCL was cut separately into two parts as shown in Fig. 4.14.

(b) The two pieces of geotextile were assembled by a staple with three sides and it left the another side for filling the core material as shown in Fig. 4.15.

(c) Then, 6.60 ± 0.15 kg/m^2 (Prongmanee and Chai, 2017) of air dried powder of the UB or PB was filled into the geotextile bag (Fig. 4.16(a)) and the remaining side was sealed by the staple. The specimen was carefully shaken to ensure a uniform distribution of the UB or the PB as shown in Fig. 4.16(b).

Fig. 4.14 The woven and nonwoven geotextile

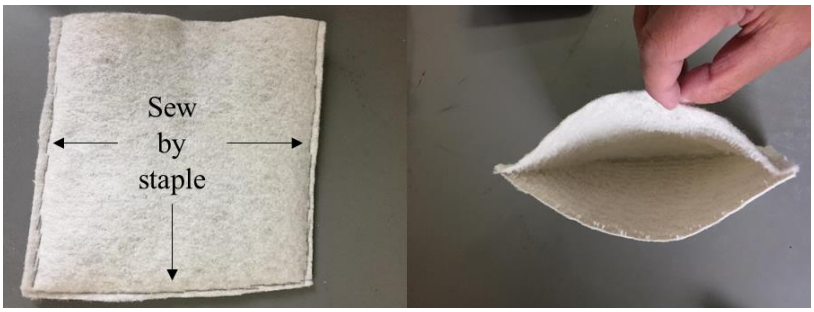

Figs. 4.15 The GCL bag

(d) The GCL bag was marked with a diameter of 150 mm and 57.3 mm of circle damaged hole (Fig. 4.17(a)). Then, the GCL sample was sewed by a yarn along the marking line. Finally, the specimen was trimmed following the marking line as indicated in Fig. 4.17(b).

(e)

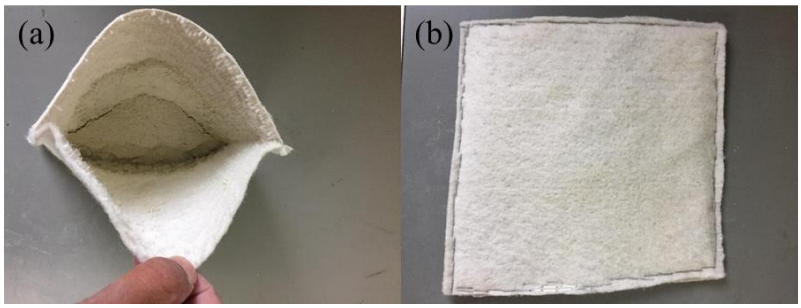

Fig. 4.16 GCL bag after fill with the sodium bentonite powder

(3) Liquids

Five different liquids namely, pH = 1, pH = 3, pH = 7, pH = 11, pH =13, were used in this section. Standard pH buffer solutions, i.e. HCl and NaOH solutions were used. By definition, pH = $-\log_{10}H^+$ concentration: pH lower than 7 is acid and pH gathered than 7 is

alkaline. Therefore, 0.001 M HCl, 0.1 M HCl, 0.001 M NaOH, 0.1 M NaOH solution can be considered as the pH value of 1, 3, 11, 13, respectively. The pH values and *EC* values are given in the Table 3.4.

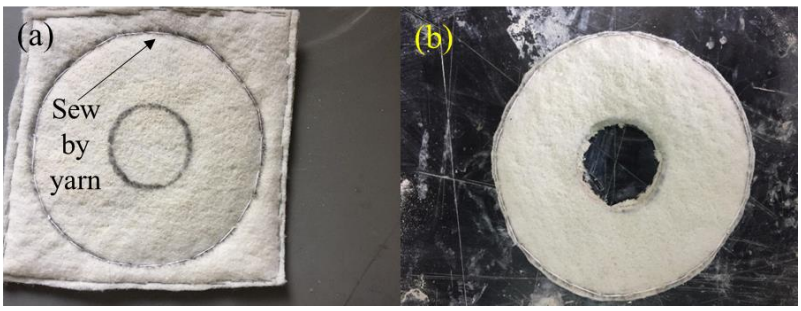

Figs. 4.17 The GCL specimen for the constant head leakage rate test

(4) Leakage rate test program

Twenty (20) cases were tested as listed in Table 4.2. The circular damage hole had a damage area of 2578.7 mm^2 (diameter of 50.8 mm) and the applied confining pressure was 40 kPa.

(5) Large scale leakage rate test methods

The detailed procedures for large scale leakage rate test are as follows:

a) The porous stones at the bottom and in the piston were saturated by boiling them for 30 minutes and kept submerged before using. The filter paper was placed on the bottom porous stone first and then the GCL specimen was set as shown in Fig. 4.18. Then, the hydrated UB or PB with the water content about their plastic limit was used to seal the gap between the specimen and the acrylic chamber. After that the piston was placed on the top of the specimen.
b) The desired liquid was filled into the cell about 1/2 of the desired water head level (320 mm) and the bottom drainage valve was closed as shown in Fig. 4.19. After that the loading system was setup.
c) A pressure of 40 kPa was applied on the top of the specimen and the displacement was recorded. The setup was kept for 24 hours.
d) The degree of saturation of the specimen was increased by a back pressure chamber contained the same test liquid as shown in Fig. 4.20. The applied back pressure of 20 kPa and the circulating liquid continued for 30 min with. After that, the liquid was filled to the desired water head level into the cylinder.
e) Open the bottom drainage valve and started the leakage rate test.

f) The amount of water flow and displacement were recorded periodically.

g) After steady state flow was reached, the leakage rate test was stopped, and the mass and water content of the hydrated bentonite entered the hole were measured.

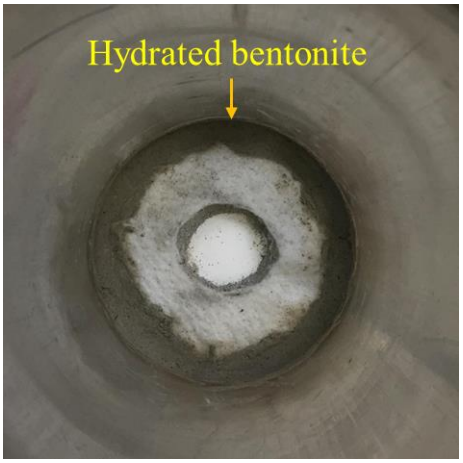

Fig. 4.18 Set-up a test specimen

(6) Results and discussions

Figs. 4.21(a) and (b) show the flow rates (Q) versus time curves of the damaged UB-GCL and the damaged PB-GCL permeated with solutions of various pH solutions. In general, Q decreased with elapse time for all tested liquids and it indicates that the GCL specimens were self-healing. In Figs. 4.21(a), it is clearly seen that the UB permeated with the solution of pH = 1 had highest Q value, while the UB with deionized water gave the lowest value of Q. The Q value is slightly increased when permeated with the solution with pH of 3 and the solution with pH of 11. The Q value is sharply increased when permeated with the pH of 1 solution and the pH of 13 solutions.

For the test results in Figs 4.21(b), the PB shows slightly changed in Q value when permeated with different liquids. For the solution with pH of 1, the PB shows increasing in the Q value, but the PB sill provided significantly lower Q value compared with that of the UB. For the solution with pH of 13, the PB yielded the lowest Q value.

The results of the flow rate of the undamaged sample of GCL is showed in Fig. 4.22. The test result shows the same tendency as the test results of the damage GCL specimen. From the flow rate, the permittivity (ψ_{hole}) of the damage hole is calculated by Eq. (4.3). The permeability of damage hole is determined by Eq. (4.4).

Table 4.2. Summary of testing programs

Case	Specimen	(o)Damaged (-) Undamaged	Liquid	Initial thickness mm	Final thickness mm
1	UB-GCL	O	0.001 M HCl	8.01	11.80
2	PB-GCL	O	0.001 M HCl	8.09	12.47
3	UB-GCL	O	0.1 M HCl	7.85	12.13
4	PB-GCL	O	0.1 M HCl	8.12	12.60
5	UB-GCL	O	Deionized water	8.16	12.39
6	PB-GCL	O	Deionized water	8.04	12.52
7	UB-GCL	O	0.001 M NaOH	8.12	12.32
8	PB-GCL	O	0.001 M NaOH	7.96	12.74
9	UB-GCL	O	0.1 M NaOH	8.14	12.30
10	PB-GCL	O	0.1 M NaOH	8.00	12.95
11	UB-GCL	-	0.001 M HCl	8.02	11.90
12	PB-GCL	-	0.001 M HCl	7.98	12.51
13	UB-GCL	-	0.1 M HCl	8.16	12.36
14	PB-GCL	-	0.1 M HCl	8.14	12.65
15	UB-GCL	-	Deionized water	8.11	12.31
16	PB-GCL	-	Deionized water	8.06	12.67
17	UB-GCL	-	0.001 M NaOH	7.88	12.42
18	PB-GCL	-	0.001 M NaOH	7.96	12.65
19	UB-GCL	-	0.1 M NaOH	8.13	12.20
20	PB-GCL	-	0.1 M NaOH	8.15	13.02

Fig. 4.19 The chamber after filling a liquid

Fig. 4.20 Back pressure chamber

$$\psi_{hole} = \frac{Q_d - Q_{ud} \cdot \left(\frac{A_{total} - A_{hole}}{A_{total}} \right)}{A_{hole} \cdot \Delta h} \tag{4.3}$$

$$k_{hole} = \psi_{hole} \cdot t_f \tag{4.4}$$

where $Q_{undamaged}$ is the steady flow rate of the undamaged sample, Q_{damage} is the steady flow rate of the damage sample, A_{total} is the total specimen area, A_{hole} is the damage area, Δh is the water head difference, and t_f is the thickness of the GCL specimen at the steady state condition.

A comparison of k_{hole} value for the solutions of different pH value is shown in Fig. 4.23. In deionized water, the value of k_{hole} of both the UB-GCL and the PB-GCL are the similar, while in acid solutions and alkaline solutions, the PB-GCL gave much lower k_{hole} than that of the UB. For the UB-GCL, the k_{hole} increases when permeated with acid and alkaline solutions, while the PB-GCL provides both increase and decrease in k_{hole} value. In acid solutions, the PB-GCL had the same tendency as the UB-GCL that the k_{hole} increase with decreasing in the pH value. However, the k_{hole} of the PB-GCL tends to decrease when it permeated with the solutions with pH of 13. As discussed in the previous section, the smaller value of k_{hole} indicates the larger volume of hydrated bentonite entered the hole, resulting in more area of damage hole to be covered by the bentonite.

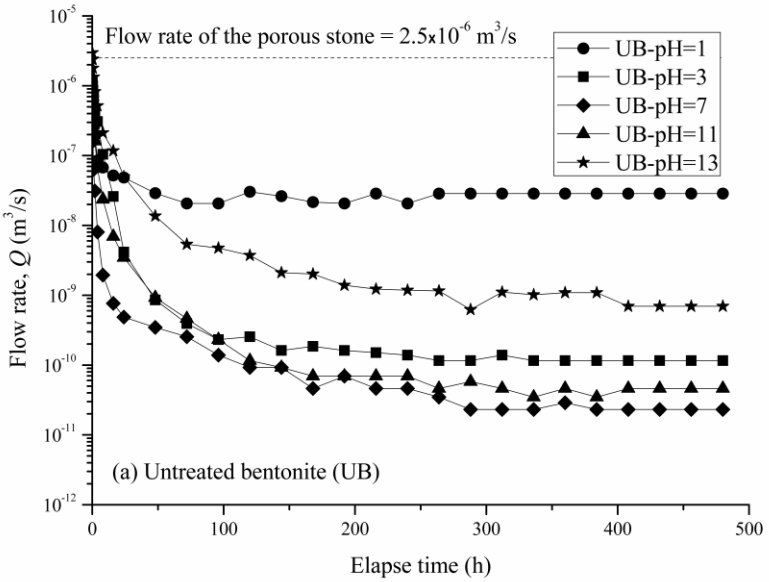

Fig. 4.21(a) Flow rate (Q) versus elapse time of the UB

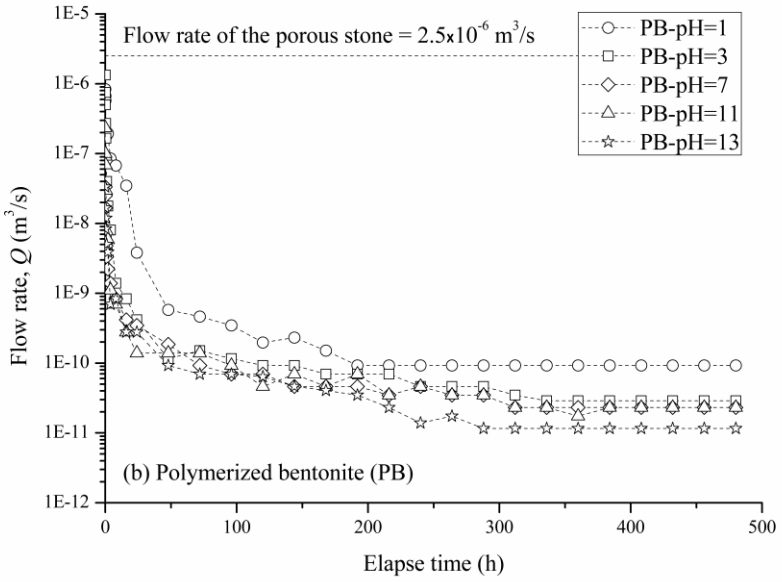

Fig. 4.21(b) Flow rate (Q) versus elapse time of the PB

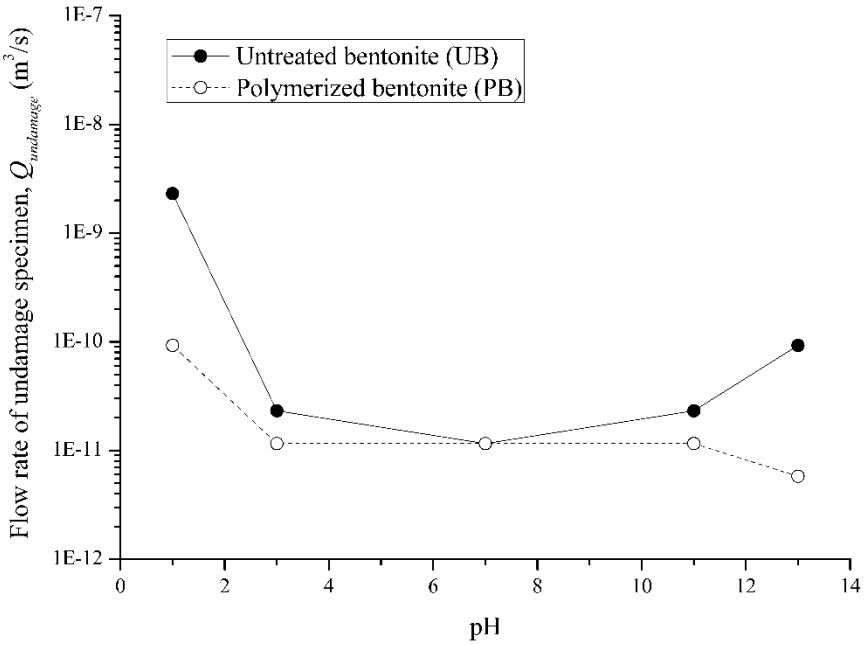

Fig. 4.22 Flow rate (Q) of undamaged sample

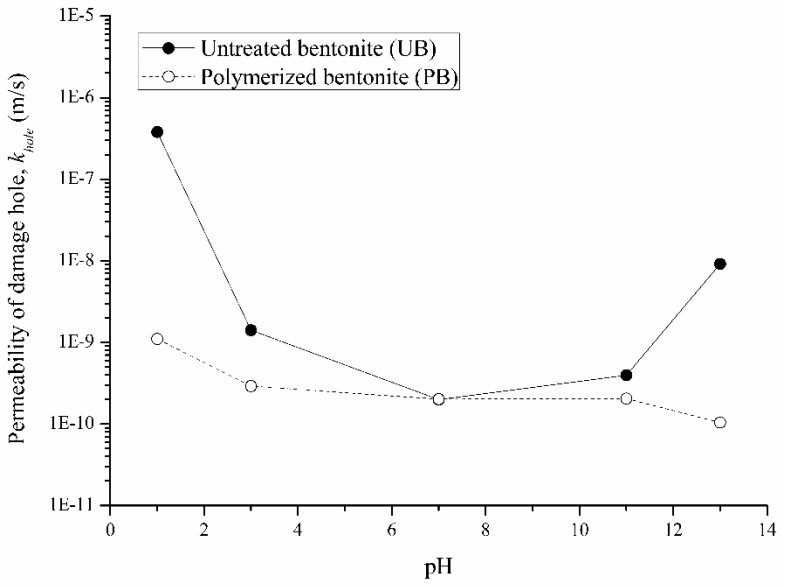

Fig. 4.23 Results of k_{hole} versus pH value

The healed specimens after the leakage rate test are shown in Figs. 4.24(a) and (b), and the calculated values of α are showed in Fig. 4.25. It shows the same tendency as the value of k_{hole} in Fig. 4.26. Thus, higher α value, lower k_{hole} can be obtained.

In Fig. 4.25, the PB shows fully self-healed for all liquids test with a damage hole of 50.8 mm in diameter, while the UB gave α = 99 % in deionized water. The value of α of the UB is slightly decreased in the range of pH of 3 and 11. However, for pH =1 and 13, the α value was significantly decreased. The test results of α confirm that the lower k_{hole} is because the PB had higher swelling potential in both the acid and alkaline solutions. The relationships between the mass (m_b) and water content (w) of the bentonite entered the damage holes versus pH are plotted in Fig. 4.26 and Fig. 4.27, respectively. The relationships follows the general trend of Fig. 4.23 and Fig. 4.25, i.e. lower the k_{hole}, higher the α and higher the value of m_b and w.

The higher swelling capacity of the PB in the solution with pH of 13 is due to the COO^- functional group (Fig. 3.20). By increasing OH^- concentration (higher pH value), it can increase the repulsive force between the chained anionic polymer, resulting in higher swelling potential compared with that of permeated in the deionized water. Based on the test results, the PB exhibited higher expansion in the strong acid solutions, and strong alkaline solutions in comparison with the UB. This indicates that for the acid and alkaline environments, the PB-GCL can be used as an effective barrier.

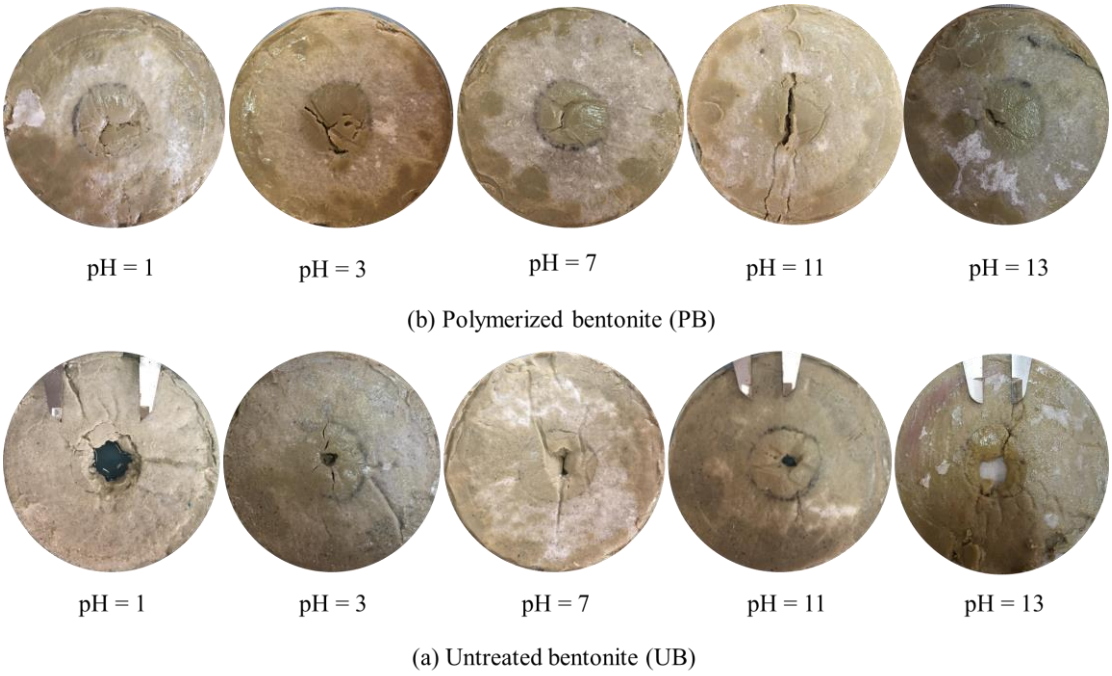

Fig. 4.24 GCL specimens after leakage rate test

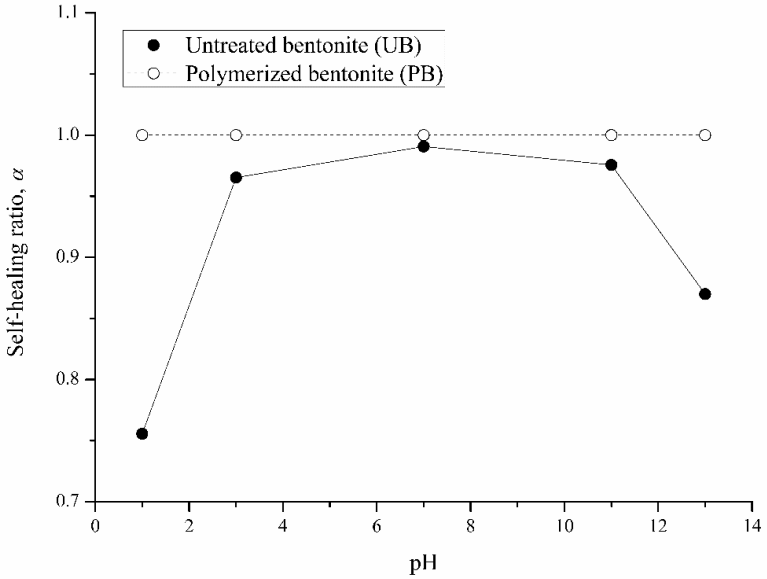

Fig. 4.25 Results of α with pH

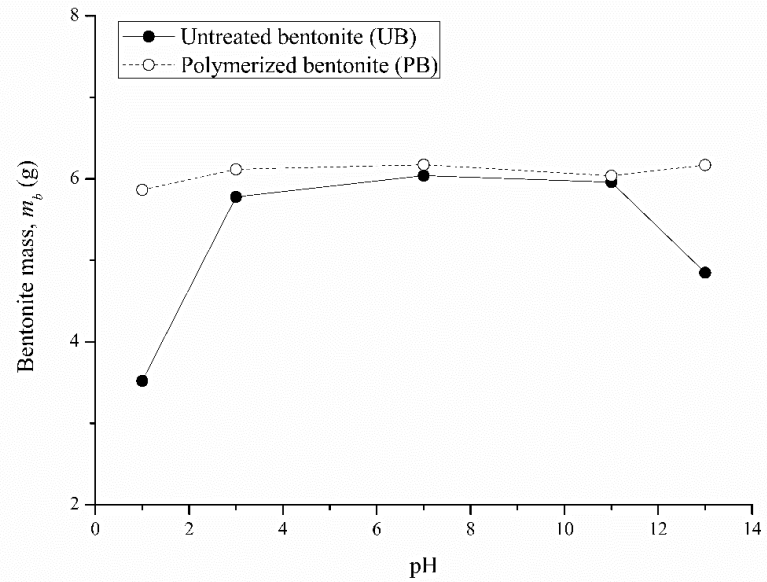

Fig. 4.26 Results of m_b with pH value

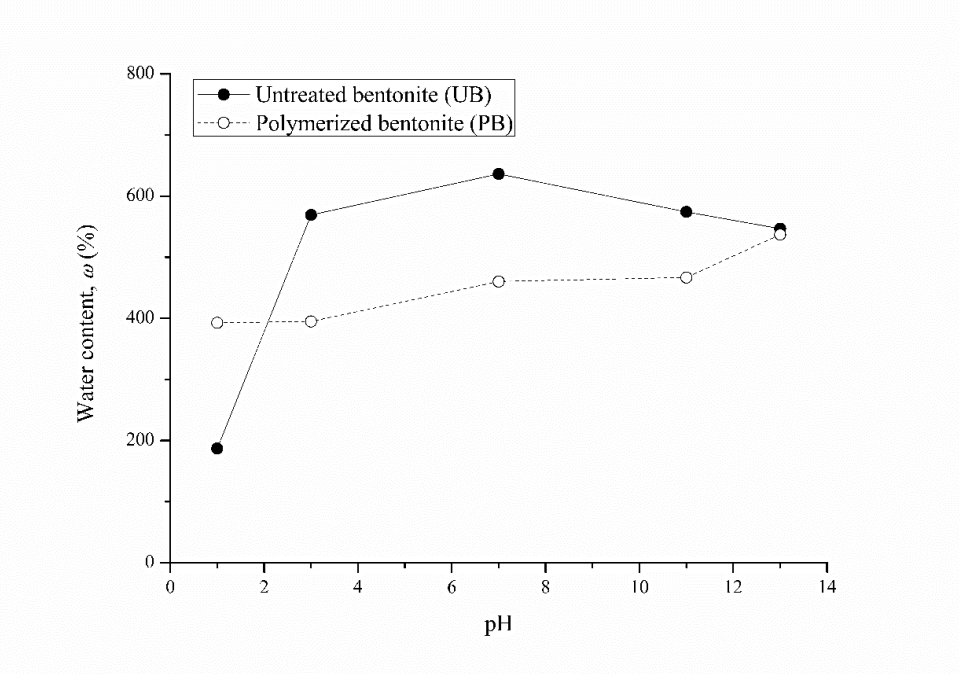

Fig. 4.27 Results of *w* with pH value

4.4 Conclusions

In this chapter, the self-healing capacity of newly material namely polymerized bentonite (PB) were evaluated through a series of laboratory leakage rate test prior recommended for the GCL material. The performance of the PB were investigate in simulate the aggressive chemical environment by considering two effect, i.e. salt solutions (concentrations and valences) and pH level. Based on the test results, following conclusions can be drawn:

1. The GCL specimen with the PB (PB-GCL) exhibited higher self-healing capacity than that of the GCL specimen with the untreated bentonite (UB)(UB-GCL). With 0.6 M $CaCl_2$ solution, for the PB-GCL specimen, 76% of a 20 mm in diameter damage hole was healed by the expanded hydrated PB, while in the case of the UB-GCL specimen, the 20 mm hole almost remained in its initial shape.
2. The permeability of damage hole (k_{hole}) of both the PB and the UB increased in acid solutions. In alkaline solutions, k_{hole} of the UB-GCL increased but for PB-GCL, in the solution with pH of 13, it resulted in the lowest value of k_{hole}. Comparing between the UB-GCL and the PB-GCL, under the same test condition, the PB-GCL shows higher pH resistant compared with that of the UB-GCL. Based on the results, it is suggested that the GCL using the PB (PB-GCL) can be used as a barrier in aggressive chemical environments.

CHAPTER FIVE
CONCLUSIONS AND RECOMMENDATIONS

5.1 Conclusions

Bentonites are widely used in barrier system because their lower permeability and high swelling pressure when hydrated. However, when bentonite meet high concentration cation or very aggressive pH solutions, their swelling capacity will dramatically reduce and their permeability will increase. Polymerizing bentonite is an effective way for maintaining low permeability and high swelling pressure of a bentonite in aggressive chemical environments.

In this study, the effective method for producing polymerized bentonite (PB) was investigated by a series of polymerization tests by varying the type of initiator, pH value, amount of monomer to be used etc. The free swelling index (FSI) was used to judge the effectiveness of the polymerization condition and optimum conditions have been proposed. The properties of the produced PB by the proposed conditions were evaluated through several series of laboratory tests compared with that of the untreated bentonite (UB). Permeability (k) of the PB and the UB in cationic solutions has been investigated by three different methods (i.e., flexible wall permeameter test, one-dimensional consolidation test, and filter press test) and the investigation of k value for both the PB and the UB in aggressive pH solutions was investigated by only one-dimensional consolidation test. Then, the value of k in aggressive pH solutions were examined through a series of one-dimensional consolidation tests.

Self-healing capacity of the geosynthetic clay liner (GCL) with the UB as core material (UB-GCL) and the GCL with the PB (UB-GCL) was investigated by small scale leakage rate tests as well as large scale leakage rate tests. The influencing factors investigated are cation concentration, valence of cation, and pH value. Based on the test results, the following conclusions can be drawn.

5.1.1 Polymerized bentonite

(1) The optimum conditions for producing PB using the free radical polymerization method are proposed as follows: using sodium acrylate as the monomer and KPS as the initiator, pH of 7.0, the initiator (I) to monomer (M) ratio, I/M, of 0.2 and the monomer content of 10% with respect of the mass of a bentonite to be polymerized. The proposed conditions have been confirmed by the test result of the FSI for the four sodium bentonites. The PBs

produced by the proposed conditions had much higher FSI values compared with those of the corresponding UBs.

(2) Based on the results of microstructure analyses, it is postulated that the function of the polymer is coating the bentonite particles without modification of the interlayer space of the bentonite particles.

(3) The produced PB had higher compression index (C_c) and swelling index (C_s) compared with that of the UB in cationic and corrosive solutions. The results of coefficient of consolidation (c_v) shows that the PB had lower c_v value compared with that of the UB for all chemical tested liquids.

(4) Results of the swelling pressure tests show that the PB yielded higher swelling pressure compared with that of the UB for three liquids tested in this study (deionized water, 0.6 M NaCl solution and 0.6 M $CaCl_2$ solution).

(5) At the same void ratio (e), the value of permeability (k) of the PB is much lower than that of the UB in chemical solutions (i.e., cationic solution and corrosive solutions).

(6) The produced PB under the proposed conditions can be effectively used as a core material in the geosynthetic clay liner (GCL) against aggressive chemical solutions.

5.1.2 Self-healing capacity of GCL with polymerized bentonite

(1) Under the same damage hole diameter (20 mm), the value of steady state permeability of damage hole (k_{hole}) for the PB-GCL is lower than that of the UB-GCL for all liquids tested. For deionized water, both the UB-GCL and the PB-GCL specimens, k_{hole} is approximately in the order of 10^{-10} m/s, whereas with NaCl solutions, the values of k_{hole} for the PB-GCL specimen is approximately one order of magnitude lower than that of the UB-GCL specimen, while using the $CaCl_2$ solutions, k_{hole} of the PB-GCL specimen is approximately 2 orders of magnitude lower than that of the UB-GCL specimen.

(2) The test result show that the PB-GCL specimen exhibited higher self-healing capacity than that of the UB-GCL specimen. With 0.6 M $CaCl_2$ solution, for the PB-GCL specimen, 76% of a 20 mm in diameter damage hole was healed by the expanded hydrated PB, while in the case of the UB-GCL specimen, the hole almost remained in its initial shape (0% healing).

(3) The permeability of damage hole (k_{hole}) of the UB-GCL and the PB-GCL increase in acid, and alkaline solutions except the PB-GCL permeated with the solution of pH =13. In the solution with pH of 13, the PB-GCL yielded the lowest of k_{hole}, with fully self-healing of a 57.3 mm in diameter damage hole. The possible reason is that the increasing in OH^-

concentration increases the repulsive force between the chained anionic polymer, and resulting in increase in swelling capacity.

(4) It is suggested that the GCL using the newly produced PB (PB-GCL) can provide better barrier performance in aggressive chemical environments.

5.2 Recommendations for further research

The present study uses the sodium acrylate as monomer for producing the polymerized bentonite (PB). For future study, other polymers such as ethyl acrylate, polyethylene glycol, polyacrylamide can be used as monomer to produce better PB with higher swelling capacity and lower permeability as well as higher resistance to chemical solutions.

REFERENCES

Ahmed, J., Tiwari, B. K., Imam, S. H., and Rao, M. A. (Eds.). (2012). Starch-based polymeric materials and nanocomposites: Chemistry, processing, and applications. CRC Press.

Ashmawy, A. K., El-Hajji, D., Sotelo, N., and Muhammad, N. (2002). Hydraulic performance of untreated and polymer-treated bentonite in inorganic landfill leachates. Clays and Clay Minerals, 50(5), 546-552.

Abels, S. and Lembens, A. (2016.) Von Badezusätzen und anderen Kosmetikprodukten. http://www.univie.ac.at/pluslucis/PlusLucis/161/S27.pdf

Armstrong, G. (2015). An introduction to polymer nanocomposites. European Journal of Physics, 36(6), 063001.

ASTM D2435. Standard Test Methods for One Dimensional Consolidation Properties of Soils using Incremental Loading. American Society for Testing and Materials, West Conshohocken, Pennsylvania, USA.

ASTM D5890. Standard Test Method for Swell Index of Clay Mineral Component of Geosynthetic Clay Liners. American Society for Testing and Materials, West Conshohocken, Pennsylvania, USA.

ASTM D5891. Standard test method for fluid loss of clay component of geosynthetic clay liners. American Society for Testing and Materials, West Conshohocken, Pennsylvania, USA.

ASTM D854. Standard test methods for specific gravity of soil solids by water pycnometer method, American Society for Testing and Materials, West Conshohocken, Pennsylvania, USA.

ASTM D4318. Standard test methods for liquid limit, plastic limit, and plasticity index of soils. American Society for Testing and Materials, West Conshohocken, Pennsylvania, USA.

Babu, G.L.S., Sporer, H., Zanzinger, H., Gartung, E. (2001). Self-healing properties of

geosynthetic clay liners. *Geosynthetic International*, 8(5), 461-470.

Bathurst, R. J., Rowe, K. R., Zeeb, B., and Reimer, K. (2007). A geocomposite barrier for hydrocarbon containment in the Arctic. *ISSMGE International Journal of Geoengineering Case Histories*, 1(1), 18-34.

Bolt, G. H. (1956). Physico-chemical analysis of the compressibility of pure clays. *Geotechnique*, 6(2), 86-93.

Bohnhoff, G. L., and Shackelford, C. D. (2013). Improving membrane performance via bentonite polymer nanocomposite. *Applied Clay Science*, 86, 83-98.

Bogdal, D., Bednarz, S., and Matras-Postolek, K. (2014). Microwave-assisted synthesis of hybrid polymer materials and composites. In Microwave-assisted Polymer Synthesis, pp. 241-294. Springer International Publishing.

Buchholz, F., Graham, A. (1998). Modern Superabsorbent Polymer Technology. John Wiley and Sons, New York.

Cowie, J. M. G., and Arrighi, V. (2008). Polymers: chemistry and physics of modern materials. (3rd ed.). Scotland: CRC Press.

Chai, J. C., and Shen, S. L. (2018). Predicting Swelling Behavior of a Na^+-Bentonite Used in GCLs. *International Journal of Geosynthetics and Ground Engineering*, 4(1), 9.

Chai, J. C, Sari, K. and Hino, T., 2013. Effect of type of leachate on self-healing capacity of geosynthetic clay liner. *Geosynthetics Engineering Journal*, 28, 93-98.

Chandra, T., and Zebrowski, J. P. (2014). Reactivity control using a Schlenk line. *Journal of Chemical Health and Safety*, 21(3), 22-28.

Choi, Y. S., Ham, H. T., and Chung, I. J. (2003). Polymer/silicate nanocomposites synthesized with potassium persulfate at room temperature: polymerization mechanism, characterization, and mechanical properties of the nanocomposites. *Polymer*, 44(26), 8147-8154.

Davis, F. J. (2004). Polymer chemistry. The School of Chemistry the University of Reading, UK.

Daniel, D.E.(1993). Introduction. In: Daniel D.E. (ed) Geotechnical practice for waste disposal. Chapman & Hall, London

Destarac, M., Guinaudeau, A., Geagea, R., Mazieres, S., Van Gramberen, E., Boutin, C., and Wilson, J. (2010). Aqueous MADIX/RAFT polymerization of diallyldimethylammonium chloride: Extension to the synthesis of poly (DADMAC)-based double hydrophilic block copolymers. Journal of Polymer Science Part A: *Polymer Chemistry*, 48(22), 5163-5171.

Deng, Y., Dixon, J. B., White, G. N., Loeppert, R. H., and Juo, A. S. (2006). "Bonding between polyacrylamide and smectite." Colloids and Surfaces A: *Physicochemical and Engineering Aspects*, 281(1), 82-91.

Di Emidio, G., Mazzieri, F., Verastegui-Flores, R. D., Van Impe, W., and Bezuijen, A. (2015). Polymer-treated bentonite clay for chemical-resistant geosynthetic clay liners. *Geosynthetics International*, 22 (1) 125-137.

Dickinson, S., Brachman, R.W.I. (2006). Deformations of a geosynthetic clay liner beneath a geomembrane wrinkle and coarse gravel. *Geotextiles and Geomembranes*, 24(5), , 285-298.

Du, Y. J., Yang, Y. L., Fan, R. D., and Wang, F., 2016. Effects of phosphate dispersants on the liquid limit, sediment volume and apparent viscosity of clayey soil/calcium-bentonite slurry wall backfills. KSCE Journal of Civil Engineering, 20(2), 670-678.

Elhajji, D., Ashmawy, A. K., Darlington, J., and Sotelo, N. (2001). Effect of inorganic leachate on polymer treated GCL material. Proc., the Geosynthetics 2001 Conference, Portland, Oregon, USA, pp. 663-670.

EPA., (2001). Geosynthetic clay liners used in municipal solid waste landfills.

EPA., (2015). Advancing sustainable materials management: 2014 fact sheet.

Fox, P.J., Triplett, E.J., Kim, R.H., Olsta, J.T. (1998). Field study of installation damage for geosynthetic clay liners. *Geosynthetics International*, 5(5), 491-520.

Forastiere, F., Badaloni, C., de Hoogh, K., von Kraus, M. K., Martuzzi, M., Mitis, F., and Perucci, C. A. (2011). Health impact assessment of waste management facilities in

three European countries. *Environmental Health*, 10(1), 53.

Gao, F. (2004). Clay/polymer composites: the story. *Materials today*, 7(11), 50-55.

Geckeler, K. E., and Nishide, H. (Eds.). (2009). Advanced nanomaterials. John Wiley & Sons.

Haraguchi, K., Ning, J., and Li, G. (2015). Swelling/deswelling behavior of zwitterionic nanocomposite gels consisting of sulfobetaine polymer–clay networks. *European Polymer Journal*, 68, 630-640.

Hu, B., Kong, Y., Zheng, R., Dong, J., Choy, K. L., and Zhao, H. (2016). Effect of C_8mimPF_6 on miniemulsion polymerization for application in new latex coating products. Faraday discussions, 190, 487-508.

Jenkins, P. L., Phillips, T. J., Mulberg, E. J., & Hui, S. P. (1992). Activity patterns of Californians: use of and proximity to indoor pollutant sources. Atmospheric Environment. Part A. *General Topics*, 26(12), 2141-2148.

Jo, H. Y., Katsumi, T., Benson, C. H., and Edil, T. B. (2001). Hydraulic conductivity and swelling of nonprehydrated GCLs permeated with single-species salt solutions. *Journal of Geotechnical and Geoenvironmental Engineering*, ASCE, 127 (7), 557-567.

Khulbe, K. C., Mann, R. S., and Khulbe, C. P. (1982). Polymerization of pyrrole by potassium persulfate. *Journal of Polymer Science Part A: Polymer Chemistry*, 20(4), 1089-1095.

Kong, D. J., Wu, H. N., Chai, J. C., and Arulrajah, A. (2017). State-Of-The-Art Review of Geosynthetic Clay Liners. *Sustainability*, 9(11), 2110.

Liu, M., and Guo, T. (2001). Preparation and swelling properties of crosslinked sodium polyacrylate. *Journal of Applied Polymer Science*, 82(6), 1515-1520.

Mazzieri, F., Pasqualini, E. (1997). Field performance of GCL: A case study. Environmental Geotechnics, Bouazza, A., Kodikara, J. and Parker, R., Editors, Balkema, Vol. 1, Proceedings of the 1stAustralia-New Zealand Conference on Environmental Geotechnics: GeoEnvironment 97, Melbourne, Australia, November 1997, pp. 289-294

Mazzieri, F. and Pasqualini, E., 2000. Permeability of damaged geosynthetic clay liners. *Geosynthetics International*, 7(2), 101-118.

McRory, J. A., and Ashmawy, A. K. (2005). Polymer treatment of bentonite clay for contaminant resistant barriers. In Waste Containment and Remediation (pp. 1-11).

Mitchell, J. K., and Soga, K. (2005). Fundamentals of soil behavior.

Mingzhu, L., Rongshi, C. H. E. N. G., and Jingjia, W. U. (1996). Preparation and swelling properties of super-absorbent polymer. 14(1), 48-56.

Miyahara, M., Kouzuma, A., and Watanabe, K. (2015). Effects of NaCl concentration on anode microbes in microbial fuel cells. *AMB Express*, 5(1), 1-9.

Mortensen, J. L. (1960). Adsorption of hydrolysed polyacrylonitrile on kaolinite. Proceedings of the 9th National Conference, West Lafayette, IN, USA, pp. 530–545.

Naka, A., Katsumi, T., Flores, G., Inui, T., Ohta, T., Urakoshi, T., and Ishihara, T. (2012). Evaluation of mineral barriers against acid rock drainage. Geotechnical Engineering *Journal of the SEAGS & AGSSEA*, 43(3), 35-42.

Ning, J., Kubota, K., Li, G., & Haraguchi, K. (2013). Characteristics of zwitterionic sulfobetaine acrylamide polymer and the hydrogels prepared by free-radical polymerization and effects of physical and chemical crosslinks on the UCST. *Reactive and Functional Polymers*, 73(7), 969-978.

Nosko, V. and Touze-Foltz, N., 2000, Geomembrane Liner Failure: Modelling of its Influence on Contaminant Transfer, *Proceedings of EuroGeo 2*, Vol. 2, Bologna, Italy, pp. 557-560.

Norrish, K., and Quirk, J. (1954). Crystalline swelling of montmorillonite, use of electrolytes to control swelling, *Nature*, 173, 255-257.

Odian, George (2004). Principles of Polymerization (4th ed.). New York: Wiley-Interscience Zohuriaan-Mehr, M. J., & Kabiri, K. (2008). Superabsorbent polymer materials: a review. *Iranian polymer journal*, *17*(6), 451.

Okamoto, M. (2003). Polymer/layered silicate nanocomposites (Vol. 14). iSmithers Rapra

Publishing.

Olad, A. (2011). Polymer/clay nanocomposites. Advances in diverse industrial applications of nanocomposites. InTech. < https://www.intechopen.com > (Mar. 22, 2011)

Onikata, M., Kondo, M., and Kamon, M. (1996). Development and characterization of a multiswellable bentonite. *Environmental Geotechnics*. Taylor and Francis, Rotterdam, 587-590.

Onikata, M., Kondo, M., Hayashi, N., and Yamanaka, S. (2000). Complex formation of cation-exchanged montmorillonites with propylene carbonate: osmotic swelling in aqueous electrolyte solutions. *Clays and Clay Minerals*, 47(5), 672-677.

Özhan H.O. (2017). "Effects of Adding Anionic Polymer to GCLs Treated with Chemical Solutions." Proc. 19th ICSMGE, Seoul, South Korea, pp. 955-958.

Prongmanee, N. and Chai, J-C. (2017) Effect of Shape of Damage Hole on Self-Healing Capacity of GCL. *Geosynthetics Engineering Journal*, 32, pp. 59-64.

Prongmanee, N., Chai, J-C., Shen, S-L., 2018. Hydraulic Properties of Polymerized Bentonites." Journal of Material in Civil Engineering, ASCE, doi;10.1061/(ASCE) MT.1943-5533.0002442.

Razakamanantsoa, A. R., Barast, G., Djeran-Maigre, I., Didier, G., and Couradin, A. (2008). Hydraulic performance of bentonite soil mixture reinforced by polymer in contact of different fluids. Proc., Journées Nationales de Géotechnique et de Géologie de l'Ingénieur, Nantes, France, pp. 133-140.

Razakamanantsoa, A. R., Barast, G. and Djeran-Maigre, I. (2012). Hydraulic performance of activated calcium bentonite treated by polyionic charged polymer. *Applied Clay Science*, 59, 103-114.

Razakamanantsoa, A., Djeran-Maigre, I., and Barast, G. (2014). Characterisation of bentonite polymer for bottom liner use. *Environmental Geotechnics*, *3*(1), 28-35.

Rozainy, M. M. R., Hasif, M., Puganeshwary, P., and Afifi, A. (2014). Combination of chitosan and bentonite as coagulant agents in dissolved air flotation. *APCBEE procedia*, 10, 229-234.

Rosin-Paumier, S., & Touze-Foltz, N. (2012). Hydraulic and chemical evolution of GCLs during filter press and oedopermeametric tests performed with real leachate. *Geotextiles and Geomembranes*, 33, 15-24.

Rosin-Paumier, S., Touze-Foltz, N., Pantet, A., Monnet, P., Didier, G., Guyonnet, D., & Norotte, V. (2010). Swell index, oedopermeametric, filter press and rheometric tests for identifying the qualification of bentonites used in GCLs. *Geosynthetics International*, 17(1), 1-11.

Rowe, R. K., Brachman, R. W., Take, W. A., Rentz, A., & Ashe, L. E. (2016). Field and laboratory observations of down-slope bentonite migration in exposed composite liners. Geotextiles and Geomembranes, 44(5), 686-706.

Ruhl, Janice L. and Daniel, David E. (1997), Geosynthetic Clay Liners Permeated with Chemical Solutions And Leachates, *Journal Of Geotechnical And Geoenvironmental Engineering*, 123(4), 369-381.

Sari, K. and Chai, J., 2013. Self-healing capacity of geosynthetic clay liners and influencing factors. *Geotextiles and Geomembranes*, 41, 64-71.

Sari, K. (2013). Investigation on self-healing capacity of geosynthetic clay liner (Doctoral dissertation, 佐賀大学).

Scalia, J., Benson, C. H., Edil, T. B., Bohnhoff, G. L., and Shackelford, C. D. (2011). Geosynthetic clay liners containing bentonite polymer nanocomposite. Proc., Geo-Frontiers 2011: Advances in geotechnical engineering, Dallas, Texas, USA, pp. 2001-2009.

Scalia, J., Benson, C. H., Bohnhoff, G. L., Edil, T. B., and Shackelford, C. D. (2014). Long-term hydraulic conductivity of a bentonite-polymer composite permeated with aggressive inorganic solutions. *Journal of Geotechnical and Geoenvironmental Engineering, ASCE*, 140(3), 04013025.

Schenning, J. A. (2004). Hydraulic performance of polymer modified bentonite.

Seiphoori, A., Laloui, L., Ferrari, A., Hassan, M., and Khushefati, W. H. (2016). Water retention and swelling behaviour of granular bentonites for application in

Geosynthetic Clay Liner (GCL) systems. *Soils and Foundations*, 56(3), 449-459.

Shackelford, C.D., Benson, C.H., Katsumi, T., Edil, T.B. and Lin, L., 2000. Evaluating the hydraulic conductivity of GCLs permeated with non-standard liquids. *Geotextiles and Geomembranes*, 18(2), 133-161.

Shackelford, C. D., Sevick, G. W., & Eykholt, G. R. (2010). Hydraulic conductivity of geosynthetic clay liners to tailings impoundment solutions. *Geotextiles and Geomembranes*, 28(2), 149-162.

Schanz, T., and Tripathy, S. (2009). Swelling pressure of a divalent-rich bentonite: Diffuse double-layer theory revisited. *Water Resources Research*, 45(5).

Stumm, W. (1992). Chemistry of the solid-water interface: processes at the mineral-water and particle-water interface in natural systems. John Wiley & Son Inc.

Sperling, L. H. (2005). Introduction to physical polymer science. John Wiley & Sons.

Sposito, G., "The Chemistry of Soils," Oxford University Press, Inc, New York, New York, 1989.

Sridharan, A., and Prakash, K., 1999. Influence of clay mineralogy and pore-medium chemistry on clay sediment formation. Canadian Geotechnical Journal, 36(5), 961-966.

Taylor, D. (1948). Fundamentals of soil mechanics. Chapman and Hall, Limited.; New York.

Tang, Q., Katsumi, T., Inui, T., and Li, Z. (2014). Membrane behavior of bentonite-amended compacted clay. *Soils and Foundations*, 54(3), 329-344.

Theng, B.K.G. (1997). Formation and Properties of Clay-Polymer Complexes, Elsevier Scientific Publishing Company, New York, New York

Theng, B. K. G. (1982). Clay-polymer interactions: summary and perspectives. *Journal of Clay and Clay Minerals*, 30(1), 1–10.

Trauger R. and Darlington J. (2000). Next-generation geosynthetic clay liners for improved durability and performance. *TR-220*. Colloid Environmental Technologies Company,

Arlington Heights, 2-14.

Von Maubeuge, K. P. (2002). Investigation of bentonite requirements for geosynthetic clay barriers. Clay Geosynthetic Barriers-Zanzinger, Koerner & Gartung (eds), pg. 155-163.

Wahl, R. R., Madison, S., DePinto, R., and Shay, B. (1998). Mechanistic studies on the decomposition of water soluble azo-radical-initiators. *Journal of the Chemical Society*, Perkin Transactions 2, (9), 2009-2018.

Wang, Y., Ma, J., Yang, S., and Xu, J. (2011a). PDMAA/Clay nanocomposite hydrogels based on two different initiations. *Colloids and Surfaces A: Physicochemical and Engineering Aspects*, 390(1), 20-24.

Wang, M., Wang, Z., Wang, J., Zhu, Y., and Wang, S. (2011b). An antioxidative composite membrane with the carboxylate group as a fixed carrier for CO_2 separation from flue gas. *Energy & Environmental Science*, 4(10), 3955-3959.

Yanovska, E., Savchenko, I., Sternik, D., Kychkiruk, O., Ol'khovik, L., and Buriachenko, I. (2017). In Situ Immobilization on the Silica Gel Surface and Adsorption Capacity of Poly [N-(4-carboxyphenyl) methacrylamide] on Toxic Metal Ions. *Nanoscale Research Letters*, 12(1), 313.

Zhang, M.Q., and M.Z. Rong, 2011. Self-Healing Polymers and Polymer Composites. A John Wiley Sons Inc., Publication, Hoboken, New Jersey.

Zdanowicz, M., Schmidt, B., and Spychaj, T. (2010). Starch graft copolymers as superabsorbents obtained via reactive extrusion processing. *Polish Journal of Chemical Technology*, 12(2), 14-17.